Report Number 94-15

research

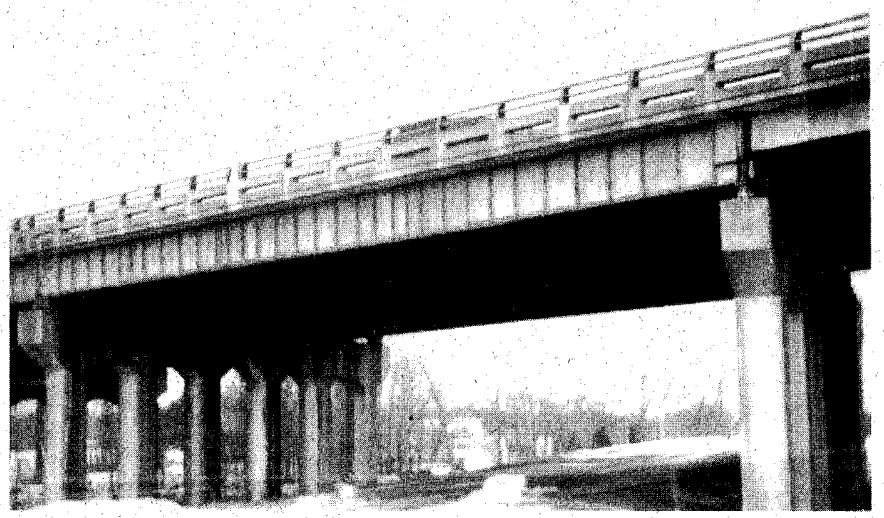

Field Instrumentation of Steel Highway Bridges

UNIVERSITY OF MINNESOTA
CENTER FOR TRANSPORTATION STUDIES

Report Documentation Page

1. Report No.	2.	3. Recipient's Accession No.
MN/RC - 94/15		

4. Title and Subtitle	5. Report Date
Field Instrumentation of Steel Highway Bridges	February 1993
	6.

7. Author(s)	8. Performing Organization Report No.
Roberto T. Leon, Theodore V. Galambos, Jeffrey J. Schmit, and Ai-Lien Teng	

9. Performing Organization Name and Address	10. Project/Task/Work Unit No.
Civil & Mineral Engineering Department University of Minnesota 500 Pillsbury Dr. SE Minneapolis, Mn 55455	11. Contract(C) or Grant(G) No. (C) Mn/DOT 67428 TOC 60 (C) Mn/DOT 68584 TOC 68

12. Sponsoring Organization Name and Address	13. Type of Report and Period Covered
Minnesota Department of Transportation Office of Research Administration 200 Ford Building-Mail Stop 330 117 University Avenue St. Paul, Mn. 55155	Final Report 1990-1992
	14. Sponsoring Agency Code

15. Supplementary Notes

16. Abstract (Limit: 200 words)

Two projects dealing with field instrumentation of bridges are described in this report. In the first project, a portable, rugged and multi-purpose bridge instrumentation system was developed. This was accomplished by using fourteen removable instruments and a portable data acquisition. The instrumentation included eight reusable strain sensors and six inclinometers, which allowed load distributions, stresses, and displacements to be measured in steel girder bridges. In the second part of the project the portable data acquisition system was used to measure strains near fatigue critical details in steel bridges to determine stress ranges under both controlled and random traffic. For this part of the project conventional strain gauges were also used.

Overall this acquisition and modelling system worked quite well for determining strains and deflections of simply supported bridges under static loadings. A new measurement technique for finding deflections, based on slope sensors, was developed and verified. This technique can now be readily used in bridge evaluation. The system should be extended now to various types of bridges including continuous span, concrete girder, and timber bridges.

17. Document Analysis/Descriptors	18. Availability Statement
Bridge Instrumentation Steel Girder Bridges Fatigue Bridge Retrofit Grouts	No restrictions. This document is available through the National Technical Information Services, Springfield, Va. 22161

19. Security Class (this report)	20. Security Class (this page)	21. No. of Pages	22. Price
Unclassified	Unclassified	153	

FIELD INSTRUMENTATION
STEEL HIGHWAY BRIDGES

Final Report to the
Minnesota Department of Transportation

Prepared By

Roberto T. Leon
Theodore V. Galambos
Jeffrey J. Schmit
Ai-Lien Teng

Department of Civil and Mineral Engineering
University of Minnesota
Minneapolis

February 1993

ACKNOWLEDGEMENTS

This project was sponsored by the Minnesota Department of Transportation (MnDOT). The researchers gratefully acknowledge this support and wish to specially thank the following engineers for their assistance in making this work possible: Donald J. Flemming (State Bridge Engineer), Ron Casellius (Research Program Coordinator), and Darab Bouzarjomehri (Bridge Design Engineer). We also want to thank the MnDOT Maintenance personnel for their logistical help during the testing of the bridges. The help of graduate students Barbara Jaeger and Don Fleming during the testing phase in also gratefully acknowledged. The project was coordinated by the Center for Transportation Studies at the University of Minnesota, and the help of engineers Amy Vennewitz and Laurie McGinnis form CTS was also greatly appreciated.

SUMMARY

The condition of the U.S.A.'s infrastructure has received much public attention during the past five years. Bridges, in particular, have received much negative publicity, since over 40% of the bridges in the National Bridge Inventory have been deemed structurally unsafe or functionally obsolete. In addition to the deterioration due to poor or limited maintenance there is concern that the increase in allowable loads that has occurred since many of these bridges were designed makes their details susceptible to fatigue failures. The conclusions regarding the structural deficiency or fatigue sensitivity of a bridge are often reached by utilizing analysis models developed for design and not for rating. These analytical models contain conservative and simplifying assumptions about both the load distribution and the material strengths. Thus most bridges have a substantial reserve capacity above the design loads, a capacity that should be utilized in the rating process if the best decisions are to be made. The main obstacle that exists in implementing this idea is that we do not know exactly how much overstrength there is in a bridge and which are the weak links in the load paths that could lead to premature failures.

To answer these questions, the Minnesota Department of Transportation sponsored the two projects dealing with field instrumentation of bridges that are described in this report. In the first project, a portable, rugged and multi-purpose bridge instrumentation system was developed. This was accomplished by using fourteen removable instruments and by basing a portable data acquisition system around a Keithley 576 DAC System and a Toshiba T3100SX portable computer. The instrumentation included eight reusable strain sensors and six inclinometers, which allowed load distributions, stresses, and displacements to be measured in steel girder bridges. In the second part of the project the portable data acquisition system was used to measure strains near fatigue critical details to determine stress ranges under both controlled and random traffic. For this part of the project conventional strain gages were used. Three bridges were tested as part of this work, one as part of the first project (Bridge 6805, now destroyed) and two as part of the second one (Bridges 61684 and 9613). The field results were compared to the analytical results from a simplified computer model, resulting in very good correlations.

For the first part of the project, for example, the maximum observed static field stress for a 100 kip load was 2.61 ksi when the two easterly lanes of a three-lane bridge were loaded. The maximum analytical stress came from the same loading condition was 3.35 ksi, while the maximum resulting middle girder deflections were 0.27" and 0.26" for the field data and analytical data respectively. The limited dynamic results show a peak stress of about 2.95 ksi which occurs in the middle west girder. An angular natural frequency was also calculated at about 20.1 rad/sec. This most likely occurs with the first mode of vibration for which a theoretical frequency of 26.6 rad/sec. was calculated. Comparisons of the field and the analytical results with two of the AASHTO code provisions shows that there exists a reasonable chance of severely underrating these bridges. AASHTO's allowable deflection is four times greater than the field deflection and twice as much as a model for all girders acting as non-composite sections. Overestimation of the field load distribution ranges from 70-100% based on current AASHTO load distribution factors.

The analytical results correspond quite well to the field results. Although there appear to be rather large discrepancies in the stress result figures, a sum of the field midspan moments and a sum of the analytical midspan moments shows that the model is about 20% conservative. This is good considering particular stress values are overestimated by as much as 40%. Many possibilities exist as to why the analytical model overpredicts the field data. Some of these include a high concrete

modulus of elasticity, excessive support restraint and uncertain transverse member stiffness, all of which are possible for Bridge 6805.

In bridges with no mechanical shear connection between the deck slab and girders, a deterministic transverse load distribution analysis is difficult because of the uncertain degree of participation of the deck slab with the various girders [Bakht and Jaeger, 1990]. This point is illustrated, in the modelling of bridge 6805, by the use of semi-composite members. Because of uncertain interaction between the slab and the longitudinal girders, average cross-sectional parameters were used to estimate the degree of slab participation. It must be noted that, in tests of designed non-composite slab on girder bridges, composite action between the girder and the slab breaks down completely as the failure limit state of the girder is approached [Bakht and Jaeger, 1990].

These conclusions were reinforced by the second part of the study. In addition, the second phase of the work, which centered on the measurement of stress range values under both controlled and ambient traffic, demonstrated that the data acquisition system can provide useful information on the estimation of the fatigue life of fatigue-critical details in the bridge. In this part of the work two multi-girder composite bridges on urban interstate highways were investigated. In the first bridge two 25 ton trucks were used to induce static and dynamic stresses. The stresses were measured near AASHTO category A, B, and C fatigue details. Acceptable correlation was shown to exist between measured and calculated static stresses. The measured dynamic stress range values, when amplified by the reliability factor specified in NCHRP Report "Fatigue Evaluation Procedures for Steel Bridges" were found to be considerably below the allowable fatigue limit for the respective details.

In the second bridge, measurements were made under ambient truck traffic. Although 18 successful dynamic data sets were obtained under heavy truck traffic, not enough measurements were obtained for a reliable estimation of the stress range spectrum. However, the measured stress ranges were always well below the fatigue limits. The use of trucks with controlled weights is a more credible means of estimating remaining fatigue life of details than measuring stress ranges in ambient traffic, unless continuous data are taken over a full day to obtain a daily spectrum. The present equipment needs to be modified for this purpose.

Overall this acquisition and modelling system worked quite well for determining strains and deflections of simply supported bridges under static loadings. A new measurement technique for finding deflections, based on slope sensors, was developed and verified. This technique can now be readily used in bridge evaluation. The dynamic data acquisition part of the system did not perform as well because of triggering problems. This was due primarily to limitations in the budget which did not account for purchasing an automatic trigger mechanism. In addition, it might be interesting to develop an easily mountable accelerometer or linear variable displacement transformer so that one could determine dynamic deflections since the current system is not equipped with such a capability. The current Keithley 576 setup is expandable to 32 channels which could accommodate additional instrumentation. The system should be extended now to various types of bridges including continuous span, concrete girder and timber bridges.

TABLE OF CONTENTS

LIST OF FIGURES

LIST OF TABLES

1. INTRODUCTION

1.1 Background

Of the more than half million bridges in the National Bridge Inventory, approximately 40 percent are reported in a recent survey to be structurally deficient, requiring safety improvements or replacement [Galambos et al, 1990]. The replacement cost for these structures may exceed 100 billion dollars. Therefore the efficient and economical acquisition of bridge loading and response information is of great importance to the vast program of inspection, repair, rehabilitation and replacement of bridges that is currently underway.

Many of the bridges rated as deficient were designed and constructed in a manner that achieved greater strength than is recognized in conventional code rating provisions. Current evaluations and rating investigations emphasize bridge condition and member dimensions. Inspection methods rarely determine bridge loads or member performance under loading. Developments in instrumentation technology, however, make it feasible to investigate existing bridges and provide more accurate site-specific load and response data for the evaluation process. This report presents the results of a pilot project to develop instrumentation suitable for obtaining bridge response data in a quick and economical manner. The criteria for selecting the instruments are discussed, the prototype data acquisition and sensor system are described, and the results of their utilization in testing three bridges composite steel bridges are evaluated.

1.2 Present Knowledge of Bridge Rating Procedures

Current rating procedures present in the American Association of State Highway and Transportation Officials (AASHTO) Specifications represent a straight extension of the design process. In other words, the rating methods mirror the design process, with all its limitations and simplifications. The rating process, however, should be very different. Many of the uncertainties in (1) the strength of materials used, (2) types and number of load repetitions, and (3) construction and design errors, which account for much of the conservatism in current design procedures, do not apply to the rating process. By the time a bridge is rated it has been "proof-loaded" structurally by innumerable overloads (legal and illegal) and the material strengths are known (either by testing during construction or in-situ measurements).

These issues have recently been addressed by Moses and Verma [1987] and Galambos, Leon and French [1990] in a series of NCHRP research projects. As a result, several new rating schemes have been proposed. The scheme in Galambos et al [1990], suggests that inelastic action (i.e. some limited yielding of the cross section), accurate load distribution factors (as opposed to the AASHTO usual S/5.5), alternate ultimate strength design concepts (autostress or shakedown), and probabilistic techniques be incorporated into a new rating process. Sample exercises have shown that rating factors could be increased by 15% to 30% without sacrificing structural reliability and safety. These gains come not only from more sophisticated analysis tools developed during the NCHRP projects, but also from the use of new rating factors, currently ignored by AASHTO. Such factors include, for example, the roadway condition (which has a direct effect on impact factors), and the level of enforcement of posted loads (which results in less likely overloads) [Moses and Verma, 1987]. Use of such factors results in a more accurate prediction of the actual strength of the structure.

The rating tools developed in Galambos et al [1990] utilize the concept of "shakedown," or a limit

state given by the ability of the structure to resist loads elastically after some initial, and minor, yielding. Shakedown, rather than ultimate strength, is the appropriate rating limit state because the loads imposed on the bridges are dynamic and cyclic [Galambos et al, 1990]. These techniques, however, require experimental verification. Issues like distribution factors (how much of the load goes to each girder), amount of composite action (whether intentional or unintentional), effect of a deteriorated deck, levels of strain actually present in the bridge under truck traffic, and effect of potential retrofit schemes need to be investigated.

An issue that has not been adequately addressed in the past is whether improvements in safety can be made at a very economical cost if the existing structural elements need not be replaced. For example, if a bridge is satisfactory from the strength standpoint but requires widening for traffic safety reasons, an accurate analysis could show that adding the necessary shoulder or lane width with new precast elements can be done without substantial structural changes. This will allow traffic to stay on the bridge while improvements are made, and save a large amount of capital funds required in the replacement process.

Before these issues can be addressed for any specific cases, an evaluation system must be devised. A review of literature on bridge testing is needed as a basis for developing this system.

1.3 Instrumentation of Bridges

There have been a number of tests on existing and model bridges over the past forty years, and list of the works can be found in the literature [Galambos et al, 1990]. There are two major groups of researchers in North America that have pioneered bridge instrumentation and evaluation for large numbers of bridges. One such group is headed by Baidar Bakht with the Ministry of Transportation of Ontario in Ontario, Canada. The other group is lead by Fred Moses at Case Western Reserve University in Cleveland, Ohio. Their accomplishments will be reviewed briefly.

1.3.1 Ontario Department of Transportation

Experience with field testing of highway bridges in Ontario, Canada, during recent years shows that nearly every bridge has some aspect of behavior that can escape the attention of even experienced bridge designers and analysts. In such cases field testing has been shown to be the most effective means of evaluating bridges [Bakht and Jaeger, 1990].

The Ministry of Transportation of Ontario (MTO) has, for many years, conducted a program of field testing of highway bridges that has included both static and dynamic tests. The dynamic tests checked the performance of the bridges, as did the static tests which also included proof tests and ultimate load tests. More than 225 bridges have been tested as part of this program in recent years. In static tests of slab-on-girder bridges the measured deflections and girder strains were found to be much smaller than calculated, indicating that the bridge is stiffer in flexure than assumed [Bakht and Jaeger, 1990].

Reasons for the difference between calculated and actual stiffnesses of slab-on-girder bridges has often been attributed to: (1) a very high modulus of elasticity of concrete; (2) interaction of the girders with secondary components, such as barrier walls and wind bracing; and (3) the presence of a high degree of composite action between the girders and deck slabs, even when they do not have any mechanical shear connection between them. The North Muskoka River Bridge was retested by

Bakht to find the reason for the discrepancy between the actual and observed stiffnesses of the girders in the original tests. The bridge has apparently simply supported girders resting on elastomeric type bearings. The retest of the bridge showed that even in the presence of elastomeric bearings, the girders develop enough bearing restraint force to reduce the applied load moments at midspan by a significant amount [Bakht and Jaeger, 1990]. Bearing restraint forces for two particular cases are shown in Figure 1.1.

In bridges with no mechanical shear connection between the deck slab and girders, a deterministic transverse load distribution analysis is difficult, if not impossible, because of the uncertain degree of participation of the deck slab with the various girders. Figure 1.2 is from a proof test reported by Bakht. It shows the actual load distribution factors for midspan girder moments compared to those obtained from two different semi-continuum method analytical models. The girders are assumed to be fully composite in one model and non-composite in the other. It can be seen that the two sets of analytical results do not envelope the actual behavior. This phenomenon emerges from the fact that the uncertain degree of composite action results in uncertain values of the effective flexural rigidities of the girders [Bakht and Jaeger, 1990].

1.3.2 Moses and Ghosn, 1983

The group led by Fred Moses has many years of experience in bridge instrumentation and evaluation and has developed a removable strain gage sensor primarily for bridge testing [Moses and Ghosn, 1983]. Moses used this type of instrument to develop a weigh-in-motion technique for trucks passing over steel girder bridges. After using trucks of known weights to obtain a reference influence surface, other vehicles passing over can be compared to the calibrated output thus "weighing" the truck traffic on the bridge. The gages were placed at midspan of each simple span bridge girder in order to obtain the critical loads.

1.3.3 Moses, Ghosn and Gobieski, 1985

Several years later Moses, Ghosn, and Gobieski [1985], used the removable strain gage sensors in bridge evaluation. As in the previous set of tests, developing a calibrated influence surface for the individual bridges is a key step in the evaluation. This time the researchers also looked into the distribution factors, impact values and the composite action of sections designed to be non-composite.

Based on the work of the previously mentioned researchers one can gain some insight to bridge rating. This knowledge gained, coupled with the fact that technology has improved data acquisition capabilities and developed better field instrumentation, presents various possibilities for developing a bridge rating system. The primary objective of which is to develop a portable and multi-purpose instrumentation system for bridges.

1.4 Objectives of the Study

The primary objectives of this project are to:

(1) Develop a portable, rugged, and multi-purpose instrumentation system for bridges.

(2) Obtain, through instrumentation, data on the field performance of a bridge in the form of influence surfaces.

(3) Compare field results with analytical results developed with a simplified computer model.

(4) Explore the use of this and similar systems in bridge fatigue studies.

(5) Explore applications to bridge rating (for example transverse load distribution, level of composite action, allowable deflections and the level of strain in the members under load for fatigue life studies).

1.5 Organization

Chapter 2 will describe the instrumentation, data acquisition setup and the method of data reduction. Results and analysis of the experimental data for Bridge 6805 will be discussed in Chapter 3. The field fatigue studies on Bridges 62864 and 9613 are covered in Chapters 4 and 5 respectively. Chapter 6 is an evaluation of the fatigue studies, while Chapter 7 contains conclusions and recommendations.

2. INSTRUMENTATION AND DATA ACQUISITION

2.1 Introduction

In general bridge designers and raters are concerned with two types of measurements in bridges. One relates to stresses, as they affect the ultimate strength and fatigue characteristics of the structure. The other relates to deflections, and how they affect the serviceability limit states. Thus any bridge instrumentation scheme must begin by looking at how to best measure stresses and deflections.

Any portable data acquisition system must consist of at least three main components: power, data acquisition, and sensors. In more detail, the system used in these studies consisted of the following parts: (a) power supply, (b) line conditioners, (c) portable computer, (d) GPIB or IEEE488 interface communications device, (e) data acquisition boards, (f) signal conditioners for the sensors, and (g) the sensors themselves. Figs. 2.1 and 2.2 show a block diagrams of the system used for the first and second projects respectively. The following sections describe the instrumentation system used in these two projects.

2.2 Power Supply and Line Conditioners

Since 120 V line power could not be assured at any of the bridge sites under consideration for these projects, power was supplied by a Honda 500 portable field generator. Portable generators, however, produce large voltage spikes that will damage computers, data acquisition boards, and sensors. Thus the power signal needs to be filtered. In this study a Clary Uninterruptible Power Supply (UPS) was used. It not only conditioned the power signal but also provided several minutes of uninterrupted power in case the generator failed. This time was sufficient to store all data to the computer hard disk and to conduct an orderly shutdown of the system.

2.3 Data Acquisition Systems

The data acquisition equipment consisted of three main components. The data acquisition box was a Keithley 576, connected through an IOtech GPIB card to a portable Toshiba T3100SX computer. Each of these will be described briefly below.

2.3.1 Portable Computer

A Toshiba's T3100SX Portable Personal Computer was used as the controller of this data acquisition system. The T3100SX uses extensive Large Scale Integrated (LSI), Complementary Metal-Oxide Semiconductor (CMOS) technology to provide minimum size, light weight, low power usage and high reliability. An 80386SX-16 32-bit microprocessor operates at 16MHz, providing speed and flexibility. The 80387SX-16 math co-processor was not included in the original package but was added later. One megabyte of CMOS Random Access Memory (RAM) was provided with the T3100SX, but three megabytes of RAM were added to improve the performance. The T3100SX contains an internal 3½" 80MB hard drive plus an internal 3½" diskette drive which accommodates 1.44MB double-sided, high-density (2HD) and 720KB double-sided, double-density (2DD) diskettes. Two NiCad battery packs are housed in the T3100SX. A plasma display offers high resolution (640 x 480 pixels) and supports 16 gray-scale levels.

Because the T3100SX cannot accept full size boards such as those needed for the IEEE488 communications board, a Toshiba Desk Station III was added. The latter allows the use of additional expansion cards with the T3100SX personal computer. Two full length 16-bit slots and one full length 8-bit slot are available for use.

2.3.2 General Purpose Interface Bus (GPIB)

An Iotech Personal488 (GPIB) series was used to monitor the communication between the Keithley 576 and the computer. The Personal488 series consists of the Driver488 software, an IEEE 488.2 compatible interface board (GP488Bplus), installation program, and other utility programs. Five jumper-selectable interrupt lines are featured on the GP488Bplus. Three 8-bit jumper-selectable Direct Memory Access (DMA) channels are also available. The Driver488 monitors all IEEE 488 bus monitoring and control lines, and generates an interrupt based on service request (SRQ) status. This device is IBM PC compatible.

2.3.3 Keithley 576 Data Acquisition Unit

A Keithley Model 576 High Speed Data Logging System was chosen for the data acquisition system. This unit includes a 16-bit 50-Khz AMM2 Analog Master Measurement Module which provides high speed multiplexing and analog to digital conversion. The AMM2 module contains quick-disconnect terminals for connection of up to sixteen single-ended channels. Fourteen of these channels were used for this project. Channels zero through five were assigned to the tiltmeters, while channels six through thirteen were used for the strain sensors.

The 576 unit is internally controlled by an MC68008 microprocessor and has 480K of user buffer space along with 5K of user program space. Digital commands are used to control the analog input and the analog-to-digital conversion process that transforms analog signals into digital information that can be used by the computer. Analog-to-digital conversion is controlled by the AMM2 module. The default analog input range accepts signals up to $\pm$ 10V full scale with 300μV resolution per bit. Accurate measurement and digitization is provided by the A/D converter. A conversion time of 16μS for the AMM2, and a sample and hold acquisition time of only 4μS allows sampling speeds of up to 50kHz.

During the static tests the acquisition system averaged each of 100 samples in the eight strain sensor and six tiltmeter channels, and stored them in a buffer. They were then downloaded to the computer for display and further processing with the aid of the ASYSTANT GPIB software (see section 2.3.4). During the dynamic tests the acquisition unit stored 8000 samples per strain channel directly to the buffer space at a rate of 1600 readings per second (1.6 Khz), resulting in about 5 seconds of data for each of the eight strain channels. The tiltmeters are static devices and cannot be used to at rates much above 0.1 Hz, and thus were not read during the dynamic tests.

2.3.4 ASYSTANT GPIB Software

ASYSTANT GPIB, by ASYST Software Technologies, was recommended as a device controller suitable for data acquisition. This software, which is menu driven, allows the user to communicate immediately (Interactive Mode) or in programmable routines (Program Mode). For doing field tests the Program Mode was used since the same programs needed to be run repeatedly. ASYSTANT GPIB can interpret only ASCII code, and therefore the rate of data transfer from the Keithley 576 to the

T3100SX is limited to 250 samples per second. This worked fine for doing static testing when a relatively small amount of data was being transferred. However, for a dynamic case when thousands of samples need to be moved this software limitation became a liability. It is recommended, that if more dynamic testing is to be done in the future, the use of a self written program that can read binary code would be advantageous. Binary code can be transferred at a rate of 30000+ samples per second.

2.3.5 Strain Gage Sensors (Static and Dynamic Tests)

Measuring strains the most practical way is through the use of strain gage sensors. The strain gage technology is well advanced, and allows the user to select the best geometry, materials, and signal conditioning for a specific application of this type of sensor. For a portable bridge testing system regular strain sensor technology presents formidable obstacles since it requires extensive surface preparation, long-term curing of the glues used, and signal conditioning capable of limiting electrical noise and drift. Many of these concerns have been addressed in the past by several researchers (including Moses et al [Moses 1983, 1985] and Bakht and Jaeger [Bakht, 1990]), and satisfactory solutions have been found. Moses, in particular, developed a demountable, full-bridge strain gage sensor for the weigh-in-motion program [Moses, 1983] that allows longitudinal strains in the girder flanges to be monitored. These sensors were adopted in this work.

These sensors, known as BWS Strain Gage Sensors (BWS), are full bridge circuits with 350 ohm foil gages. They have an effective gage length of 5", an overall length of 7¼" and a range of $> \pm 2000$ microstrain. Full bridge circuits have favorable properties such as greater output signal and automatic compensation of errors [Hoffmann, 1973] (i.e. temperature errors). For this application, the sensors were mounted to the top of the bottom flange with two C-clamps, one at either end of the 7¼" aluminum gage plate, attempting to keep the axis of the sensor parallel to the girder axis. Because of many rivets in the flanges of Bridge 6805, it was nearly impossible to keep the strain gage sensor axis parallel to the girder. An idea of the error introduced can be gleaned from assuming an alignment error of 10°. Using a Mohr's circle approach it can be shown that a 10° rotation causes a 6% error in the strain output [Beer, 1981], an error that can be considered small for such a large misalignment.

The strain sensors respond immediately to any strain change, and therefore they can be used for dynamic as well as static loading cases. For this project the signal conditioning and power were provided by an Analog Devices AC1300 transformer and board with eight 3B18 modules. The AC1300 board converts the 120 AC volts to ± 15 volts DC which is used to power the eight 3B18 signal conditioners used for these sensors. The output signal from the BWS devices is proportional to the input voltage, in this case on the order of 6 mV per V per microstrain. The signal was then filtered, amplified 1000 times, and relayed to the Keithley acquisition system.

Five-conductor cables (Belden 8723), 100 feet long were used to supply power to and return the signal from each of the eight strain gage sensors. The wire was 22-gage and contained a single wrapped shield and an aluminum foil shield for all five conductors.

2.3.6 Strain Gage Sensors (Fatigue Studies)

For the fatigue studies the stresses are highly localized. Both the long gage length of the BWS (7 in.) and the geometry of the details under study made the use of regular, quarter-bridge strain gages necessary for this part of the study.

Tokyo Sokki FLW-06-3 gages were used for this portion of the work, as they contain long built-in leads and waterproofing that made their application much simpler than conventional strain gages. The gages are 0.5 in long and 0.3 in. wide and allow readings up to 20000 microstrains to be made. The FLW-06-3 is not a precision gage, and long experience in the laboratory indicated that strains could be resolved to -/+ 2 microstrains. This was deemed more than acceptable as a compromise to simplify and speed field installation.

The Tokyo Sokki strain gages were connected to a bank of MicroMeasurements 2120 signal conditioners and amplifiers that provided similar signal conditioning and amplification as the Analog Devices units described above.

2.3.7 Deflection Measurements

There are many types of transducers that can be used for deflection measurements. The most commonly used are: (1) linear variable differential transformers (LVDTs) in which the inductance of a magnetic field formed by two coils is disturbed by a moving core and the corresponding change in voltage recorded; (2) linear potentiometers, in which a sliding sensing element is directly attached to a long resistor, and a measurement of a change in voltage proportional to the change in resistance is made; and (3) mechanical devices such as dial gages and levels. In all cases the measurements must be made versus a fixed reference. This makes it difficult to apply to bridges because often the midspan and other critical locations of the bridge are not accessible from below (stream, river, swamp, etc.) or are very high and preclude, within reasonable time and economic constraints, the building of a platform to use as reference frame.

This research project took a different approach to measuring deformations, based on the well-known differential equation of the elastic curve. This equation tells us that deformations can be obtained from successively integrating the loads, then the shear diagram, then the curvature diagram (M/EI), and finally the slopes (Fig. 2.3, [Sack, 1984]). It is tedious and difficult to carry out three successive integrations, particularly since both the boundary conditions and the EI must be known in order to evaluate the integral. As with any process involving integration, moreover, the errors accumulate with each step, resulting in a large uncertainty in the final product (the deflections, in this case). The ideal measurement is then one that limits the number of integrations so that the constants can easily be evaluated, and does not require a knowledge of the modulus of elasticity and moment of inertia of the cross sections. This is the case if one can make direct measurements of slope, which leads to the selection of inclinometers, described below (Section 2.3.8), as the instrumentation of choice for this project.

2.3.8 Applied Geomechanics Tiltmeters

The Applied Geomechanics Model 800 tiltmeter is an uniaxial sensor that incorporates a high precision electrolytic tilt transducer as the internal sensing element. Measured angular movement is referenced to the vertical gravity vector, eliminating the need to locate an external datum. The high-gain model ($\pm 0.5°$ range) was chosen since rotations were expected to be small and high sensitivity (0.0001°) was needed. This model also is equipped with internal electronic signal conditioning; therefore additional conditioning was not needed as for the strain sensors. For this application, the tiltmeters were mounted to a ¼" aluminum backplate which was epoxied to the girder web in the first test. Due to problems with epoxy drying time during the first test, donut magnets glued to the backplate were used in the remaining tests.

The tiltmeter transducer operates similar to a spirit level. As the transducer tilts, internal platinum electrodes are covered or uncovered by a conductive fluid. This process produces a change in the electrical resistance to a signal passed through the transducer. Six wires of eight-conductor shielded cables (Carol E60233-8), 100 feet each were used to power the tiltmeters and return the analog output signal. The cables are 24-gage with one aluminum foil shield. Two power supply units were combined to send ± 12 volts DC to the tiltmeters. A range of $+10$ to $+15$ volts or -10 to -15 volts is recommended since in these ranges the tiltmeter voltage output remained constant. A voltage of ± 12V was used in this application with no drift in output voltage. Small variations of voltage have no effect on the output as long as the recommended range is maintained. The tiltmeters can be utilized either in a common (single-ended) or differential mode, and the single-ended was chosen.

2.4 Data Reduction Methods

Once the data for the tiltmeters and strain sensors was obtained and stored on the hard drive in the field, it could be brought back to the office for reduction and analysis. The data was tabulated and plotted to show the distribution of stresses and deflections. An analytical grid model developed by Weaver and Gere [Weaver, 1980], which was also used by Barker [Galambos et al, 1990] at the University of Minnesota, was chosen as the simplified model with which to compare the reduced field data.

2.4.1 Data Reduction for the BWS Strain Sensors

The main task for the reduction of the BWS strain sensor data was to convert the voltage output obtained from the strain sensor to a stress value. This was done by using the ASYSTANT GPIB software commands. Conversion factors as well as an electronics and cabling error factor were used to manipulate the output into a stress value in kips per square inch (ksi). The electronics and cabling loss factors were computed by installing the sensors on a long steel strap and testing the strap in a Riehle 30 kip testing machine. The loads divided by the area provided known stress values, while the voltages from the sensors were read by the computer in exactly the same fashion as in the field. By taking a ratio of the actual stress versus the sensor output a corrected calibration factor could be computed. The calibration factors provided by the manufacturer turned out to be quite accurate when the cable lengths were short and the sensing equipment was simple (P-3500 Micro Measurements, for example). However, the data acquisition impedance and cabling added significant losses to the strain sensor output so that a new calibration factor, labelled cabling and electronic loss factor, had to be computed.

The strain sensor calibration constants and loss factors for the electronics and cabling are shown in Table 2.1. Since the standard deviation of the average calibration constant was small, the average calibration constant will be used for each channel. Multiplying the output voltage by the electronics and cabling loss factor, and 29,000 ksi, for Young's Modulus, then dividing by the calibration constant and the input voltage of 3.33V a stress value in ksi is obtained. For example, using channel 6 values and a voltage output of 350μV, which is amplified 1000 times, the solution is:

$$\sigma = \frac{350mV * 1.14 * 29{,}000ksi}{1.81mV/V/\mu\epsilon * 3.33V} = 1.92ksi$$

The final computer output was given in ksi. Only an approximate electronics and cabling factor was

used in the field and thus the proper factor was applied to each channel's data after returning to the laboratory. Then tabulating and plotting were all that remained for the data reduction of the strain sensor readings.

Most of the necessary conversions were carried out using the GPIB software, and this turned out to be very beneficial while the testing was being done, as it provided a rough idea of whether or not reasonable field results were being obtained.

2.4.2 Reduction Methods of Tiltmeter Output

Calibration factors were also applied to the output voltage from the tiltmeters. This time the data was converted to list the output in milliradians. The tiltmeter calibration constants and the electronics and cabling loss factors are presented in Table 2.2. The electronics and cabling loss factor for the tiltmeters was much less than for the strain sensors. This is attributed to the fact that the tiltmeter's output is a signal in volts, whereas the strain sensors send a return signal in microvolts. A microvolt loss is negligible when using the tiltmeters but can be very substantial for the strain gage sensors. These factors for the tiltmeters were computed by clamping the tiltmeters to an 8 ½ foot angle then placing a rocker support directly beneath the tiltmeter and raising the other end incrementally with 1/8 inch thick disks. The calculated angle could then be compared to the data acquisition output.

Since the standard deviations found were small, using the averaged calibration constants was deemed satisfactory. The ASYSTANT GPIB software was used to multiply the calibration constant and the electronics and cabling loss factor with the output voltage from the tiltmeters, thus producing the final computer output in milliradians.
The tiltmeters were used to calculate the deflections at the centerline of the middle girder of Bridges 6805 and 62864. In order to do that a method of converting the rotations to deflections was developed. Since rotations are the derivatives of deflections, a best fit cubic line can be placed through the tiltmeter values, using curve fit software developed by Golden Software, Inc. [Golden Software, 1987]. The choice of a cubic polynomial is based on the assumed deflection curve for a bridge. Once the curve was fit, the coefficients of the cubic equation were listed by the program. The next step was to integrate this equation to a fourth order equation, which can provide deflections. Using Quattro Pro Version 3.0, a table was set up with the fourth order coefficients to produce deflections at any desirable point along the middle girder. Table 2.3 is an example of data reduction to obtain deflections from the field data.

The cubic equation from the curve fit is:

$$\theta = 6.85x10^{-13}x^3 - 2.73x10^{-10}x^2 + 1.52x10^{-7}x - 2.00x10^{-4}$$

After integrating with respect to x the fourth order equation is:

$$\Delta = 1.71x10^{-13}x^4 - 9.12x10^{-11}x^3 + 7.59x10^{-8}x^2 - 2.00x10^{-4}x$$

Now, inserting positions of desired deflection from the south support (0") up to midspan (667"), the deflections can be obtained. The results are only accurate along the portion of the girder where the rotations are known, in this case from the south support to midspan. Table 2.4 shows the results of this computation.

This method of calculating deflections was verified by comparison with the analytical model. The analytical model that is used in this study provides output of rotations as well as deflections for each node. The rotation values for each of the four nodes corresponding to tiltmeter locations were entered into the curve fit program. The cubic coefficients were integrated and checked at the tiltmeter locations for accuracy compared to the deflections from the analytical model. This was done for five random cases while the analytical model was being developed and in no case was there a difference of more than 1%. Thus it is felt that this method of rotation reduction using four data points is sufficient to provide good results.

3.0 STATIC AND DYNAMIC TESTS ON BRIDGE NO. 6805

3.1 General Bridge Information

Minnesota's Department of Transportation (MN/DOT) Bridge No. 6805 was located on Trunk Highway 280 (TH 280), between University and Como Avenues, and crosses over the Great Northern and Northern Pacific railroads as well as a University of Minnesota service road. This was an eleven-span bridge with a total length of just over 1000 feet. Figures 3.1 and 3.2 give details of this bridge. This bridge was demolished shortly after the completion of these tests as part of a project to widen TH280.

In this project the fourth span from the south end, which consists of five girders with 9 foot spacings (Fig. 3.3) on a highly skewed plan (Fig. 3.4), was of particular interest. Span no. 4 was chosen since it is easily accessible from the service road below, simply-supported, and contained deep riveted steel plate girders (Fig. 3.5). The girders were at an approximate elevation of 30 feet from the service road, but with the use of a cherry-picker, provided by MN/DOT, access of the girders was gained easily.

This was an ideal bridge for this project since it is conveniently located a couple of miles from the University of Minnesota. However, this particular span was skewed, 27° at the north end and 36° at the south end. This may present some analysis problems, namely that simple analysis programs (software) are not available to do an "exact" analytical study of highly skewed bridges.

Complete plans and maintenance records for Bridge No. 6805 were available from MN/DOT. For the analysis, all dimensions and nominal material resistances for the main members were taken from the original records. Originally the deck was designed with a minimum thickness of seven inches. It was assumed that by the present time the deck had been thickened to eight inches due to patching and overlays. Most likely the concrete strength over time has also increased. Based on this the decision was made to assume a concrete strength of five kips per square inch (5 ksi). Both of these assumptions with regard to deck thickness and concrete strength are believed to be conservative, since the deck was probably thicker due to successive paving operations and the concrete stronger due to aging. Thus the analytical model used to model the bridge will probably exhibit less lateral load transfer than the actual bridge. Each girder has three moments of inertia because cover-plates were added to the bottom flange of the girders near their centerlines. See Table 3.1 and Figs. 3.3, 3.6 and 3.7 for location of cover-plates, girder lengths and other details.

3.2 Rating Criteria

Before instrumenting and loading of the test bridge takes place one should review the criteria that is of concern when rating bridges. The rating criteria that is used in the assessment of bridges fall into four categories:

(1) Strength (overload, ultimate);

(2) Serviceability (working loads);

(3) Fatigue and fracture;

(4) Others: impact, fire, scour....

Methods of observing each of these criteria have been developed. Knowledge of the bridge strength can be obtained through the analysis of strains in the bridge. Some confidence on the level of service can be acquired by measuring the deflections. Fatigue and fracture, on the other hand are difficult, if not impossible, to measure. Thus extensive and careful inspection must be done in order to do a thorough fatigue study. This is also true of some of the other criteria such as impact and scour. This part of the study will look at the strength and serviceability of span no. 4, but fatigue, fracture and other criteria were not investigated.

3.3 Instrument Location

With eight strain gage sensors and only five girders it was decided to place five sensors at the midspan of each of the five girders since the girders are simply-supported and this would be a critical location. This is similar to the placement used by Moses and Ghosn [1983] who placed sensors at midspan of the five simply-supported bridges that they tested. A transverse load distribution can be obtained with this method of sensor placement. The remaining three sensors were used to develop a longitudinal stress distribution along the middle girder. Since changes in the moment of inertia (I) exist along the girders, the decision was made to place the sensors near the points where I changes. Thus a sensor was placed at each of the two I changes and the last was mounted in the highest moment of inertia zone, between midspan and the nearest change in moment of inertia (Fig. 3.8).

The tiltmeters were positioned on the middle girder in order to obtain a representative idea of the rotations along the girder. Four of the six tiltmeters that were purchased for this project were mounted on the middle girder and the other two were used one girder to the west as a system check (Fig. 3.9). The largest rotation is at the support of a simply-supported member, thus a tiltmeter was positioned as near the support as possible. From there the tiltmeters were placed at the eighth-span, quarter-span, and mid-span. This placement should give reasonable representation for a curve fit and was consistent with a simplified analytical model that indicated that four slope measurements would give a very good approximation to the exact deflected shape for a simply-supported beam. The last two tiltmeters were placed approximately the same as the first two, but on the adjacent girder to the west.

3.4 Loading Method

This three-lane bridge was loaded with 50 kip ($\pm$0.5 kips) sanding trucks provided by MN/DOT. For the purposes of this study, the center of gravity of the trucks was assumed to be the point of the applied load (Fig. 3.10). Static and dynamic tests were conducted, with the emphasis being on the static test data.

Five loading passes were done to obtain the bridge response under static loading. Each pass consisted of a reading every 15 feet along each lane the bridge (Fig. 3.11). Extra readings were taken during each pass to ensure that all possible loading positions that might influence the span of interest were obtained. This was especially critical since a skewed span was being tested. The five static passes consisted of one truck in each of the three lanes individually, two trucks in the westerly two lanes and then two trucks in the easterly two lanes (Fig 3.12). The last two passes were done since random occurrences of heavy side-by-side trucks are extreme loading cases that need to be considered [Moses, 1983].

Five attempts were made to complete a dynamic pass in which the trucks were travelling approximately the speed limit, 55 mph. However, since manual triggering of the acquisition program was being used and only a five second window of data collection was available at 1600 Hertz, most data was missed and only one pass was recorded in its entirety. In this successful pass two trucks were being driven in the two west most lanes, travelling at 57 mph.

3.5 Results of Data Reduction

The results shown here are those using the reduction methods described previously in Section 2.5. The following subsections look at four types of data for the static tests: (1) field stresses, (2) analytical stresses, (3) field deflections, and (4) analytical deflections. Another, separate section, describes the dynamic portion, and deals exclusively with field stresses. An attempt will not be made here to model the dynamic case because the tiltmeters require a relatively long time to stabilize, due to the nature of a fluid sensor, and thus deflections could not be monitored for the dynamic passes.

The comparisons made in this section are between a simple analytical model of Bridge No. 6805 utilizing a stiffness approach and the results obtained in the field tests. Because small rotations and strains were observed in the field a first order elastic model should be adequate for a simple analysis. A nodemap for the analytical model is shown in Figure 3.13. It consists of 140 members and 95 joints. The program is a straight implementation of the grid program described by Weaver and Gere [1980], which utilizes three degrees of freedom per joint (vertical displacement, bending rotation, and torsional rotation). There were 90 beam elements for the main members, the slab was modelled as a beam using uncracked section properties [Galambos et al, 1990], and the cross bracing type diaphragms were modelled following the recommendations of Cheung et al [1985]. The equations for the modelling of the slab are:

$$I = \frac{L_x * t^3}{12} \tag{3.1}$$

$$J = \frac{E_c}{G_c} * \frac{L_x * t^3}{12} \tag{3.2}$$

where,

- $I \equiv$ moment of inertia
- $J \equiv$ torsional rigidity
- $L_x \equiv$ representative strip of slab
- $t \equiv$ thickness of the slab
- $E_c \equiv$ modulus of elasticity of concrete
- $G_c \equiv$ shear modulus for concrete

The equation for the moment of inertia of the diaphragm is:

$$\lambda I_d = \frac{a_d s^3 h^2}{6 l_d^3} \tag{3.3}$$

where:

$$\lambda = \frac{a_d s^3}{3a l_d^3} \tag{3.4}$$

and,

$s \equiv$ girder spacing
$h \equiv$ height of diaphragms
$a_d \equiv$ cross-sectional area of diagonal members
$l_d \equiv$ length of diagonal members
$a \equiv$ cross-sectional area of horizontal members

3.5.1 Stress Results

Many analytical model runs were made utilizing a simplified grid model in order to determine a best match to the field stresses. Three main parameters were studied: (1) effect of end diaphragms, (2) effect of varying the stiffness of the transverse members, and (3) effect of considering various amounts of composite action. The best match was determined by looking at the transverse distribution of stresses at midspan associated with a load at midspan. The comparisons were between the field data and the analytical results obtained by extracting the midspan moments from the analytical model, and converting them to stresses. Figure 3.14 shows a typical result for this phase of the work.

There were five comparisons, one for each of the five different loading cases, for each of the twelve models utilized (See Table 3.2)[1]. In the first set of analysis, the effects of diaphragms at the supports (Model 1) versus no end diaphragms (Model 2) was studied . In a rectangular span it would be expected that the end diaphragms would have little effect on the distribution of loads near midspan especially since the W-section has a relatively small torsional rigidity. This was definitely not the case for this bridge as the end diaphragms had a significant effect on the midspan stress distribution due to the skewness of the bridge. Based on this results the element mesh was adjusted to reflect the exact position of the diaphragms, and the Model 1 geometry was used in the rest of the studies. Both Models 1 and 2 overestimate the stresses near the load position but typically underestimated them away from the load. This indicated that the lateral load distribution in the model is not as extensive as the distribution of the actual bridge, requiring stiffer transverse members (slab and diaphragms) in the model. The underestimation by the model does not imply lack of safety, since by AASHTO Standards all the girders would have been designed for the worst case loading.

[1] Complete results are shown in J.R. Schmit's thesis, available from the MnDOT Library [Schmit, 1992].

The next set of studies were intended to highlight the effect of varying the stiffness parameters of the transverse slab members on Model 1. The case labelled 100% is the original model (Model 1) with the slab being 8" thick and having a concrete strength of 5 ksi. From this point the slab parameters were cut by 50% (Model 3), increased by 50% (Model 4), and increased by 100% (Model 5). The latter would correspond to a slab thickness of 10", with the concrete strength and hence its modulus of elasticity remaining constant. There was little difference in the curves for varying transverse member stiffnesses for most of the load cases. Even though the differences for models 3 through 5 were slight, the curve for the 200% members (Model 5) showed a better distribution of stresses in all five load cases. This indicated that there was more transverse capacity in these members than can be assumed based on initial observations. As for the end diaphragm studies, conservatism in the loaded region versus unconservatism in the other regions was very noticeable.

In Fig. 3.14, the first curve corresponds to a model for which the entire bridge is acting non-compositely (Model 6), while the second curve is the case of full composite action for all five girders (Model 1). For the next model (Model 7), the east girder (E1, Fig. 3.3) was assumed to act as a non-composite member while the other four longitudinal members acted compositely. Here the stress seemed to be better predicted than for the other two curves except in the two load cases where the truck(s) were in the east lane(s). Model 8 assumed both the E1 and E2 girders to act in a non-composite fashion, while the other three girders are still acting fully compositely. This model showed a better match to the field data in all but the middle lane loaded case.

The last set of studies dealt with the possibility of partial composite action. Model 9 assumed that the east girder (E1) was acting in a semi-composite manner, while the other four girders remained fully composite. Semi-composite implies that the member is acting in less than a fully composite manner. Specifically in this case, the girder sections have been modified to an average (neutral axis, moment of inertia and torsional stiffness values) of the fully non-composite section and the fully composite section. This does not correspond to any real case, but was intended to model partial composite action. The East lane of the bridge, which corresponds to girders E1 and E2, was an acceleration lane for a ramp carrying heavy traffic from an industrial park. It was felt that over the years this heavy traffic could have decreased the amount of interaction between the girders and the deck. Model 10 assumed that both E1 and E2 girder were acting in a semi-composite manner. Better transverse stress distribution was seen for this case in all of the load cases except for the truck loadings in the west lane(s). Two other models (Models 11 and 12) were used to try combinations of non-, partially, and fully composite action for the two East beams.

Figures 3.15 through 3.19 show what appeared to be the best three options based on the stresses obtained from the studies described above. The first curve has the E1 and E2 girders non-composite (Model 8). Curve number two is from the model for the E1 and E2 girders semi-composite (Model 10). The third curve assumes the E1 girder to be semi-composite and the E2 girder to be non-composite (Model 12). In each case the west three girders were modelled as fully composite. As a reminder the transverse stress distribution in these figures is at midspan for load cases near midspan. The five data points for each curve are for the five longitudinal members of the span. When the east lane (Fig. 3.15) was loaded Model 12 seemed to have the best fit with good trend characteristics and stress distribution. However, more conservatism exists in the east girder than for the other two curves. The second curve best predicts the field data when the middle lane (Fig. 3.16) is loaded. The stress distribution is the best and the peak value on the middle (M) girder is good. By a very small margin, Model 10 depicts the field data better when the west lane is loaded (Fig. 3.17) and has a slightly better transverse stress distribution. When trucks are in the east two lanes

(Fig. 3.18) Model 10 shows less conservatism than Model 8 and shows a better trend than Model 12. Again when the west two lanes (Fig. 3.19) are loaded, Model 10 predicts the field data best, showing conservatism in four of the five girders. Based on the stresses from these various models the best fitting model is when the east (E1) plus middle east (E2) girders are acting as semi-composite members while the west three girders are modelled with full composite action (Model 10).

3.5.2 Field Stress Distributions

Surface plots were generated to show a type of influence surface for the transverse field stress distribution (Figs. 3.20-3.29). These influence surfaces are similar to influence lines in that the load is moving linearly in the longitudinal direction of the bridge span. However, they differ from the influence line in that five sets of stress data are being collected, one set at each of the girder midspan points, thus producing data in three dimensions (longitudinal and transverse position and vertical stress) for each linear load case. Essentially five influence lines are being developed with each load case and are then being placed in a three dimensional plot. With nine longitudinal loading positions each surface has 45 actual data points. The rest of the points on the surface are generated using the Kriging method, which is available in the Grapher Software [Golden Software, 1988]. The X-axis shows the longitudinal position of loading at every 15 feet. The Y-axis marks the five girder positions spaced at 9 feet from east to west. The Z-axis is the stress axis in ksi. These ten figures are to be observed in pairs (i.e. Figs. 3.20 and 3.21). Each pair consists of a three dimensional surface plot and a topographic view of that particular surface. For ease of viewing some of the surface plots have been rotated 180°, but the corresponding topographic views have not. Please keep this in mind when looking at these figures. The center of the key box, in the surface plot figures, is north and may help distinguish between rotated and non-rotated plots. Figures 3.20 and 3.21 are for loading in the east lane. This surface plot has been rotated 180° and is viewed north to south from left side to right side of the page. The second pair of plots is for the middle lane loaded (Figs. 3.22 and 3.23) and the surface plot has been rotated 180°. The west lane is loaded in Figures 3.24 and 3.25. Here no rotation has occurred as well as in the fifth pair of plots (Figs. 3.28 and 3.29) where the west two lanes have been loaded. In the fourth pair of figures the surface plot has been rotated 180° where the east two lanes are loaded (Figs. 3.26 and 3.27).

Looking at the influence surfaces it can be seen that the peak stresses are occurring very near the midspan of the loaded lane. These figures have been adjusted in order to align the midspans. It is also apparent in these figures that the peak stresses for the east loading cases (Figs. 3.20, 3.21, 3.26 and 3.27) are in the east (E1) girder. However, the peak stresses for the west loading cases (Figs. 3.24, 3.25, 3.28, and 3.29) are in the middle west (W2) girder. This is because the west girder (W1) is covered by a four foot sidewalk whereas the east girder is within the east lane.

Similar plots were made for the results of the analytical models. Different from the field plots, the analytical plots show unloading on the side away from the load. The unloading is predicted in three of the loading cases; the east lane (Fig. 3.30), the west lane, and the east two lanes. Based on the field stresses measured, no unloading was observed in any of these three cases.

3.5.3 Stress Conclusions

Twelve analytical models were developed in the process of determining a best fit model. In each of these models the overall trends appeared to follow the field data quite well. Since the trends match quite well it is safe to assume that the field data is good. However, the analytical stresses in the

loaded regions tend to greatly overpredict the field data whereas opposite the loaded regions, the analytical results are slightly unconservative. As a check, one could add the analytical moments for the five transverse positions and compare this to the sum of field moments at these same five positions. This was done for a truck at midspan of the middle girder where the peak analytical stress is 36% greater than the peak field stress. This comparison shows that the analytical moments are 20% greater than the field moments. This is much better and shows that the model predicts the total system load better than can be seen by the stress distribution figures. However the full scope of the modelling predictions cannot be analyzed by looking solely at the stresses.

3.6 Analysis of Deflection Data

The comparison of the reduced rotation data with that predicted by the models constituted the second half of the analytical phase for Bridge 6805. The stresses at midspan were used to predict the bridge behavior in the transverse direction. The longitudinal deflections were used to model the longitudinal effects. Figure 3.31 shows a typical result of this phase of the analysis. The X-axis displays the longitudinal distance from the south support in inches. Symmetry of deflections about midspan is assumed in order to show a curve plot along the full length of the span. The tiltmeters were placed between the south support and midspan and thus the data reduction method used only predicts deflections from the South support to midspan. Because of skewness, symmetry cannot be assumed. However all the load cases are for loads near midspan and the results are for the middle girder so the assumption of symmetry is reasonable.

3.6.1 Deflection Results

The following five figures (Figs. 3.32 through 3.36) display the deflections of the best three models (Models 8, 10, and 12). The first curve is from the model in which the E1 plus E2 girders are assumed to be behaving as non-composite sections (Model 8). This curve is typically the most conservative of the three options being reviewed. The second curve depicts the model where the E1 plus E2 girders are participating as semi-composite longitudinal members (Model 10). Curve number two overall has a close fit to the field data curve. However, this curve is slightly unconservative when the east lane is loaded (Fig. 3.32) and when the west two lanes are loaded (Fig. 3.35). The third curve, consisting of the east girder semi-composite and the middle east girder non-composite, remains conservative with overall deflections better matching the field curve than does the first curve. In all three models listed in this section, the three westerly most girders (M, W2 and W1) are acting as fully composite members. Because of the close prediction of deflections and looking back to the stresses the best choice appears to be Model 10. Thus, of the twelve models analyzed, the model with E1 plus E2 acting semi-compositely was chosen for the final analysis.

3.6.2 Deflection Conclusions

Many of the twelve models were shown to be unconservative or overly conservative. Only four models made very good matches to the field data and with the help of the stress results, they were narrowed down to the one model which was used for the final analysis (Model 10).

3.7 Discussion of Model Parameters

Now that the final model has been chosen some details on the bridge model parameters should be listed. This structure is a slab on girder bridge with five girders spaced at 9 feet. See the cross-

section diagram (Fig. 3.3). For the purposes of the model the slab was assumed to be 8" thick with a concrete strength of 5 ksi. The effective concrete width for the longitudinal composite members is the girder spacing of 9' = 108" (Fig. 3.7). The transverse slab members were modelled with an effective width of 15' = 180". This is equivalent to the longitudinal load spacing. The steel plate girders are made of a 60" x 3/8" web with four 6" x 6" x 3/4" angles used for the flanges. The web was stiffened with 5" x 3½" x 3/8" angles (Fig. 3.6) but these were not taken into account in the model. The bottom flanges were built up with as many as two 12" x 3/4" cover-plates.

The end diaphragms are W 30 x 108 sections for a total of eight end diaphragms. The cross bracing type diaphragms consist of two diagonal members and two horizontal members, one at the top and the other at the bottom. The top member is a 4" x 4" x 3/8" angle, the two cross members are 4" x 3" x 3/8" angles and the bottom member is a WT 4 x 14. The section specifications can be found in the LRFD Manual [AISC, 1986]. There are a total of 16 cross bracing type diaphragms.

3.8 Comparison with AASHTO Code

The AASHTO Specifications for Highway Bridges [AASHTO, 1983] allows for a maximum live load deflection of L/800. For a span of 1335" the allowable deflection is 1.67". The maximum deflection that was observed during the field tests was about 0.27" for a 100 kip loading (two trucks side-by-side). AASHTO requires a minimum loading of an HS20-44, which is a 72 kip truck. For this study it will be assumed that two trucks are side-by-side for a total AASHTO loading of 144 kips. This is a 44% greater load than used in the field study so assuming linear elasticity the maximum field deflection would be 0.39". This is still ¼ the maximum allowable deflection. In the same respect, looking at the analytical deflection for a non-composite model (since this is how the span was designed) one sees about a 0.52" deflection. Multiplying by 1.44 one obtains a maximum analytical deflection of 0.75". This conservative model still has a maximum deflection less than ½ of the allowable. If the design and/or rating procedure is assuming that deflections near the allowable are occurring, then underrating of Bridge 6805 may occur.

The AASHTO code also recommends a distribution factor of

$$\Delta = \frac{S}{4 + 0.25S} \tag{3.5}$$

[AASHTO, 1983] for bridges with girder spacings greater than six feet. This factor becomes 1.44 for a 9' girder spacing, which is the case for this project (Fig. 3.3). As an example results from a 50 kip truck placed in the east lane will be analyzed. This should be a good example since the truck's center of gravity will be between the two girders. Based on the analytical model in which the center of load is placed 42" from the east girder the code would require that:

$$30.56\ \textit{kips} * 1.44 = 44.0\ \textit{kip load}$$

$$19.44\ \textit{kips} * 1.44 = 28.0\ \textit{kip load}$$

be applied to east and middle east girders respectively. Table 3.3 shows the ratios of the field and the best analytical moment distributions applied to a 50 kip load. From this table one can quickly calculate that the AASHTO load overestimates the field load by as much as 70-100% in the loaded region. AASHTO also overestimates the analytical model, which was based on the design case of

all girders having non-composite behavior. This overestimation ranges from 35-70%. For the east lane loading of span 4 the AASHTO code is overly conservative with its distribution factor of 1.44. A factor of 1.44 may be reasonable for design but when rating this bridge if the distribution just presented is not taken into account underrating will occur.

These two code provisions along with a high degree of composite action (for which this span was not designed) could present problems for bridge rating personnel that have no access to the field data. Similar situations most likely exist when rating other bridges.

3.9 Discussion of Dynamic Field Stresses

Since only one dynamic pass was recorded in its entirety and no data was obtained for dynamic deflections, this section presents only the field stresses and a comparison to the static stresses. The one good pass consisted of two trucks in the westerly lanes travelling at 57 mph. Figures 3.37-3.41 show the dynamic response of the strain gage sensors at midspan of the five longitudinal members. The X-axis shows the number of samples (8000) taken during the pass and the Y-axis displays the raw data units (in thousands) which are the resulting output from the Keithley 576. Raw data units were used for the dynamic program because they demand less memory. Therefore more samples could be taken than if real number data was taken (i.e. voltages). Each of these five figures contains five seconds of data or 1600 samples/second.

Scaled values were taken from the dynamic figures (Figs. 3.37-3.41) in order to calculate maximum stresses for each girder. The apparent no load value was subtracted from the peak raw data count and converted to a voltage. Then multiplying by the cabling and loss factor and the modulus of elasticity (29,000 ksi) plus dividing by the calibration constant and the input voltage, a stress value can be determined.

The maximum stress for each girder respectively from east to west is: 0.83, 1.32, 2.23, 2.95, and 2.35 ksi. Figure 3.42 shows the transverse stress distribution for the five girders during the dynamic loading. The trends look quite similar to those of the static field and analytical results (See Figure 3.43 for the comparison of the static and dynamic curves.) The dynamic curve (fifth curve) shows much higher stresses than the static field curve (fourth curve) and the dynamic curve tends to compare much better with the analytical results. Better load distribution can be seen in the dynamic curve than in the analytical curves. This implies that the transverse members are carrying more load than can be assumed by initial observations. The static analytical model underestimates the sum of midspan moments by 6%. Thus the analytical model predicts the dynamic midspan response much better than the static response.

3.9.1 Calculation of the Angular Natural Frequency

As a point of interest (since the dynamic data acquired was limited and no in-depth analysis was done) it was decided to go ahead and calculate the angular natural frequency and estimate a first mode shape for span no. 4. From some free vibration results obtained during one of the incomplete dynamic tests one can estimate the period, T, of the span. It can be seen from Figure 3.44 that eight peaks and eight valleys exist within a range of 4000 samples. Thus it is safe to use 500 samples to approximate the period. With a sampling rate of 1.6 kHz, T is equal to 0.3125 seconds. The equation relating the angular natural frequency, ω, to the period is:

$$T = \frac{2\pi}{\omega} \tag{3.6}$$

thus

$$\omega = \frac{2\pi}{T} \tag{3.7}$$

Based on the free vibration data, the angular natural frequency is:

$$\omega = \frac{2\pi}{0.3125} = 20.1 \ rad/\text{sec.} \tag{3.8}$$

The theoretical equation for the angular natural frequency [Paz, 1985] is:

$$\omega_n = n^2\pi^2\sqrt{\frac{EI}{mL^4}} \tag{3.9}$$

where:

ω_n ≡ theoretical angular natural frequency
n ≡ mode shape
E ≡ modulus of elasticity
I ≡ moment of inertia
m ≡ mass per unit length
L ≡ length of span

This equation for the theoretical frequency is an approximation because it assumes uniform girders and that both ends are simply supported. To do this calculation it was decided to use the parameters of the middle girder and assume full composite action. Because there are three different cross-sections along the middle girder, ratios were used to approximate the moment of inertia and the mass per unit length. The material densities were obtained from AASHTO [1983]. The theoretical angular natural frequency then becomes:

$$\omega_n = (1)^2\pi^2\sqrt{\frac{(29{,}000{,}000)(108{,}718)}{(0.244)(1335)^4}} = 26.6 \ rad/\text{sec.}$$

where
the first mode shape was used. Considering the approximations these frequencies compare reasonably well and gives more confidence in the field results that were obtained. The theoretical frequency is about 30% greater than the actual frequency which indicates that this span is less stiff than what was assumed. This possibly occurs due to the partial composite action in some of the longitudinal members.

4. FIELD MEASUREMENTS OF STRESS RANGE DATA FROM CONTROLLED TRAFFIC ON BRIDGE NO. 62864

4.1 Purpose of the Field Tests

This chapter discusses an application of the methodology and the equipment described in the previous parts of this report. A composite steel bridge was instrumented and subjected to controlled traffic consisting of two fully loaded trucks in order to measure the static and the dynamic response of possible fatigue sensitive details. An analytical study was performed so that the theoretical model could be validated by comparing measured and calculated stresses.

4.2 Description of the Bridge

The bridge selected for this study is MnDOT Bridge No. 62864. It is located under Interstate I-35E in St. Paul, Minnesota. It is situated between Jefferson Avenue and Randolph Avenue and crosses over an express service road. It was designed for HS20 loading and an alternate loading according to the 1969 A.A.S.H.O. design specifications. The design drawings are dated 2-10-71. The crossing consists of two bridges, one carrying the northbound traffic on I-35E toward St. Paul, and the other supporting the southbound traffic. The field tests were performed on the northbound bridge.

This bridge has a three-span continuous structure with five parallel longitudinal steel girders, attached in the regions of positive moment to an 8.5 inch thick concrete slab to form a composite bridge. The total length of the bridge is just over 200 feet. It is a skewed and a curved bridge, skewed 39° at the north end and 32° at the south end. Figure 4.1 shows a drawing of the cross section of the bridge, and a plan view is presented in Fig. 4.2. The solid horizontal lines represent the five longitudinal girders, and the solid diagonal lines are the support lines. The horizontal dashed lines define the traffic lanes (right and left lanes) and the right shoulder lane.

The steel girders in the south span were instrumented. The underside of the span slopes from the south end of the bridge down to the access roadway which is below the center lane of the bridge. The south span was thus easily accessible from below with a ladder (10 to 20 ft. high). The complete design data of this bridge are presented in the drawings entitled "Fed. Proj. No. I-35E-4(95)104.

4.3 Description of the Instrumentation and the Data Acquisition System

The principal data taken on this bridge consist of strain gage readings. There were also five tilt-meters installed at the center of the test span on the main longitudinal girders. Since the main interest was on fatigue behavior, the information obtained from the tilt meters is not evaluated here.

The strains were measured by 1) full-bridge clamp-on BWS Strain Gage Sensors and 2) standard wire resistance strain gages. The former measures the average strains over a five inch gage length, while the latter gives the strain at a point on the test beam.

The workings of the BWS Strain Gage Sensors are described earlier in this report. Their location is diagrammed in Fig. 4.3. Five gages were placed at the center of the test span on each of the longitudinal girders (Channels 6 through 10), two were located over the support (Channels 12 and 13), and one was placed where the moment of inertia of the girder cross section changed, ten feet

south of the first interior support (Channel 11). The BWS Strain Gage Sensors were clamped to the inner face of the bottom flange.

The wire resistance strain gages were placed near fatigue critical details on the main longitudinal girders in the test span. They were attached with their long side parallel with the longitudinal axis of the girders in order to measure the normal strains due to the longitudinal bending moment in the girder. Strain gages connected to Channels 0 and 1 and 3 and 4, were located over the interior support on the north end of the test-span on beams 3 and 4, respectively. Channels 0 and 3 are on the web near the stiffener and the top flange, while Channels 1 and 4 are on the inside face of the bottom flange near the bearing stiffener. The detailed locations of these gages are given in Figs. 4.4 and 4.5, respectively. Two additional strain gages (Channels 2 and 5) were placed about nine feet south of the support on the inside face of the bottom flange at the welded flange splice (see Figs. 4.6 and 4.7).

The data acquisition and data storage process is described in an earlier part of this report.

4.4 Load Application

The stresses calculated from the measured strains represent only the live load contribution since it is not possible to measure the strains due to the dead load on an existing bridge. It is, however, important to recognize that as far as fatigue resistance is concerned only the stress range is of significance. In the bridge under discussion (No. 62864 on 35E) the live load was applied through two standard MnDOT dump trucks loaded with sand so that the total weight of each was within a few hundred pounds of 25 tons, or 50 kips ($\pm$ 0.6 kips).

The field tests on this bridge were performed on July 24, 1992. The day was clear and sunny. While the loading trucks were on the bridge, the right lane, and thus also the right shoulder lane, were blocked off to normal traffic. The lane locations are marked on the plan-view of the bridge in Fig. 4.1. The left traffic lane was kept open to permit normal traffic to pass by slowly northward. Thus it was possible to have, in addition to the loading trucks, also some additional ambient traffic present in the left lane. Attempts were made to obtain static load readings, i.e., the truck remained standing in a pre-defined location while the signals from all the channels were recorded, when there were no other vehicles on the bridge. This was not always successful, and thus there is some unquantifyable variability of the data. However, this part of I-35E is restricted to vehicles weighing less than 9 kips, and so the traffic mix consisted only of personal vehicles. The occasional simultaneous presence of these vehicles on the bridge does not affect the results in a significant way.

Static loading was accomplished by moving the trucks along the center of each respective lane, stopping every 15 feet until the strains from each of the 13 channels were recorded. Three passes were made to obtain the static readings from: 1) one truck in the shoulder lane, 2) one truck in the right lane and 3) one truck each in the shoulder and right lane. The lane definitions and the locations of the truck stops are shown in Fig. 4.8. It would have been desirable to have had the bridge completely closed during the test loading (a 15-20 minute period at most) but it was not possible to obtain permission to do so.

Dynamic testing was accomplished by driving the two trucks side-by-side at 60 mph in the shoulder and the right lane. During the dynamic testing the acquisition unit was being used to collect and store one thousand samples per strain channel at a rate of 200 samples per second. It took a number

of runs where only partial data was recorded until the timing was perfected for effective data acquisition. Two successful passes were recorded resulting in complete traces.

4.5 Analytical Model

The forces and stresses due to the static loading were calculated in order to make a comparison between measurement and prediction. The following assumptions were made: 1) the response of the material in elastic; 2) the deformations are small and 3) there is no interaction between axial and flexural effects in the members. According to the design drawings furnished by the Minnesota Department of Transportation (MN/DOT), every longitudinal girder in Bridge No. 62864 consists of composite sections in the approximate positive moment regions (i.e., shear connectors fasten the slab to the girder) alternating with non-composite sections in the approximate negative moment regions over the interior supports (i.e., no shear connectors).

The bridge is modeled as a grid for analysis. The members are diagrammed in the nodemap of Fig. 4.9. The longitudinal girders are divided into beam segments between locations where the moment of inertia changes. The diaphragms (i.e., the channels perpendicular to the longitudinal members) are shown in their locations in Fig. 4.9. The slab is modeled as a series of uncracked concrete transverse beams located at the places marked by dashed lines in Fig. 4.9. The bridge model consists of 180 beam elements and 137 joints. It was analyzed by a grid analysis program given by Weaver and Gere (1980).

4.6 Static Live Load Stresses

The static live load stresses were calculated from the strains measured by the 13 channels of strain sensors due to the loads from the trucks weighing 50 kips as they stopped at 15 foot intervals along the longitudinal axis of the bridge. Figures 4.10 through 4.24 present representative results for each of the gage locations. The complete set of curves for each of three truck-lane combinations and each channel are given by Teng (Teng, 1992). The curves in Figs. 4.10 through 4.24 are the straight connecting lines between the plotted stress values at the point of the gage location as the truck moves along the bridge. These curves are thus influence lines for the stresses. The field data are recorded each time the truck stops at 15 ft intervals. The predicted analytical values are computed for the same points by the grid program, as described above. For the analysis, the truck is idealized as a point load of 50 kip magnitude acting in the center of the lane.

The ordinates in Figs. 4.10 though 4.24 are the location of the centroid of the truck from the south end of the center of the right traffic lane (see Fig. 4.8), and the ordinates are the stress values. Three runs of strain recording were made: one 50 kip truck in the shoulder and the right traffic lanes, respectively, and two trucks side-by-side in the shoulder and right lane. An examination of the curves in Figs. 4.10 through 4.24 shows that 1) the stresses are relatively small, the maximum recorded stress being 2.6 ksi, with most of the other stresses below 2 ksi, and 2) the general correlation between analysis and field measurement is reasonable, considering the idealizations made in the model. Further implications of the data presented will be discussed later in this report.

4.7 Dynamic Stress Range Data

Two successful traces of dynamic response were obtained on Bridge No. 62864 on I-35E. The data were obtained during the passage over the bridge of the two 50 kip trucks travelling side-by-side in

the shoulder and the right traffic lanes at 60 mph. Each data channel, i.e., six strain gages and eight BWS strain sensors, recorded 1000 readings during 5 seconds. A trace showing stress versus time from one of these (Channel 12, a BWS strain sensor located on the inside surface of the bottom flange at the interior support of the fourth girder from the east, see Fig. 4.3) is shown in Fig. 4.25. The noise was filtered from this trace and the resulting image is shown in Fig. 4.26. From this, and from the corresponding traces of the other 12 channels, the bar charts of Figs. 4.27 and 4.28 were constructed. The charts show the measured and filtered stress ranges, i.e., the difference between the maximum and the minimum stress recorded by the device during the passage of the trucks. The significance of the results from these dynamic runs will be discussed in Sec. 6 of this report.

5. FIELD MEASUREMENTS OF STRESS RANGE DATA FROM RANDOM TRAFFIC ON BRIDGE NO. 9613

5.1 Description of the Bridge

The purpose of this test was to measure the stress ranges at fatigue-critical locations on a heavily travelled bridge during the off-commuter period when it is subjected to considerable truck traffic: cement transport vehicles, concrete mixer trucks, vehicles loaded with bricks, construction machinery, etc. The north-south artery I-35W is one such road in the Twin Cities area which fulfills the requirement of loading stated above. The other condition of selection was that the bottom of the bridge should be easily accessible for placing the strain sensors.

Bridge No. 9613 on the northbound lane of I-35W south of downtown Minneapolis was chosen for this study. This bridge, one of twin structures, carries the separate northbound traffic over East Minnehaha Parkway and Minnehaha Creek. It consists of five parallel continuous steel beams acting compositely with an 8.5 inch thick reinforced concrete slab. The spacing between the girders is 10 ft. This bridge is a four-span continuous bridge on a 41° skew. The spans are 65 ft. - 88 ft. - 110 ft. -88 ft. consecutively from the south abutment to the north abutment. The plan view of the bridge is shown in Fig. 5.1. The instrumented portion of the bridge in the second span from the south end at the vicinity of pier No. 3. The five continuous longitudinal girders are haunched at either side of each of the three interior piers. The clearance of the test span was less than 15 ft. above East Minnehaha Parkway, and therefore it was easy to set up the equipment on the sidewalk and to install the strain gages.

5.2 Instrumentation and Data Acquisition

Strains were measured by three kinds of devices on this bridge: clamp-on BWS Strain Gage Sensors, wire-resistance uni-directional strain gages and wire-resistance rosette strain gages. The BWS sensors and the uni-directional gages measured normal stresses perpendicular to the main girder cross section while the rosettes measured the principal strains in the plane of the web.

The BWS strain gage sensors were clamped to the inside face of the bottom flange at the first interior support on each of the main girders at the north end of the test span (pier 2), as shown in Fig. 5.2. The data from these sensors is recorded via channels 0 through 4.

The uni-axial and the multi-axial strain gages were attached to beam No. 2, which is essentially under the right wheel line of trucks travelling in the right lane. Strain gages were attached in the first panel (between the diaphragm at pier 2 and the next transverse stiffener) north of the interior support at pier 2. Since it was possible to take data from 16 dynamic channels only, the same channel numbers were used for different strain gages in two rounds of data acquisition runs. In Round One, 11 dynamic data runs were recorded, while in Round Two, 8 dynamic data runs were taken. The locations of the uni-axial and the rosette strain gages are shown, together with their channel numbers, in Figs. 5.3 through 5.7 for both rounds of data acquisition runs. Table 5.1 lists the details of the locations of the gages, and Figs. 5.8 and 5.9 diagram the locations again for further clarity.

5.3 Load Application

Bridge testing was performed on August 11, 1992 on a clear cool summer day. Since traffic could

not be slowed, diverted or stopped, only dynamic data could be obtained. This means that the 5 second burst of 1000 readings per channel was recorded under the ambient normal mid-afternoon traffic flow. The traffic that day was always dense, consisting of a mix that contained many heavy vehicles such as cement container vessels, concrete mixer trucks, and vehicles carrying masonry, fabricated steel and construction equipment.

Data taking commenced when a lookout at a vantage point from which oncoming traffic could be observed gave a radio signal that a heavy vehicle, or a group of such vehicles, was approaching the bridge. It took some initial trial and error samples before the technique of timing the start of data-taking was successful, but eventually eighteen dynamic passes were successfully recorded.

The fact should be kept in mind that neither the weight nor the speed of the loaded vehicles was known. The data thus represents only a narrow window of observation, and it does not necessarily represent extreme possibilities.

5.4 Dynamic Stress Range Data

The signals from the active channels were recorded simultaneously for each of the eighteen dynamic passes under vehicles of unknown weight and speed. Because of the nature of electronic signals, the dynamic results from the field measurements had to be filtered digitally to reduce spurious noise effects from the data. Noise can take many forms, from slowly changing voltages produced by electrode contact potentials, to the broad spectrum random noise produced in high gain amplifiers. In general, noise can be reduced by the use of a filter without too great a change in the actual signal itself. By using a software package DADISP3.0 (DSP, 1991), the raw strain-time traces (1000 data points taken during a 5 sec. interval for each of 16 channels) were filtered and the maximum stress range was determined for each run. Typical bar chart results are presented in Figs. 5.10 through 5.14. The charts give the maximum stress range for each run for which data was taken from that particular sensor. A complete set of bar charts for each sensor is given by Teng (1992).

The charts in the figures presented in this report are for the following strain sensor and gage locations:

a) at pier No. 2, bottom flange, beam 2, average over 8 in (Fig. 5.10)
b) at pier No. 2, bottom flange, beam 2, near stiffener (Fig. 5.11)
c) at flange splice, on bottom flange (Fig. 5.12)
d) on bottom of web, near stiffener, rosette (Fig. 5.13)
e) on bottom on web, near flange splice (Fig. 5.14)

The significance of the results will be discussed in Sec. 6 of this report.

6. EVALUATION OF STRESS-RANGE DATA

The purpose of making the stress range measurements on the I-35E and I-35W bridges was to determine their magnitudes under controlled weight and under normal day-time heavy traffic. Following is a discussion of the significance of the obtained data in regard to the fatigue life of the details on these bridges.

6.1 Fatigue Life of Bridges

One possible limit state of parts of a highway bridge is the development of fatigue cracks in critical connection details. These fatigue fractures may grow and eventually damage enough of the cross section so that the entire member has failed, or their growth may be arrested naturally or by human intervention such as by introducing crack arrestors of various kinds. Various typical fatigue problems are discussed in the book by J. W. Fisher (1984).

Over the period of the quarter century starting in 1960, field and laboratory studies, as well as observations of successful and unsuccessful details in installed bridges have isolated the situations which are fatigue prone, and, therefore, very few fatigue problems exist, or are expected, in properly designed modern steel bridges. However, there is always the question as to how this satisfactory behavior will continue if the truck weights increase and/or the Average Daily Truck Traffic (ADTT) increases. This question has been under intense investigation, and there are a vast number of papers and research reports available on the subject. It is not the intent here to review this voluminous material. However, two recent references, namely the papers by Raju, Moses and Schilling (1990) and Hakin, South, Mohammedi and Polepeddin (1993) will be discussed in some detail as they relate to the research performed in this project.

The research by Hakin and his colleagues from the Illinois Department of Transportation describe an extensive project where 15 steel bridges were instrumented with strain gages to measure the stress ranges under ambient traffic at typically two to four active gages per bridge. The gages were placed as close as possible to the fatigue detail to be investigated. Continuous readings were taken under mixed traffic using a single-channel microprocessor-based data-acquisition device which uses a method known as "rain-flow" counting to produce a stress range histogram from which the equivalent applied constant amplitude stress range can be determined by using Miner's hypothesis. Readings were taken for 3 to 8 hours, and the data were then linearly extrapolated to get a daily histogram for each bridge. From the data measured on the individual bridges, a composite histogram was produced for the details investigated for the steel bridges of the State of Illinois. Various theoretical studies were then performed to study fatigue damage or remaining fatigue life.

The paper by Raju, Moses and Schilling (1990) describes a general method of evaluating the fatigue life of details in steel bridges which was published as NCHRP Bulletin 299 (Moses, Schilling and Raju, 1988). This Bulletin contains the background research and the resulting recommendations for both the evaluation of existing bridges and for new designs. The recommendations for fatigue evaluation are appropriate for the evaluation of the research performed in this project.

The fatigue life can be determined as follows (Sec. 6.3, Moses et al 1988):

(a) The fatigue life is infinite and no further fatigue calculations are required if
where,

$$R_s S_r < S_{FL} \quad (16)$$

R_s = reliability factor
S_r = nominal stress range
S_{FL} = limiting stress range for infinite life

(b) The finite remaining life can be determined by

$$Y_f = \frac{fK \times 10^6}{T_a C(R_s S_R)^3} - a \quad (17)$$

where,

Y_f = remaining fatigue life in years
K = detail constant depending on the AASHTO fatigue detail category
T_a = estimated lifetime average daily truck volume in the outer lane
C = stress cycles per truck passage
f = 1.0 for calculating "safe life" and 2.0 for calculating "mean life"
a = present age of bridge in years.

The "safe life" is a 97.7 percent probability that the actual life will exceed this predicted remaining life. The mean life is the best estimate of the remaining life of the fatigue detail, because there is about a 50 percent probability that the actual life will exceed this value.

The recommendations in the NCHRP Bulletin contain many particulars about how the various parts of Eqs. 1 and 2 are to be determined. These will not be repeated here. The next section of this chapter will only utilize those parts of the NCHRP Bulletin which are necessary to interpret the test data from this project.

It should be mentioned here that there is a large literature on the remaining life of fatigue details, and that there is by no means agreement on the best way to proceed. Because of the many uncertainties and variabilities inherent in the loading, the stress analysis and the fatigue process itself, the results of any evaluation should be tempered by judgment and experience before any drastic remedial action is taken in any given situation.

6.2 Examination of the Test Results of Bridge No. 62864

This bridge is on northbound I-35E, and strains were measured in 13 locations of the south span under one or two 50 kip trucks producing either static or dynamic response, as already discussed in Chap. 4 of this report. The histogram of Fig. 6.1 shows the comparative bar charts of the static stress range and the dynamic stress ranges from runs where two trucks were side-by-side, one in the shoulder lane and the other one in the right traffic lane. Also shown are the stress range values from the analysis. Since the analytical values of the stresses do not give an exact trace of the experimental values (see Figs. 4.15-4.29), the stress range values can be even more divergent, as demonstrated in Fig. 6.1. The static versus the dynamic values should reflect the influence of impact. With some exceptions this is verified by the lower static stress ranges as compared to the dynamic ranges. The exceptions can be explained by the presence of other traffic due to smaller vehicles on the bridge during the static runs. The significant data as far as the fatigue evaluation is

concerned are due to the two dynamic runs. The strain sensors on this bridge were located at three AASHTO fatigue category details:

(a) Detail A, base metal with rolled surface; sensors 6 through 10 and 12 and 13 were BWS strain sensors which were clamped to surfaces away from groove wells or fillet welded connections.

(b) Detail B, Channel 11 is also a BWS strain sensor, and it was attached to the bottom flange at a butt-welded flange splice.

(c) Detail C, Channels 0 through 5 were uni-directional strain gages located near the toes of transverse stiffener welds.

The maximum measured dynamic stress ranges for each fatigue detail category are as follows (see Fig. 6.1)

Category A, $(S_r)_{max}$ = 2.5ksi
Category B, $(S_r)_{max}$ = 2.7ksi
Category C, $(S_r)_{max}$ = 2.2ksi

These values of the maximum stress range are the result of two 50 kip trucks side-by-side, moving across the bridge at 50 mph. The significance of these values will now be interpreted in accordance with the criteria set forth by Moses, Schilling and Raju (1988). This publication provides several criteria for determining the factored stress range R_sS_r (Eq. 1), depending on the way the stress range is determined by various types of field measurements or calculations of differing degrees of sophistication. The one alternative which is appropriate for the measurements taken on this bridge is as follows:

A "fatigue" truck is moved across the bridge and measurements of the stress ranges due to this event are used. This "fatigue" truck is approximately of the same weight but of somewhat different overall dimensions as the trucks used on this bridge. The weight of the "fatigue" truck is 54 kip, so in order to have an equivalent reading, the stress ranges taken in the tests need to be increased by the factor 54/50 = 1.08. The stress ranges one would obtain from the "fatigue" truck (see comparison between the test truck and the "fatigue" truck in Fig. 6.2) are not the same, to be sure, but the test truck with its shorter length will generally give higher values. Furthermore, the readings on the bridge were taken with two trucks side-by-side. According to Moses, Schilling and Raju only one "fatigue" truck is required for the fatigue evaluation.

The "fatigue" truck is calibrated such that the fatigue damage caused by a certain number of passes of this equivalent truck is the same as the fatigue damage caused by the same number of passages of trucks of different weights in the traffic stream. The weight of the "fatigue" truck was determined from actual traffic spectra obtained from Weigh-in-Motion studies conducted nationwide that included 30 sites and over 27,000 trucks (Raju, Moses, Schilling, 1990).

The "reliability" factor accounts for the probabilistic variations of the loading, the fatigue process and the material properties. For the case of this bridge the value of R_s is determined by the formula (Moses, Schilling and Raju, 1988).
where R_{so} = 1.35 for redundant members, the basic reliability factor (all the sensors were placed

$$R_S = R_{SO} \times F_{S1} \times F_{S2} \times F_{S3} \quad (18)$$

on redundant members in this bridge)
F_{S1} = 0.85 for data obtained directly in the field
F_{S2} = 1.00 if the "fatigue" truck was used
F_{F3} = 1.00 no analysis was performed with assumed distribution factors

Therefore, $R_S = 1.35 \times 0.85 \times 1.00 \times 1.00 = 1.15$

The total factored stress range, upgraded for the weight of the fatigue truck is then

$$R_S S_r = 1.15 \times 1.08 S_{r50} = 1.24 S_{r50}$$

where S_{r50} is the maximum stress range measured in the field. This value of $R_S S_r$ will be compared to the limiting stress range S_{FL}, which is also tabulated in the report by Moses, Schilling and Raju (1988). These values of S_{FL} are based on the 1989 AASHTO specification provisions. Following is a summary:

Category	S_{r50}	$R_S S_r$	S_{FL}
A	2.5 ksi	3.1 ksi	8.8 ksi
B	2.7 ksi	3.4 ksi	5.9 ksi
C	2.2 ksi	2.7 ksi	4.4 ksi

The fatigue requirements of the proposed AASHTO Load and Resistance Factor Design (LRFD) specification (AASHTO, 1992) are similar, but they are more liberal. The AASHTO "fatigue" truck is identical to that in the NCHRP report (Moses, Schilling, Raju), but the measured or calculated stress range need not be multiplied by a reliability factor. The design limiting stress range for the LRFD specification is set at one-half of the constant amplitude fatigue threshold $(\Delta F)_{TH}$ for the given detail. The comparison with the proposed LRFD specification is, therefore:

Category	S_{r50}	$(54/50)S_{r50}$	$(1/2)(\Delta F)_{TH}$
A	2.5 ksi	2.7 ksi	12 ksi
B	2.7 ksi	2.9 ksi	8 ksi
C	2.2 ksi	2.4 ksi	6 ksi

According to these analyses, Bridge No. 62864 has details which have a very high probability of not experiencing fatigue damage even if the truck loading is considerably increased. Even by the most conservative estimate the fatigue truck could be increased in weight by 4.4/2.7 = 1.63, or by about 60 percent. This means that the mix of traffic could include a very high proportion of extremely heavily loaded trucks, beyond anything ever experienced in this country on a public highway. It should be recalled that presently the maximum permitted vehicle weight on this stretch of I-35E is

9000 lbs!

6.3 Examination of the Test Results of Bridge No. 9613

This bridge is on the northbound lane of I-35W in South Minneapolis and it crosses Minnehaha Creek. The traffic on this portion of I-35W is very heavy, carrying about 5000 trucks per day on three lanes. Strain gage readings were taken during the afternoon of a clear August day prior to the afternoon rush hour commuter traffic. The traffic mix contained a fairly large percentage of trucks. A total of 19 strain traces were obtained for 5 gage locations, 11 traces for 3 locations, 8 traces for 5 locations and 5 traces for 2 locations over a period of about 4 hours. Readings were made when a lookout signalled the approach of one or more big trucks, mostly cement container trucks, concrete mixers and trucks loaded with construction equipment.

The maximum stress range values obtained from this bridge are summed up below (further particulars are given in the table below, and sample maximum stress range bar-charts are presented in Figs. 5.10 through 5.14) for the AASHTO fatigue detail categories A, B, C:

Detail Category	$(S_r)_{max}$	$R_s(S_r)_{max}$	S_{FL}
A	1.9 ksi	2.2 ksi	8.8 ksi
B	4.3 ksi	4.9 ksi	5.9 ksi
C	3.3 ksi	3.8 ksi	4.4 ksi

In this table $(S_r)_{max}$ is the maximum observed stress range, R_s is the reliability factor and S_{FL} is the limiting stress range for infinite life. Moses, Schilling and Raju (1988) define the reliability factor for the case where the stress range is determined from ambient traffic as the product $R_S = 0.85 \times 1.35 = 1.15$, where 0.85 reflects the fact that data from ambient traffic is used, and 1.35 is the basic reliability factor for redundant members. From the data presented above, it can be seen that there is a comfortable margin between the measured and the lower-bound permissible values.

This statement must be, however, qualified by the following observations:

(a) Not nearly enough runs were recorded to build a stress range histogram so that a meaningful Miner's hypothesis cumulative stress range value can be determined.

(b) At least eight hours of continuous data should have been obtained to adequately characterize the truck traffic between morning and evening rush hours. The equipment we used is clearly not suitable for such data acquisition.

(c) The best that can be said about the data is that it represents typical values of stress ranges. By taking the maximum stress range, we are conservative because we assume that all trucks produce the same stress range. On the other hand, there is little chance that the haphazard way of selecting the stream of traffic under which a set of readings were taken contains the heaviest vehicles using the highway during the day the observations were made.

7. SUMMARY, CONCLUSIONS AND RECOMMENDATIONS

7.1 Summary

A portable, rugged and multi-purpose instrumentation system was developed during this project. This was accomplished by using fourteen removable instruments where possible and non-reusable strain gages where access was difficult. The data acquisition system was based around a Keithley 576 A/D device and a Toshiba T3100SX portable computer.

7.1.1 Static Tests

Stresses the main members of two composite bridges were obtained through the sue of the portable data acquisition system. The field results were then compared to the analytical results from a simplified computer model. For Bridge 6805, the maximum observed static field stress for a 100 kip load was 2.61 ksi when the two easterly lanes were loaded. The maximum analytical stress came from the same loading condition and was 3.35 ksi. For the same load case, the maximum resulting middle girder deflections were 0.27" and 0.26" for the field data and analytical data respectively. The analytical data here is from the best computer model as determined in Chapter 3. The best model consisted of the easterly two girders behaving as semi-composite members while the other three girders were modelled as fully composite members. The definition of semi-composite is given in Section 3.5.5.

Comparisons of the field and the analytical results with two of the AASHTO code provisions shows that there exists a reasonable chance of underrating bridges and in particular Bridge 6805. AASHTO's allowable deflection is four times greater than the field deflection and twice as much as a model for all girders acting as non-composite sections. Overestimation of the field load distribution ranges from 70-100%. These two facts coupled with the idea that span 4 has a high degree of composite action gives an indication that this bridge would be underrated without the availability of field instrumentation data.

In general, the analytical results correspond quite well to the field results. Although there appear to be rather large discrepancies in the stress result figures, a sum of the field midspan moments and a sum of the analytical midspan moments shows that the model is about 20% conservative. This is good considering particular stress values are overestimated by as much as 40%.

7.1.2 Dynamic Tests

For Bridge 6805, the limited dynamic results showed a peak stress of about 2.95 ksi which occurs in the middle west girder. An angular natural frequency was also calculated at about 20.1 rad/sec. This most likely occurs with the first mode of vibration for which a theoretical frequency of 26.6 rad/sec. was calculated. For the other two bridges, extensive dynamic data was acquired, and good correlation with static analysis was obtained.

7.1.3 Stress Range Determination and Evaluation

The field-testing equipment described in Chapter 2 and 3 was used to obtain live-load stress range data from two bridges in the Twin Cities area. This field testing equipment consisted of strain sensors attached to specific locations on the main girders of the bridges, and of data acquisition

paraphernalia to convert the electric signals generated by the sensors into stress values. The summary of the design and evaluation of the equipment is described in previous parts of this report. It is here reiterated that the total data collection procedure worked very satisfactorily, and the sensors were sharp enough to pick up meaningful live load data from truck traffic on the bridges.

Stress range values were obtained from two bridges. Each of these crossings were on a major urban interstate road system. The bridges are located on the northbound lanes of I-35E in South St. Paul, and I-35W in South Minneapolis, respectively.

The first bridge, No. 62864 of the MnDOT on I-35E, was subjected to controlled traffic under both static and dynamic loading from one and/or two 50,000 lb weight dump trucks. Only one of the two traffic lanes was closed off to public traffic during the testing. However, the public traffic weights are mandated to not exceed 9,000 per vehicle, so there were no trucks in the open lane while the measurements were taken. No significant disturbance of the data is believed to have occurred because of the occasional presence of these light vehicles. It would, of course, be desirable to have the whole bridge closed off while the test trucks are on the bridge, but this is a luxury one cannot afford on a major urban interstate route.

The static runs were made with the test trucks stopping every 15 ft along the bridge while readings were taken. Three combinations of vehicles were used: one truck each in the shoulder lane and the right traffic lane, respectively, and both trucks side-by-side in both lanes. The dynamic runs were made by both trucks side-by-side in the shoulder and the right traffic lanes, travelling at 60 mph.

Stress range data were obtained from 3 static runs and from two dynamic runs at 14 locations in various parts on the main longitudinal girders of the southern span of this three-span bridge. The locations were selected to correspond to AASHTO fatigue detail categories A, B and C. The locations and types of gages are presented in Figs. 4.3 through 4.6.

The live load stresses for the static runs were also calculated using a grid model, and the comparisons between the predicted and the measured stresses for representative gage locations are shown in Figs. 4.10 through 4.24. The summaries of the measured static stress ranges, the calculated stress ranges and the two dynamic stress ranges are presented in the histograms of Fig. 6.1.

The second bridge, MnDOT Bridge No. 9613 on I-35W, was tested under ambient truck traffic. The data were obtained on a typical working-day afternoon while there was a very heavy mix of trucks in the traffic stream. Strain sensors were again placed at AASHTO fatigue detail categories A, B and C at various locations on the main longitudinal girders. No runs were made with controlled weight vehicles, and the traffic was never interrupted during the tests. The gage locations are shown in Figs. 5.1 through 5.8, and maximum stress range values for selected gage locations are given in Figs. 5.9 through 5.13.

In summary, then, stress range values were obtained from two bridges under controlled-weight vehicles and under ambient truck traffic. The purpose of these tests was to be able to make some conclusions about the fatigue life of the various details which were instrumented.

7.2 Conclusions and Recommendations

7.2.1 Static and Dynamic Tests

Overall this acquisition and modelling system worked quite well for the simply supported and continuous bridges with static loading. A new measurement technique for finding deflections was developed, and it can be readily used for bridge evaluation. The application of this system should now be extended to various types of bridges including continuous span, concrete girder and timber bridges.

The dynamic data acquisition system had limitations. Because the sampling time allotted was only five seconds, more times than not the interesting data was missed. To alleviate this one should consider reducing the sampling rate below the current rate of 1600 Hz. Another option would be to develop a program that accepts binary code, to control the Keithley 576, then one could increase the data transfer rate by over 100 times that of using ASYSTANT GPIB Software. Doing this could allow continuous dynamic monitoring of actual traffic loading. Setting up a trigger mechanism is also recommended. It might be interesting to develop an easily mountable accelerometer or linear variable displacement transformer so that one could determine dynamic deflections since the current system is not equipped with such a capability. The current Keithley 576 setup is expandable to 32 channels which could accommodate additional instrumentation. Compatible hardware can be purchased to expand the Keithley 576 to over 200 channels.

7.2.2 Fatigue Life Determinations

Two kinds of methods were used to acquire information on the stress ranges in existing steel bridges under truck traffic:

1. using trucks of controlled weight, and
2. using ambient truck traffic.

1. The weight of the trucks used was 50 kips each. This weight is approximately equal to the proposed "fatigue" truck (Moses, Schilling and Raju, 1988) in the new AASHTO Load and Resistance Factor Design (LRFD) specification for highway bridges. This truck is a statistical average vehicle which represents the fatigue-damage producing stress cycles on the Nation's bridges. This truck, together with the load factors that are associated with it, account for the load spectrum, the change of traffic volume and weight with time, and the statistical variabilities of the significant parameters which affect loading and resistance. Thus the analysis of the I-35E bridge under controlled loading is a valid and acceptable method of fatigue rating details on bridges.

   The maximum stress ranges obtained in the field from such a controlled weight test were always below the factored limiting stress range for infinite life for all the three detail categories on which data were taken. The ratios between the measured and factored maximum stress ranges and the permissible ones were 0.35, 0.56 and 0.61, respectively, for AASHTO fatigue detail categories A, B and C. This means that the selected details in this bridge have a very high probability of not experiencing fatigue distress in the lifetime of the bridge even if the general truck weights increase considerably.

   Using a controlled truck weight and configuration precisely equal to the actual fatigue vehicle, which is shown in Fig. 6.2, would sharpen the data, and this should be considered in future

tests of this kind. Furthermore, the comparisons between the measured and predicted stress range values could be also improved by more realistic modelling of the bridge structure, and then no field tests would be required. This would be a satisfactory approach for straight right bridges, but field tests would still be desirable for sharply curved and skewed geometries.

2. The type of data taken under ambient truck traffic on the I-35W bridge is of much less value than that obtained from the controlled vehicles on the I-35E bridge, because it is not at all guaranteed that the samples taken are representative of the spectrum of truck traffic on the bridge during the day. All that can be said is that the random sampling of the traffic resulted in maximum stress range data which did not exceed the lower bound infinite life fatigue limits for the three detail categories which were instrumented. While this is of some limited value and is certainly worth much more than no observations at all, it is not enough to base decisions on whether or not repairs or modifications are to be considered. In order to get more assuring data another different kind of scheme must be used under ambient traffic. This is the method described by Hakin, South, Mohammadi and Pelepeddin (1993) in which continuous strain data from one sensor is fed directly into a microprocessor that uses the "rainflow counting method" to provide the stress range histogram for the truck on the bridge during the period of data taking (say eight hours).

REFERENCES

(1) The American Association of State Highway and Transportation Officials, Standard Specifications for Highway Bridges, Thirteenth Edition, 1983,with Interim Specifications through 1986, Washington, D.C., 1987.

(2) American Institute of Steel Construction, Manual of Steel Construction, Load and Resistance Factor Design, First Edition, Chicago, Ill., 1986.

(3) Analog Devices, Inc., The 3B Series Signal Conditioning I/O Subsystem, User's Manual, Norwood, Massachusetts, 1986.

(4) Applied Geomechanics, Inc., Model 800 Engineering Tiltmeter and Model 870 Readout Module, User's Manual, Santa Cruz, California, January, 1991.

(5) Asyst Software Technologies, Inc., Asystant GPIB Software Manual, Rochester, New York, 1988.

(6) Bakht, B. and Jaeger, L.G., Bridge Testing-A Surprise Every Time, Journal of Structural Engineering, American Society of Civil Engineering, Vol. 116 No., May 1990.

(7) Beer, F. and Johnston, E., Mechanics of Materials, 1st Edition, McGraw-Hill Company, 1981.

(8) Borland International, Inc., Quattro Pro Software Manual, Version 3.0, Scotts Valley, California, 1991.

(9) Cheung, M.S., Jategaonkar, R., and Jaeger, L.G., Effects of Intermediate Diaphragms in Distributing Live Loads in Beam-and-Slab Bridges, Canadian Journal of Civil Engineering, 1986.

(10) DADISP, "The DADISP Worksheet, Data Analysis, and Software Users Manual", DSP Development Coropration, Cambridge, MA, 1991.

(11) Galambos, T.V., Leon, R.T., French, C.W., Barker,M.J., Dishong, B., Inelastic Rating Procedures for Steel Beam and Girder Bridges, Preliminary Draft of Final Report, Department of Civil and Mineral Engineering, University of Minnesota, Minneapolis, Minnesota, March, 1990.

(12) Golden Software, Inc., Grid Software, Version 1.79E, Golden, Colorado, 1987.

(13) Golden Software, Inc., Grapher Software, Version 1.79E, Golden, Colorado, 1988.

(14) Hanin, C., South, J.M., Mohammadi, J., and Polepeddi, R.K., Accurate and Rapid Determination of Fatigue Damage in Steel Bridges", ASCE J. of Structural Engineering, Vol. 119, No. 1, 1993, pp. 150-168

(15) Hoffmann, K., Fundamentals of the Strain Gauge Technique: How to Avoid or Minimize Errors in Strain Gauge Measurement, Hottinger Baldwin Messtechnik, GmbH, 1973.

(16) Hoffmann, K., Fundamentals of the Strain Gauge Technique: Applying the Wheatstone Bridge Circuit, Hottinger Baldwin Messtechnik, GmbH, 1973.

(17) IOtech, Inc., Personal488 User's Manual, Cleveland Ohio, Revision 3.0, December, 1990.

(18) Keithley Instruments, Inc., Model 576 High Speed Data Logging System, User's Manual, 2nd Edition, Cleveland, Ohio, October, 1990.

(19) Moses, F. and Ghosn, M., Instrumentation for Weighing Trucks-in-Motion for Highway Bridge Loads, Final Report Department of Civil Engineering, Case Western Reserve University, Cleveland, Ohio, August, 1983.

(20) Moses, F., Ghosn, M. and Gobieski, J., Weigh-in-Motion Applied to Bridge Evaluation, Final Report Department of Civil Engineering, Case Western Reserve University, Cleveland, Ohio, September, 1985.

(21) Moses, F. and Verma, D., Load Capacity Evaluation of Existing Bridges, Final Report, Department of Civil Engineering, Case Western Reserve University, Cleveland, Ohio, October, 1987.

(22) Moses, F., Schilling, C.G., and Raju, S.K., "Fatigue Evaluation Procedures for Steel Bridges", NCHRP 299, Transportation Research Board, Washington, D.C., 1988.

(23) Paz, Mario, Structural Dynamics Theory and Computation, 2nd Edition, Van Nostran Reinhold, New York, 1985.

(24) Raju, S.K., Moses, F., and Schilling, C.G., Reliability Calibration of Fatigue Evaluation and Design Procedures, ASCE J. of Structural Eng., Vol. 116, No. 5, 1990, pp. 1356-1369.

(25) Sack, R.L., Structural Analysis, 1st Edition, McGraw-Hill, Inc., 1984.

(26) Schmit, J.R., "Field Instrumentation of Brdiges", a Thesis prsented to the Graduate School of the University of Minnesota in partial fullfillment of the requirements for the degree of Master of Science, March 1992.

(27) Teng, Ai-lien, "Remaining Fatigue Life of Steel Bridges", a Thesis prsented to the Graduate School of the University of Minnesota in partial fullfillment of the requirements for the degree of Master of Science,December 1992.

(28) Toshiba Corporation, Toshiba T3100SX Portable Personal Computer, Reference Manual, Irvine, California, 1st Edition, May 1990.

(29) Toshiba Corporation, Toshiba Desk Station III Manual, Irvine California, September, 1990.

(30) Weaver, W. and Gere, J.M., Matrix Analysis of Framed Structures, 2nd Edition, Van Nostran Reinhold, New York, 1980.

TABLES

Table 2.1 Strain sensor calibration factors

Strain Sensor Calibration Values			
Strain Gage Channel Number	Strain Gage Calibration Constant (Mv/V/$\mu\epsilon$)	Electronics and Cabling Loss Factor	
		Loss Factor	St. Dev.
6	1.82×10^{-3}	1.14	0.03
7	1.83×10^{-3}	1.16	0.03
8	1.79×10^{-3}	1.20	0.02
9	1.77×10^{-3}	1.14	0.03
10	1.80×10^{-3}	1.15	0.03
11	1.83×10^{-3}	1.25	0.03
12	1.84×10^{-3}	1.03	0.05
13	1.80×10^{-3}	1.24	0.06
	Average 1.81×10^{-3}		
	St. Dev. 0.02×10^{-3}		

Table 2.2 Calibration factors for tiltmeters

Tiltmeter Calibration Values		
Tiltmeter Channel Number	Tiltmeter Calibration Constant (μradian/Mv)	Electronics and Cabling Loss
0	1.7508	1.01
1	1.7489	1.06*
2	1.7425	1.02
3	1.7417	1.03
4	1.7461	1.03
5	1.7474	0.98
	Average 1.7462	Average 1.01
	St. Dev. 0.0036	St. Dev. 0.02

* Channel 1 was providing erratic values during its calibration and therefore was not included in the average. Also the location of the channel 1 tiltmeter was not critical to this study.

Table 2.3 Parameters for curve fitting

Input for Curve Fit		Curve Fit Output
Distance from Support (in)	Rotation (radians)	Cubic Equation Coefficients
60	-0.00019126	-0.000199532
203	-0.00017425	1.51811×10^{-7}
368	-0.00014654	-2.7347×10^{-10}
667	-0.00001653	6.8546×10^{-13}

Table 2.4 Sample computation of deflections

Distance from Support (in)	Analytical Deflections	Field Deflections	Ratio
0	0.000	0.000	--
60	-0.0157	-0.0117	1.34
203	-0.0513	-0.0378	1.36
368	-0.0851	-0.0646	1.32
667	-0.114	-0.0924	1.23

Location and Lengths of Span 4 Coverplates					
Girders	"X"	"Y"	"Z"	"Q"	"R"
WEST	115.125	17.353	27.353	79.0	59.0
M WEST	113.117	16.380	26.380	79.0	59.0
MIDDLE	111.219	15.401	25.401	79.0	59.0
M EAST	109.271	14.427	24.427	79.0	59.0
EAST	107.312	13.448	23.448	79.0	59.0

Where:

(X) Girder length
(Y) Distance from south support to 1st plate
(Z) Distance from south support to 2nd plate
(Q) Length of 1st coverplate (12" x .75")
(R) Length of 2nd coverplate (12" x .75")
* All lengths in feet

Table 3.1 Details of girders

Model Number	1	2	3	4	5	6	7	8	9	10	12
End Diaph.	Y	N	Y	Y	Y	Y	Y	Y	Y	Y	Y
Slab 100%	Y	Y					Y	Y	Y	Y	Y
Slab 150%				Y							
Slab 200%					Y						
Slab 50%			Y								
Non-Composite						Y					
East Girder Non-Comp.							Y				
East and MidE Non-Comp.								Y			
East Girder Semi-Comp.									Y		
East and MidE Semi-Comp.										Y	
East Semi MidE Non-Comp.											Y

Table 3.2 Details of analytical models

Table 3.7 Midspan load distributions for east lane loading

Girder	Field Moment (k-in)	Field Ratios	Field Load (kips)	Analytical Moment (k-in)	Analytical Ratios	Analytical Load (kips)	AASHTO Code (kips)
East	4666	0.438	21.90	5625	0.507	25.35	44.00
Middle East	3487	0.327	16.35	4570	0.412	20.60	28.00
Middle	1802	0.169	8.45	1316	0.119	5.95	0.00
Middle West	653	0.061	3.05	162	0.015	0.75	0.00
West	54	0.005	0.25	-583	-0.053	-2.65	0.00
SUM	10662	1.000	50.00	11090	1.000	50.00	72.00

Moments and loads are based on a 50 kip truck

Table 3.3 Comparison of load distributions

ROUND	CHANNEL	TYPE	LOCATION
1	5	Uniaxial	Top Flange Center of Panel
1	6	Uniaxial	Center of Web Center of Panel
1	7	Uniaxial	Bottom Flange Center of Panel
1	8, 9, 10	Rosette	Bottom of Web Near Diaphragm
1	11, 12, 13	Rosette	Bottom of Web Near Stiffener
1	14	Uniaxial	Bottom Flange Near Diaphragm
2	5	Uniaxial	Same as Channel 14 in Round 1
2	6, 7, 8	Rosette	Top of Web Near Diaphragm
2	9, 10, 11	Rosette	Bottom of Web Near Flange Splice
2	12	Uniaxial	Bottom Flange Near Flange Splice
2	13	Uniaxial	Bottom Flange at Flange Splice
2	14	Uniaxial	Bottom Flange Near Flange Splice

Table 5.1 Location of gages

CHANNEL NO.	MAXIMUM MEASURED STRESS RANGE	AASHTO DETAIL CATEGORY
0	1.9 ksi	C
1	2.6 ksi	C
2	1.9 ksi	C
3	2.0 ksi	C
4	1.9 ksi	C
5 (1st round)	1.2 ksi	B
6 (1st round)	1.9 ksi	A
7 (1st round)	1.7 ksi	B
14 (1st round) & 5 (2nd)	2.0 ksi	C
15 (1st round)	2.0 ksi	C
Rosette No. 1 (1st round)	1.3 ksi	C
Rosette No. 2 (1st round)	3.3 ksi	C
Rosette No. 1 (2nd round)	1.3 ksi	C
Rosette No. 2 (2nd round)	2.0 ksi	C
12 (2nd round)	3.6 ksi	B
13 & 14 (2nd round)	4.3 ksi	B

Table 6.1 Maximum stress range values for bridges

FIGURES

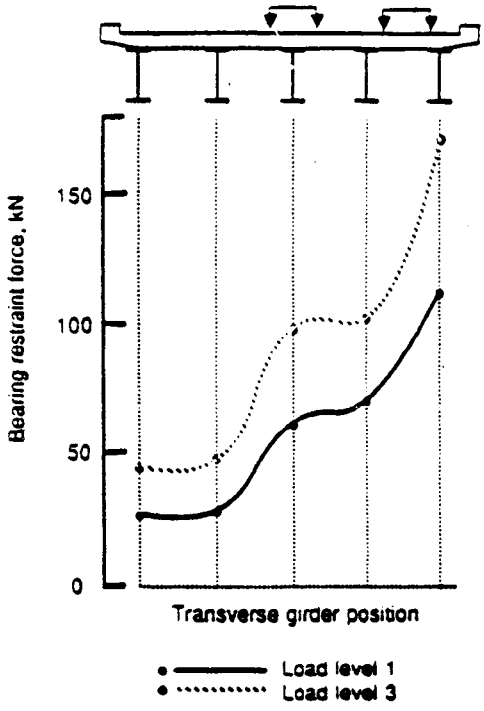

Figure 1.1 Bearing restraint forces in slab-on-girder bridge with elastomeric bearings

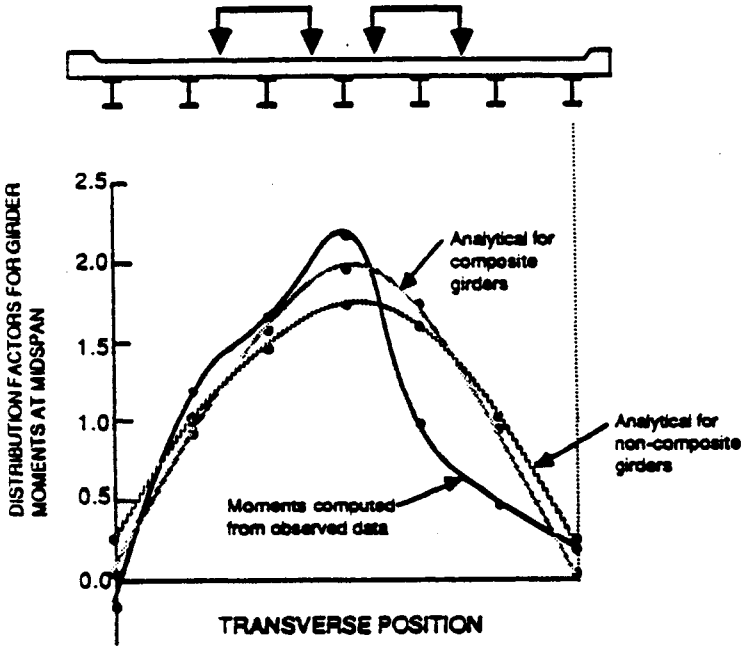

Figure 1.2 Actual and analytical distribution factors for midspan girder moments

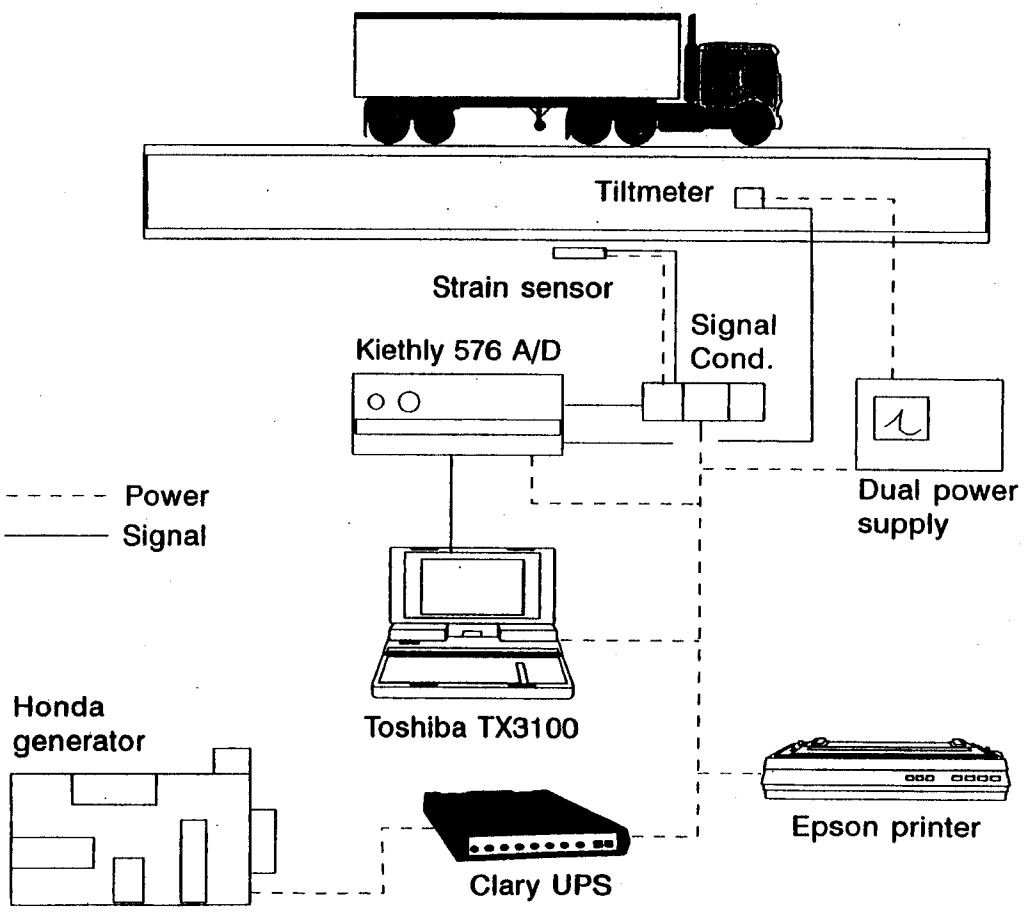

Figure 2.1 Flow diagram for data acquisition without quarter-bridge strain gages

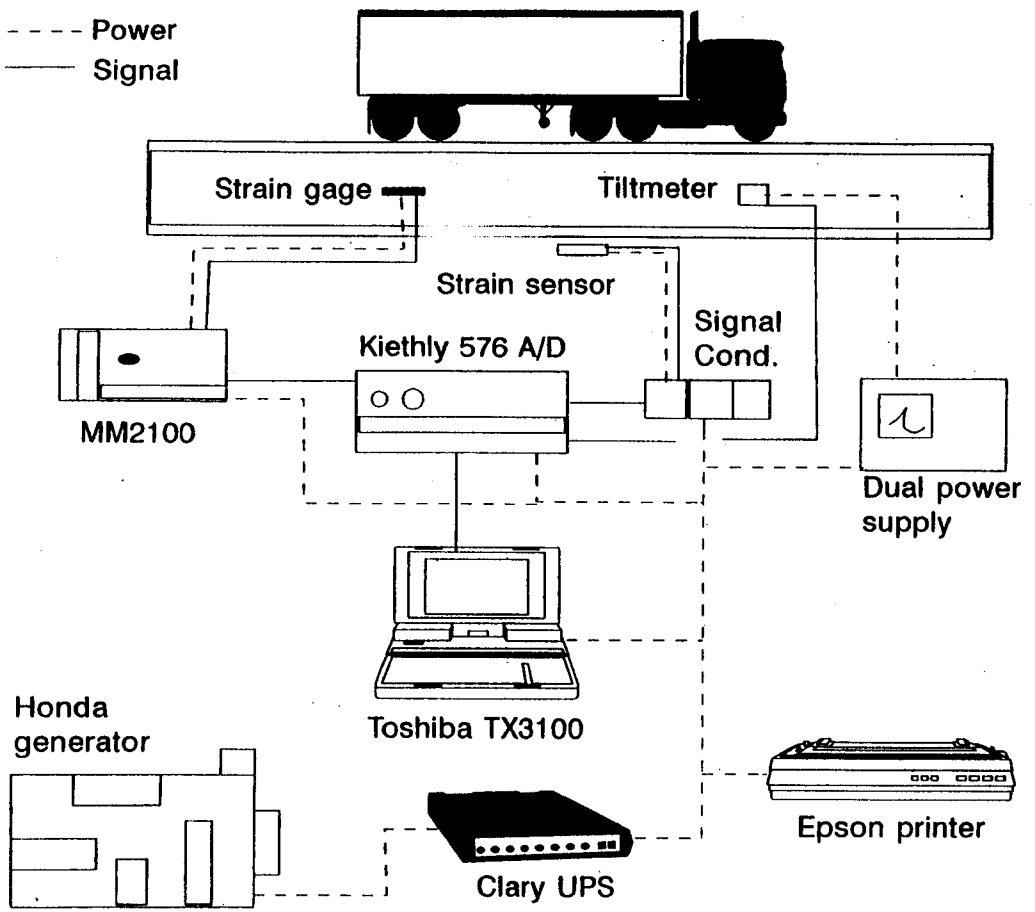

Figure 2.2 Flow diagram for data acquisition with quarter-bridge strain gages

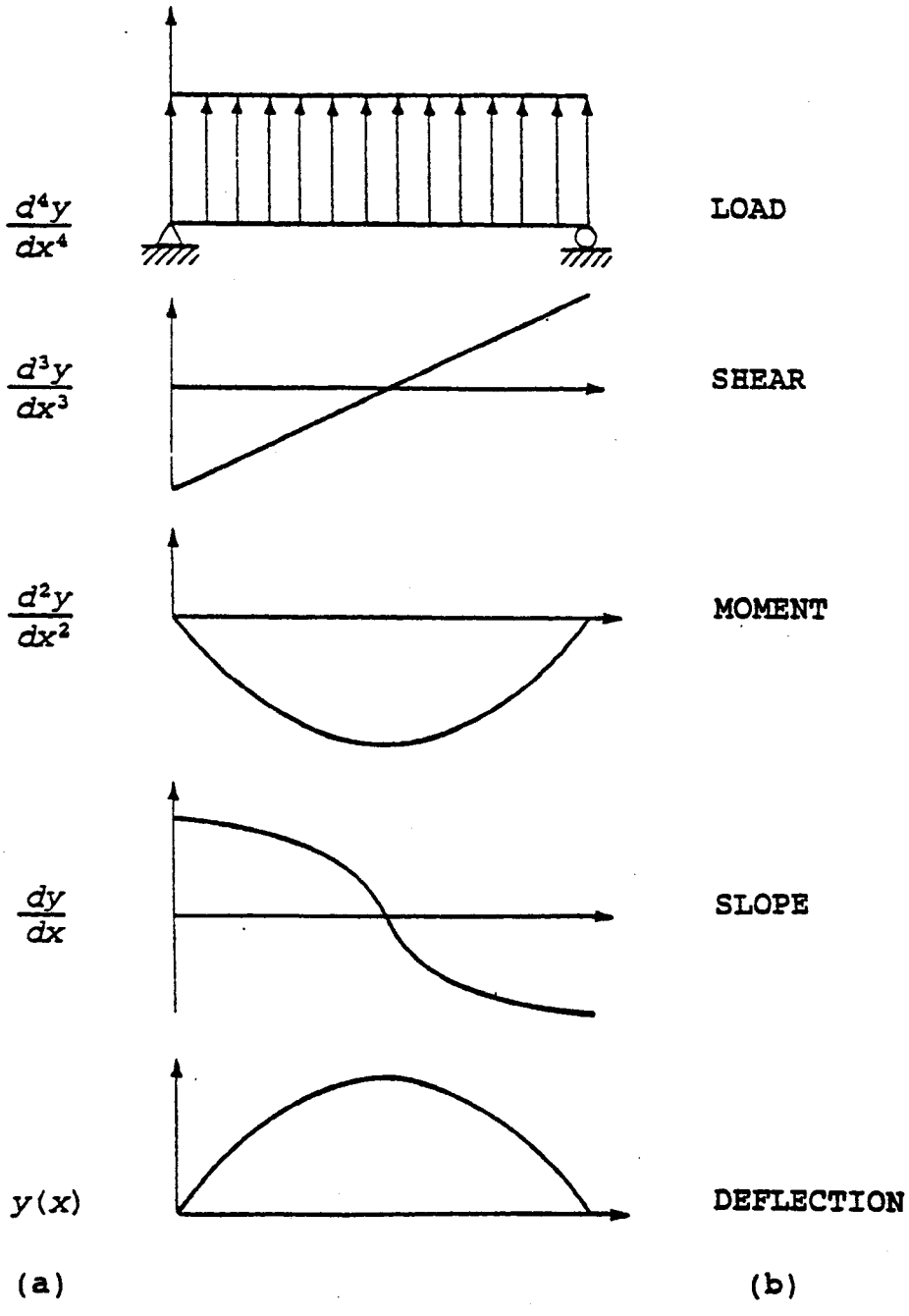

Figure 2.3 Computation of deflections by integration

Figure 3.1 Elevation drawing of bridge 6805

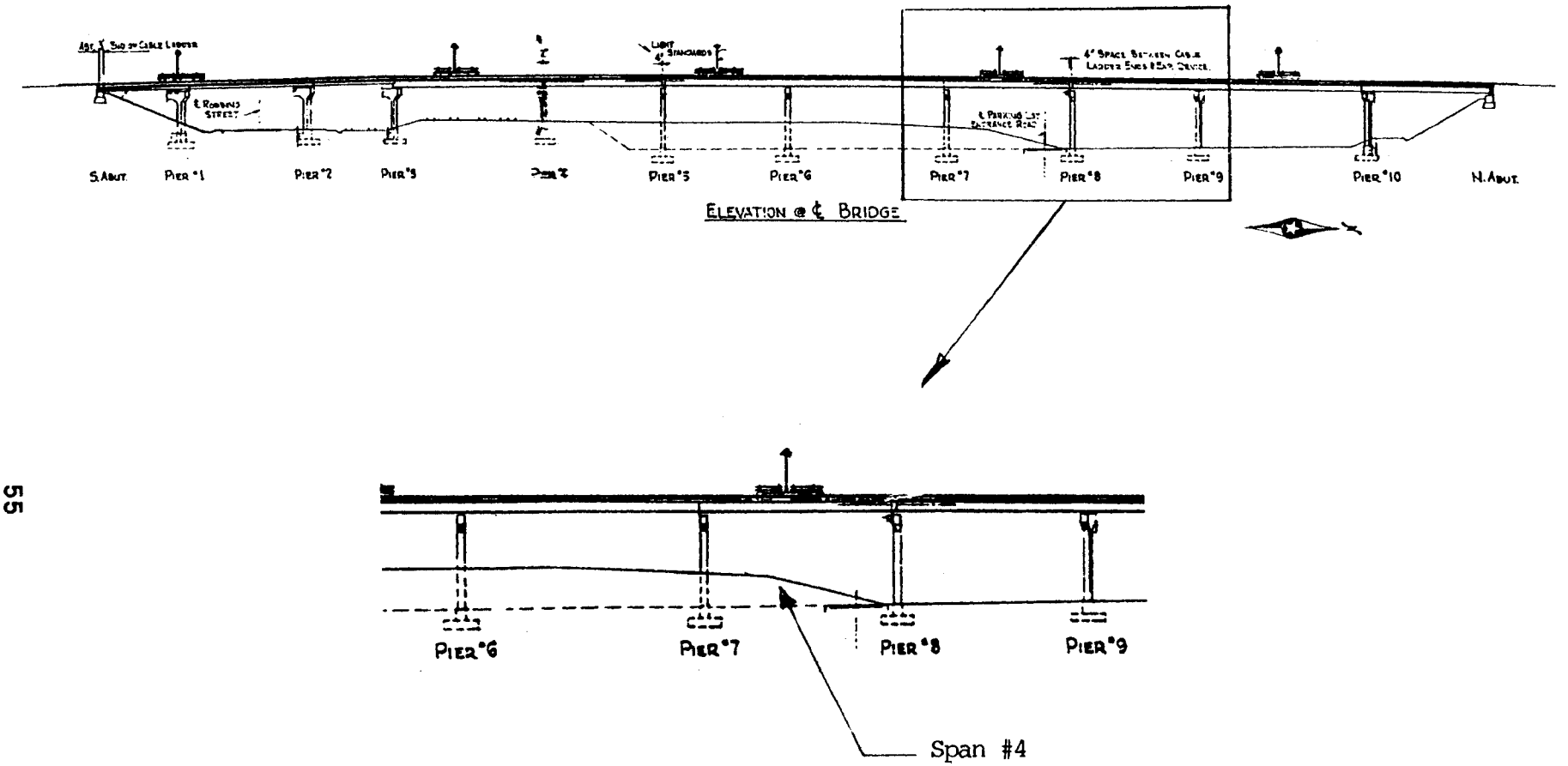

Figure 3.2 Elevation view of span 4 of bridge 6805

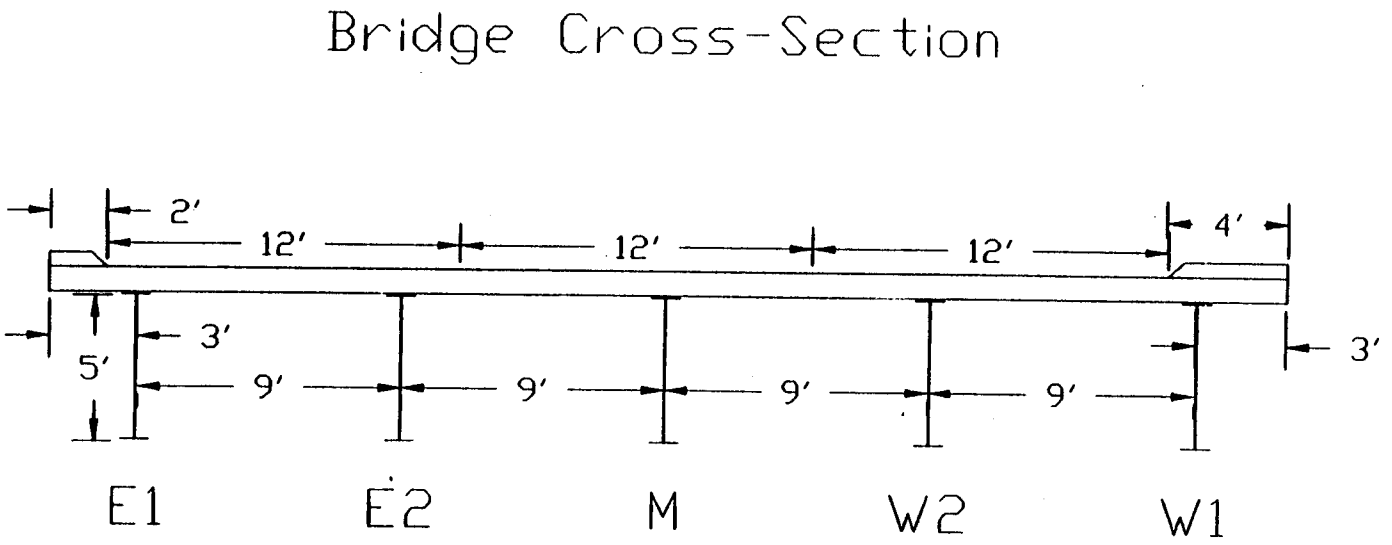

Figure 3.3 Cross-section of span no. 4 looking South

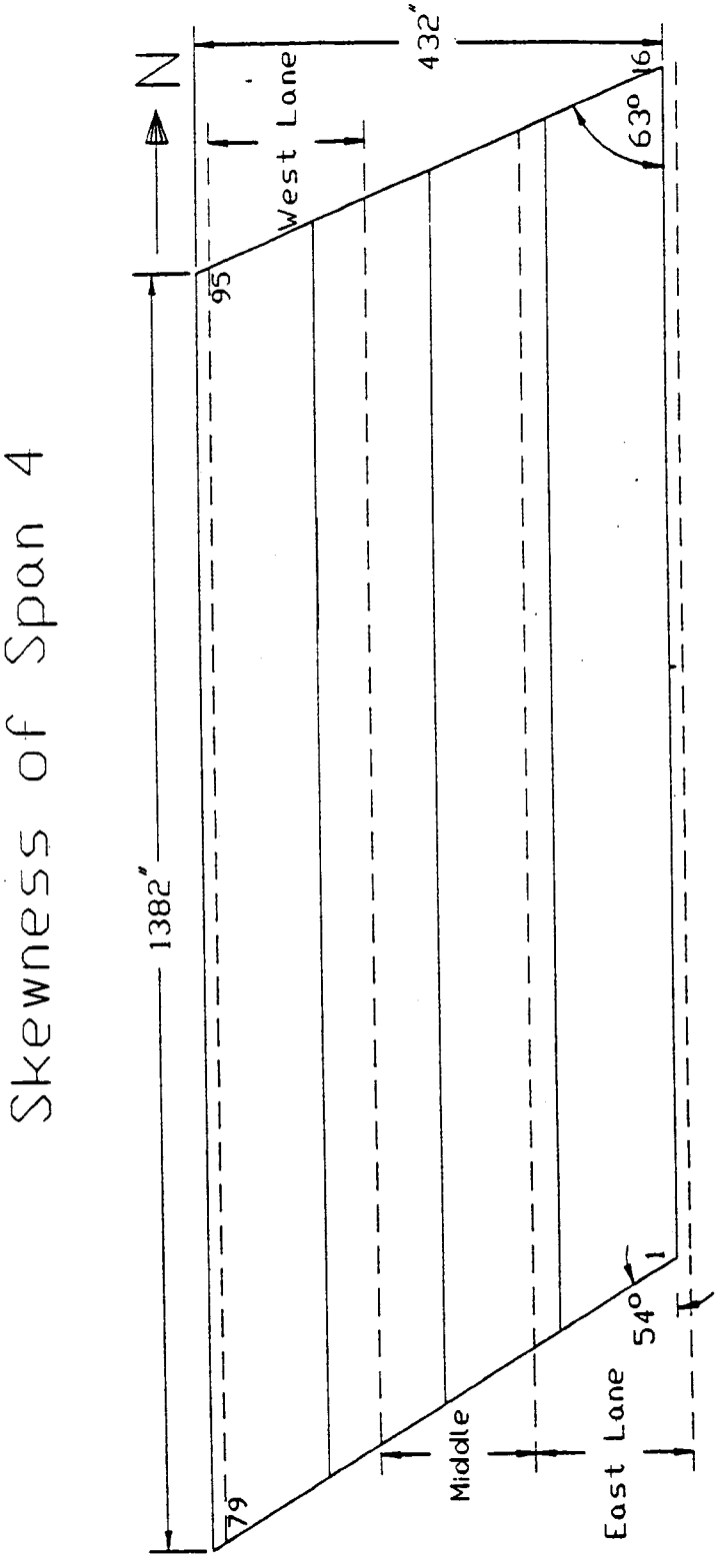

Figure 3.4 Plan view of span no. 4

Figure 3.5 View of typical girder

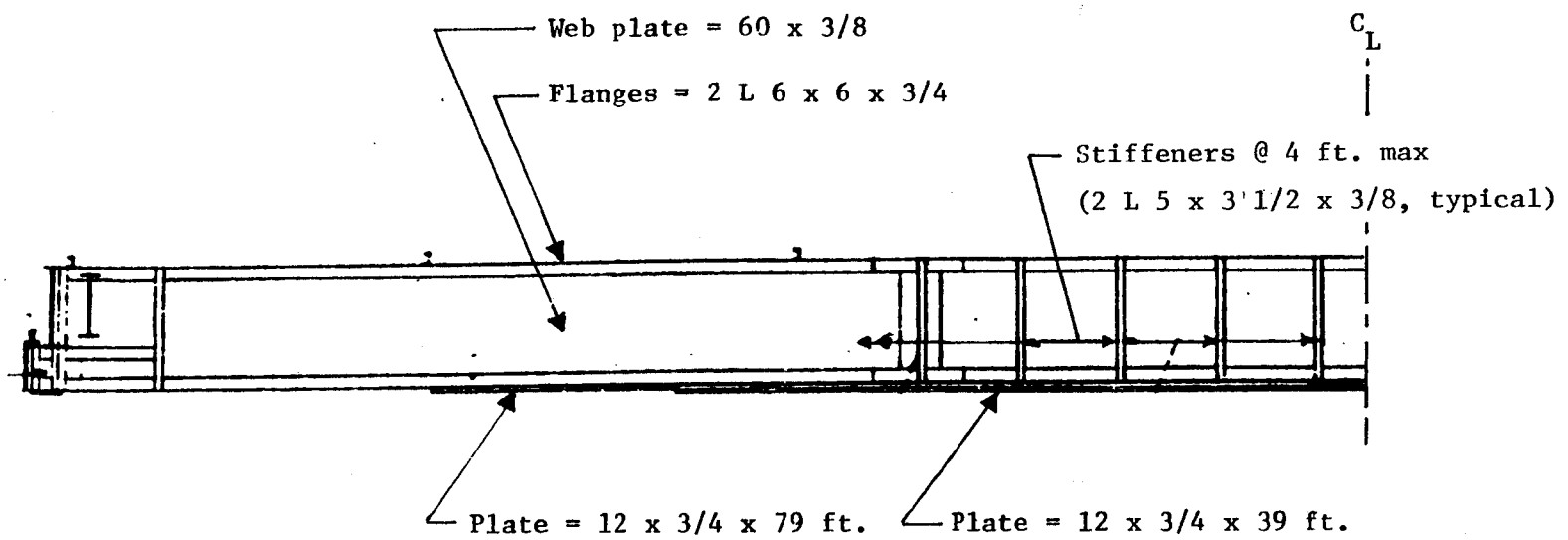

Figure 3.6 Details of typical girder for span no. 4

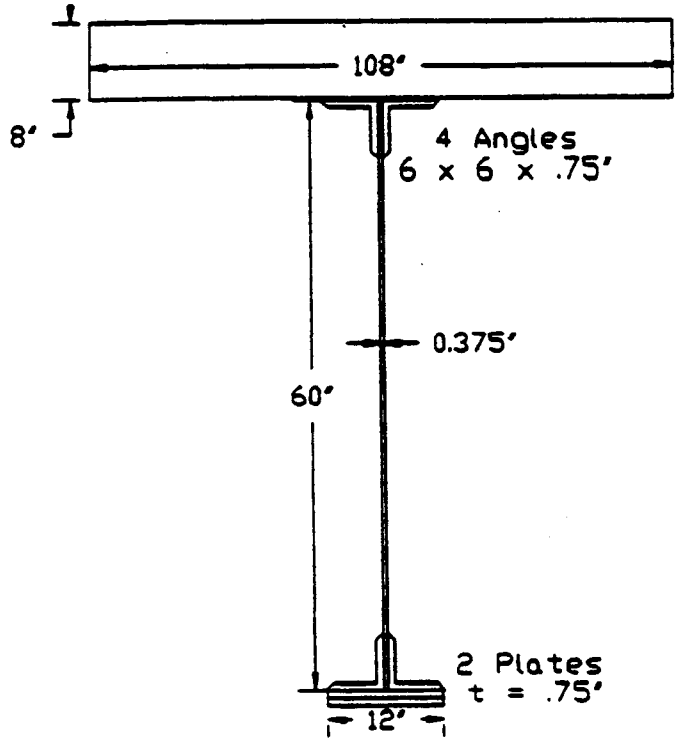

Girder Cross-Section

Figure 3.7 Typical girder cross-section for span no. 4

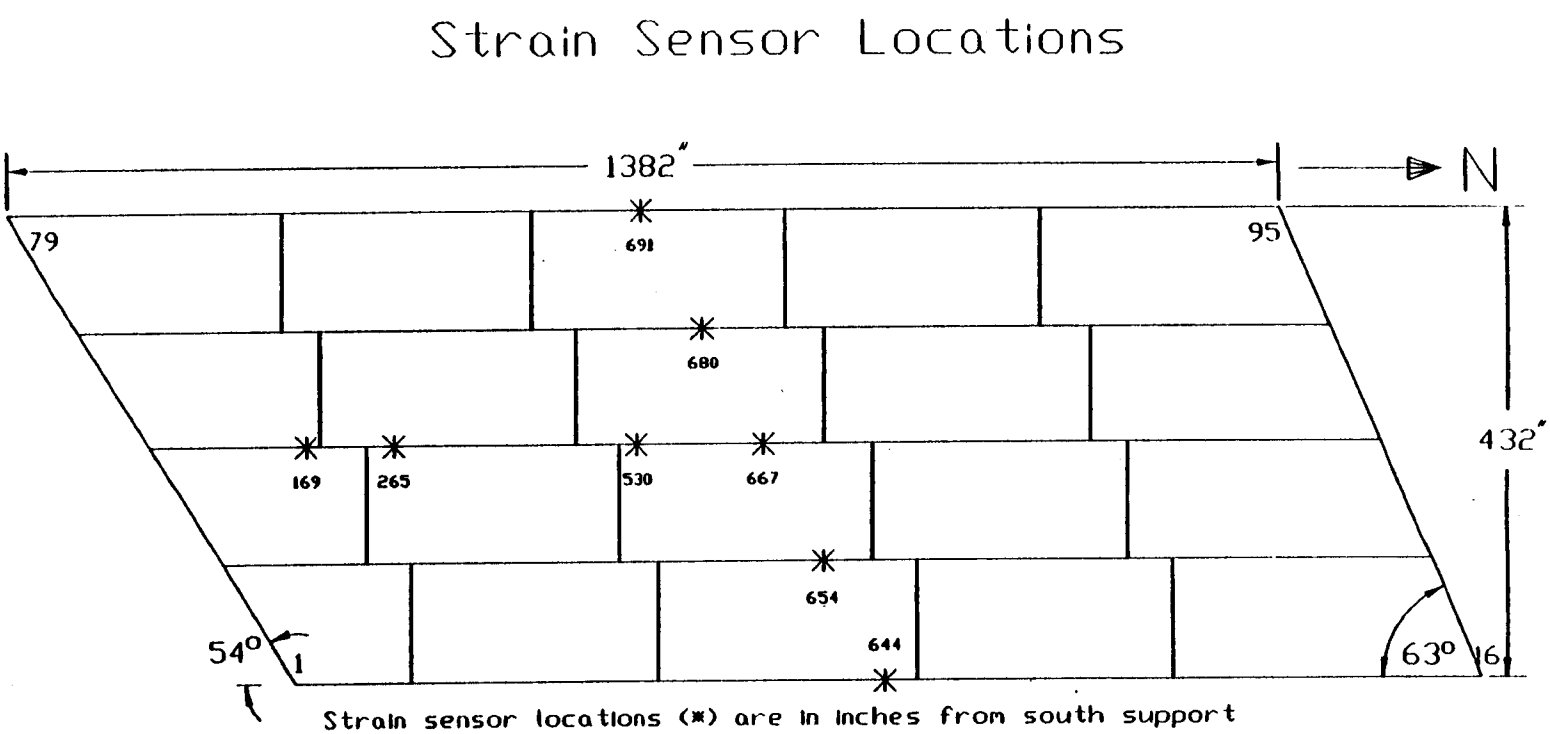

Figure 3.8 Location of strain sensors

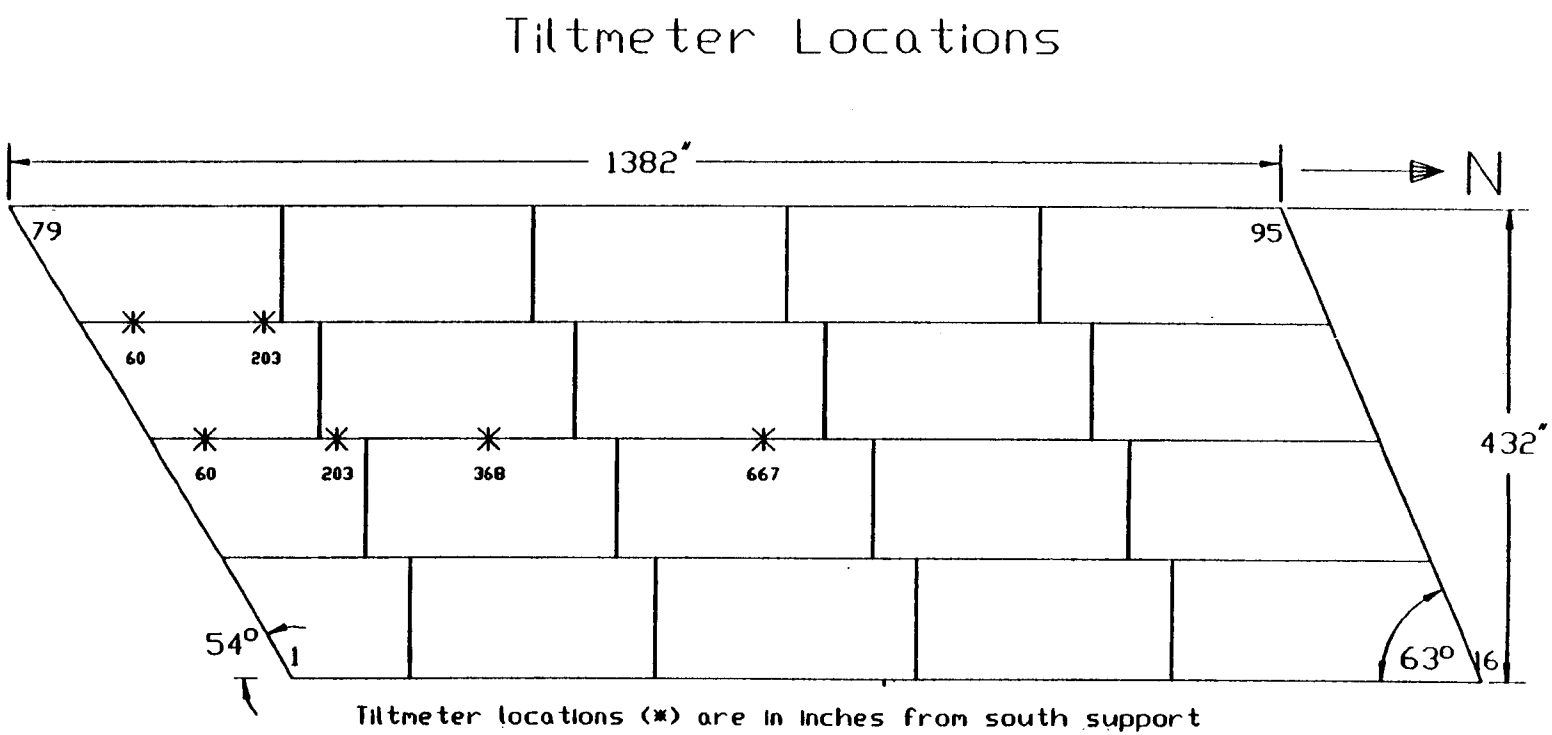

Figure 3.9 Location of tiltmeters

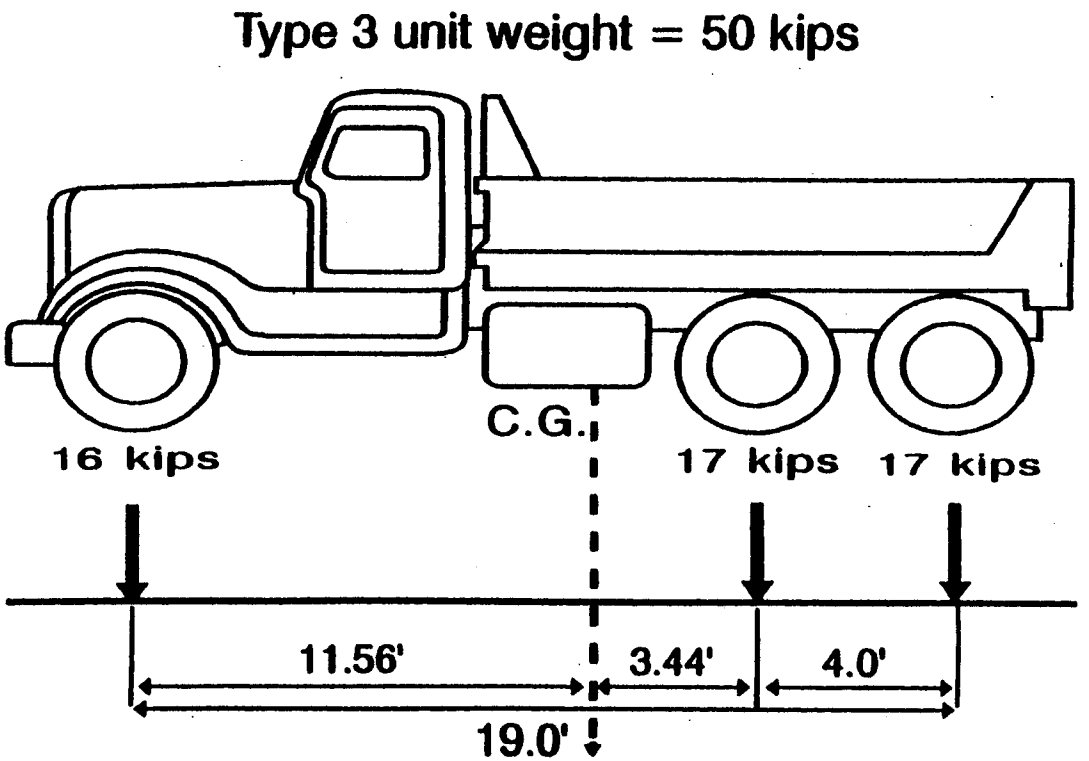

Figure 3.10 AASHTO type 3, 50 kip truck showing center of gravity

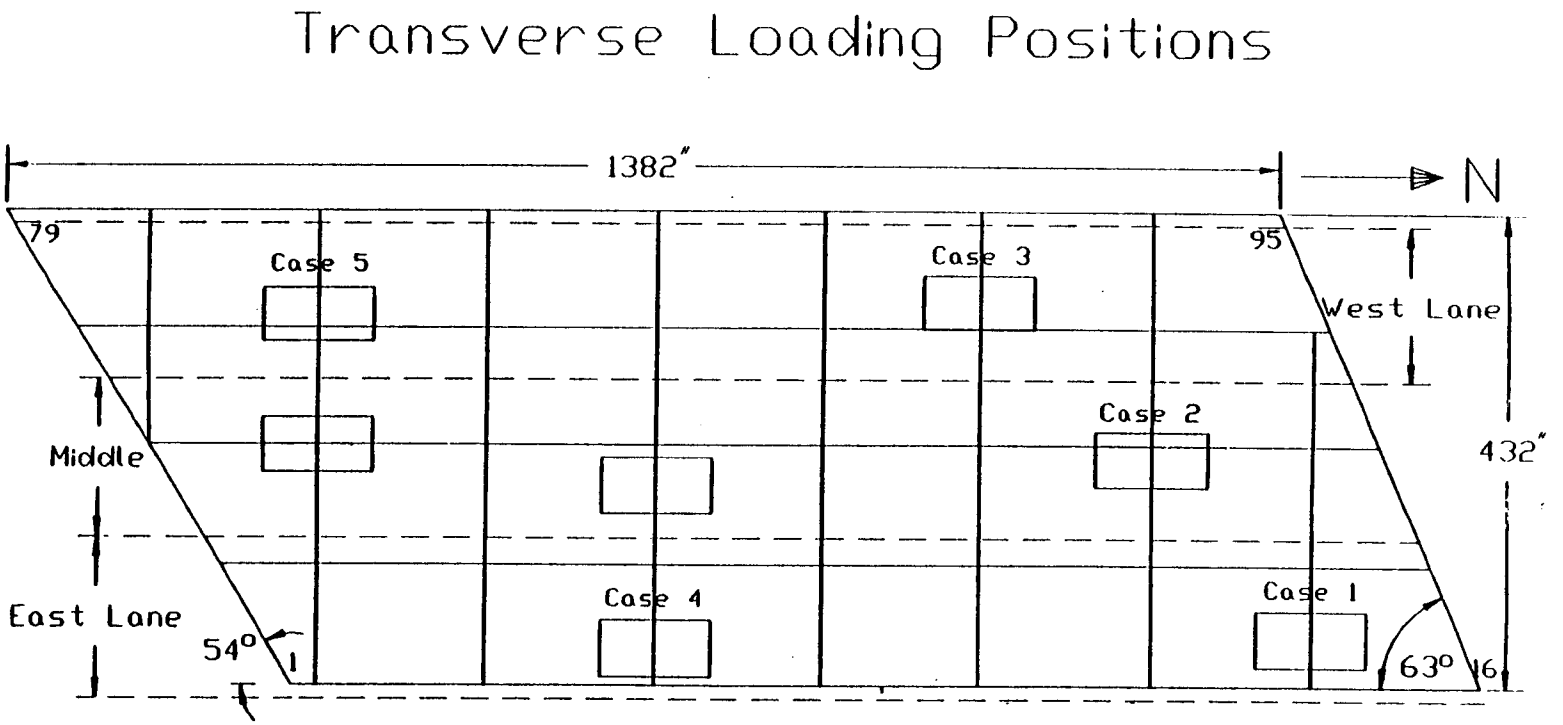

Figure 3.11 Transverse loading positions for the five loading cases

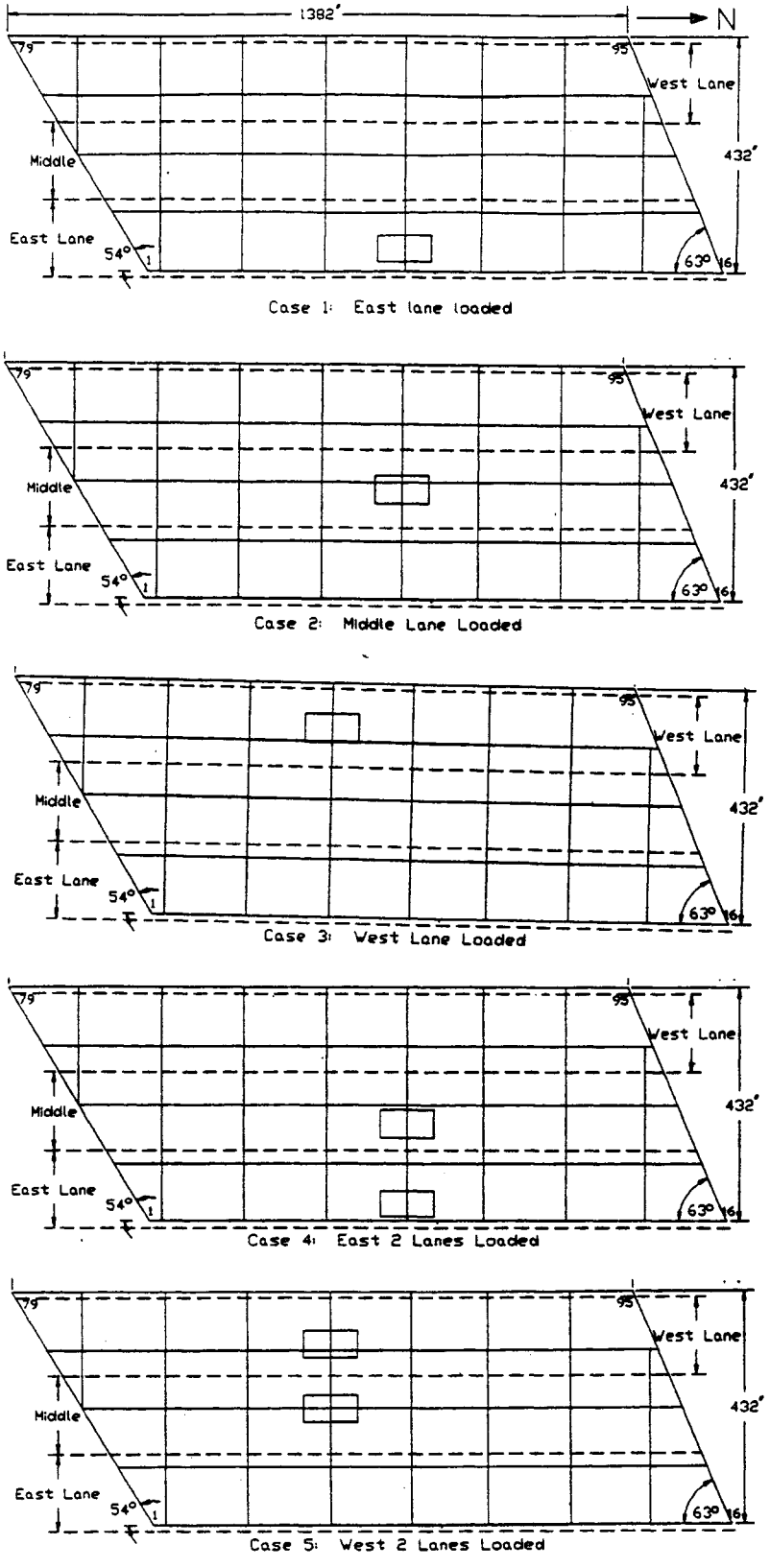

Figure 3.12 Midspan loading positions

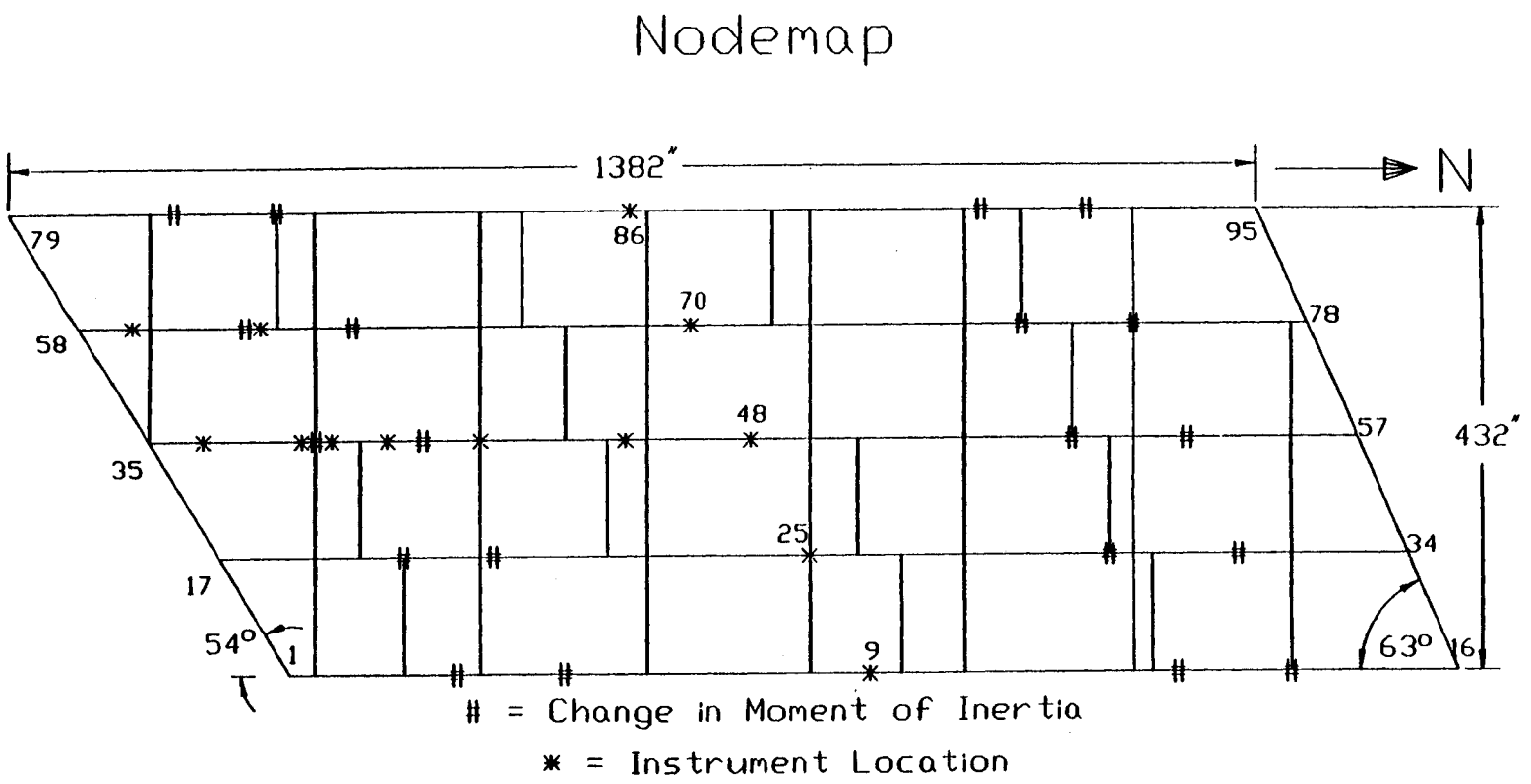

Figure 3.13 Nodemap for analytical grid model

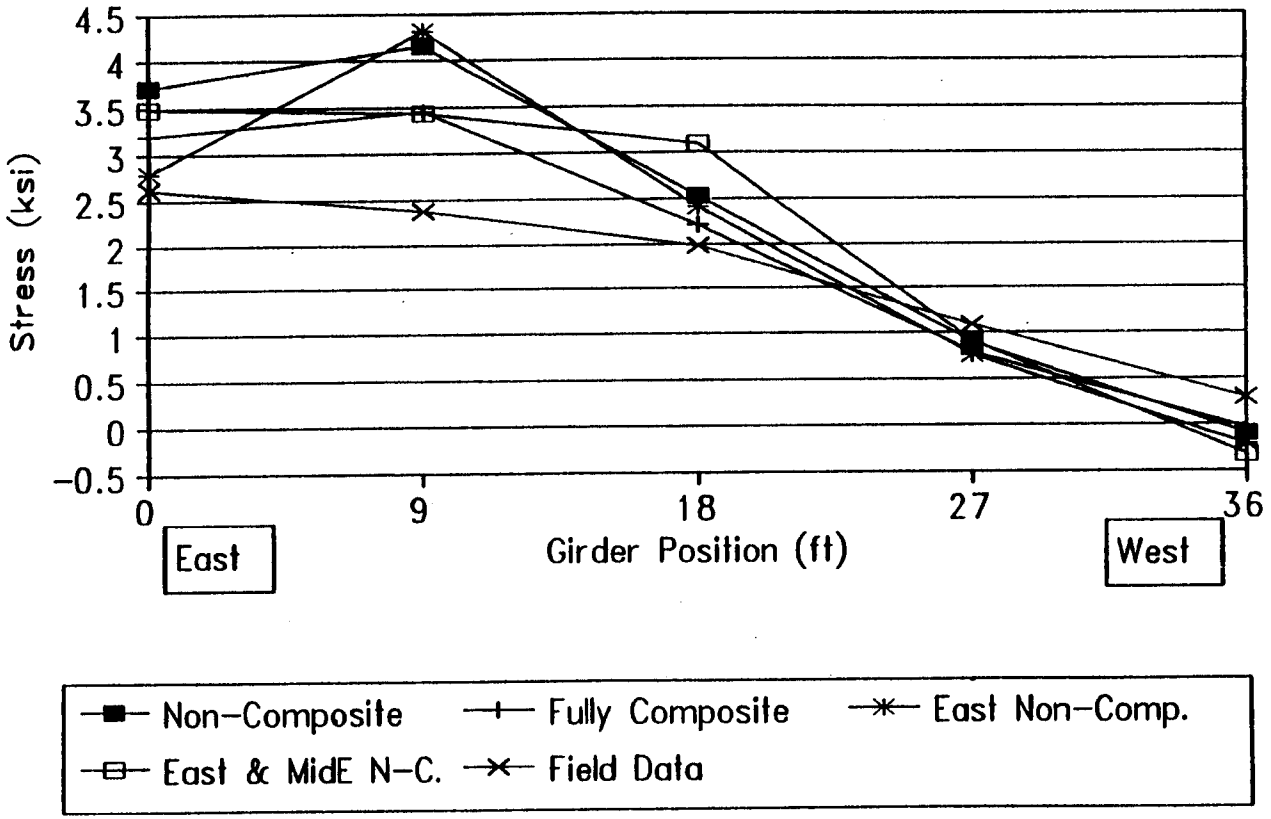

Figure 3.14 Transverse stress distributions comparing different levels of composite action

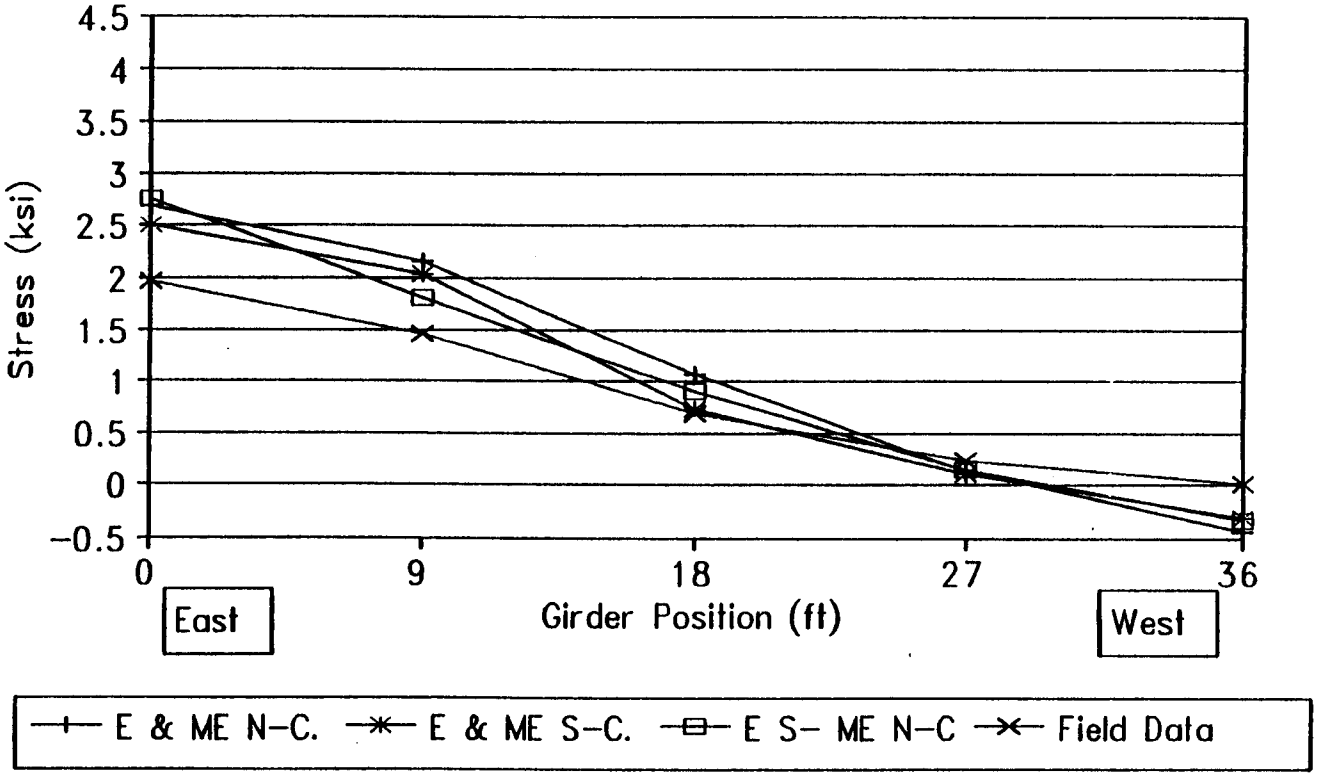

Figure 3.15 Middle girder stress distribution comparing the best three analytical models (east lane loaded)

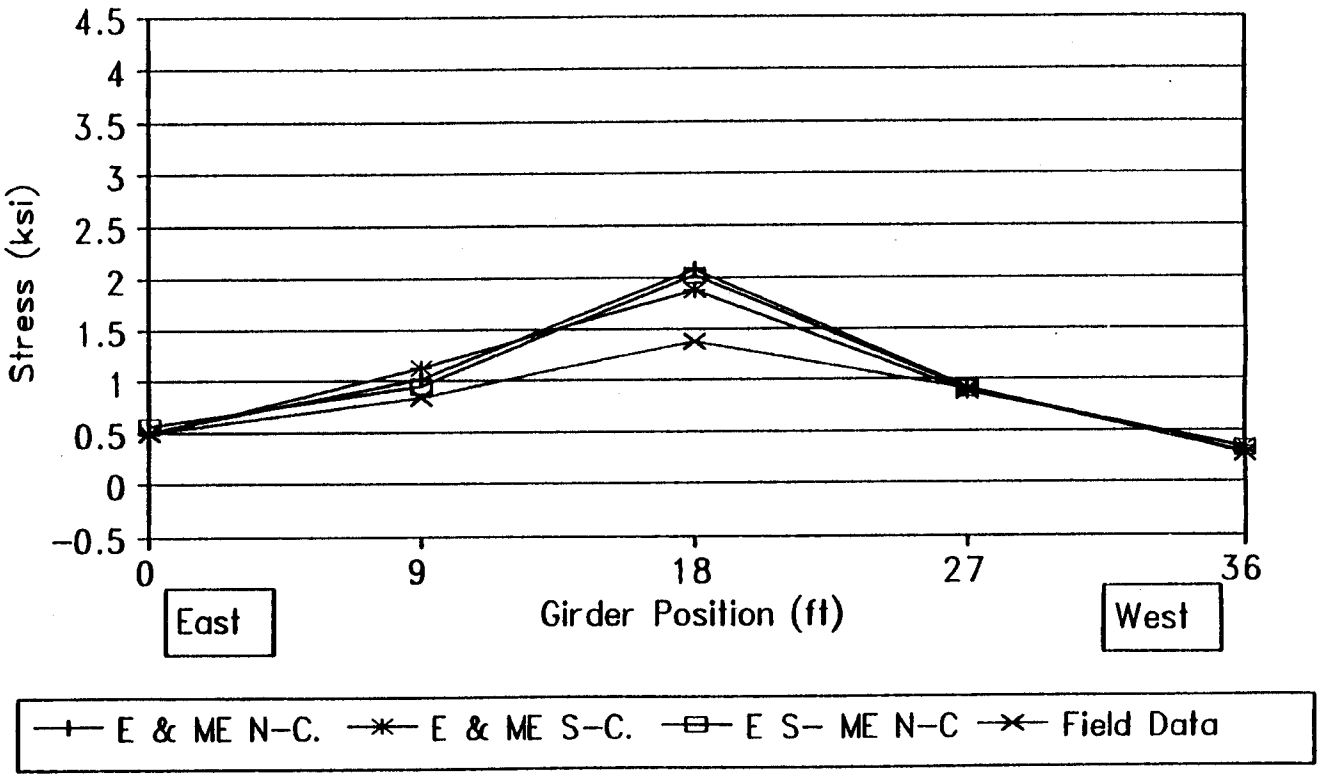

Figure 3.16 Middle girder stress distribution comparing the best three analytical models (middle lane loaded)

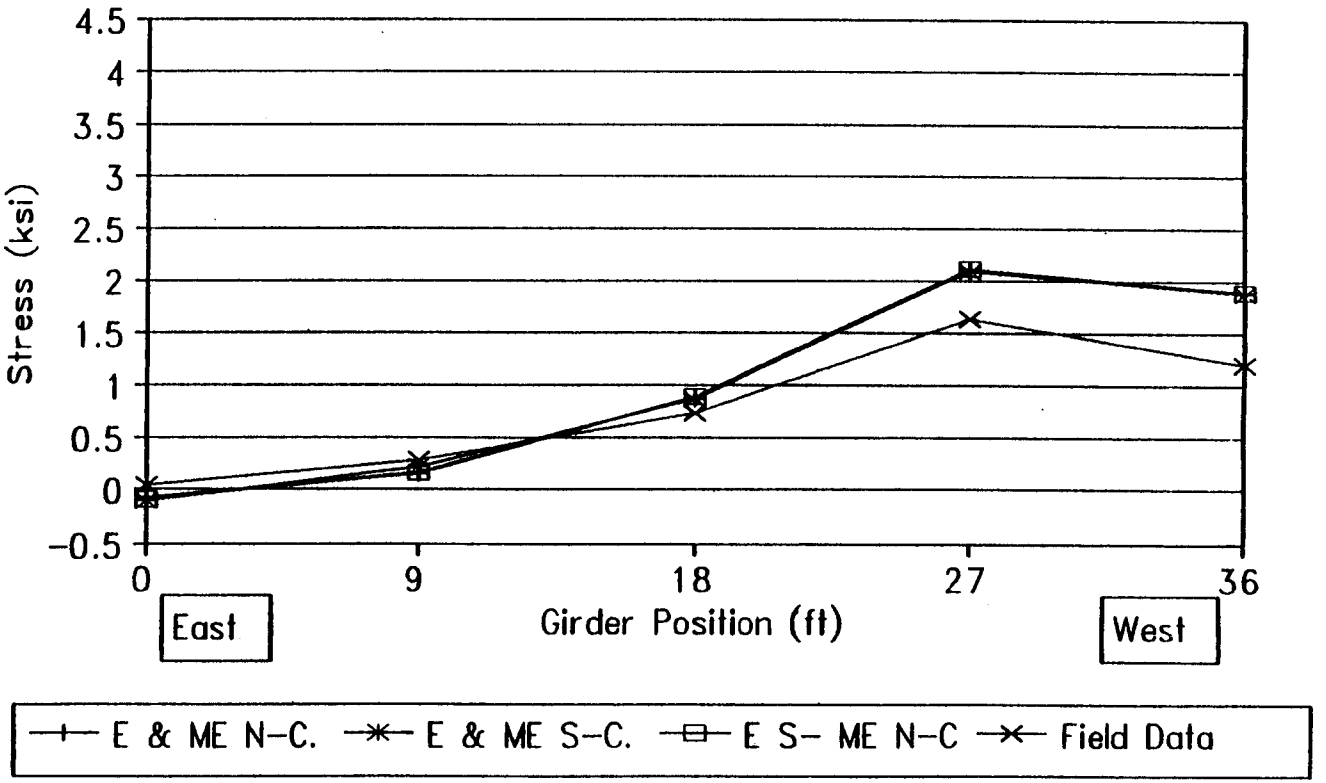

Figure 3.17 Middle girder stress distribution comparing the best three analytical models (west lane loaded)

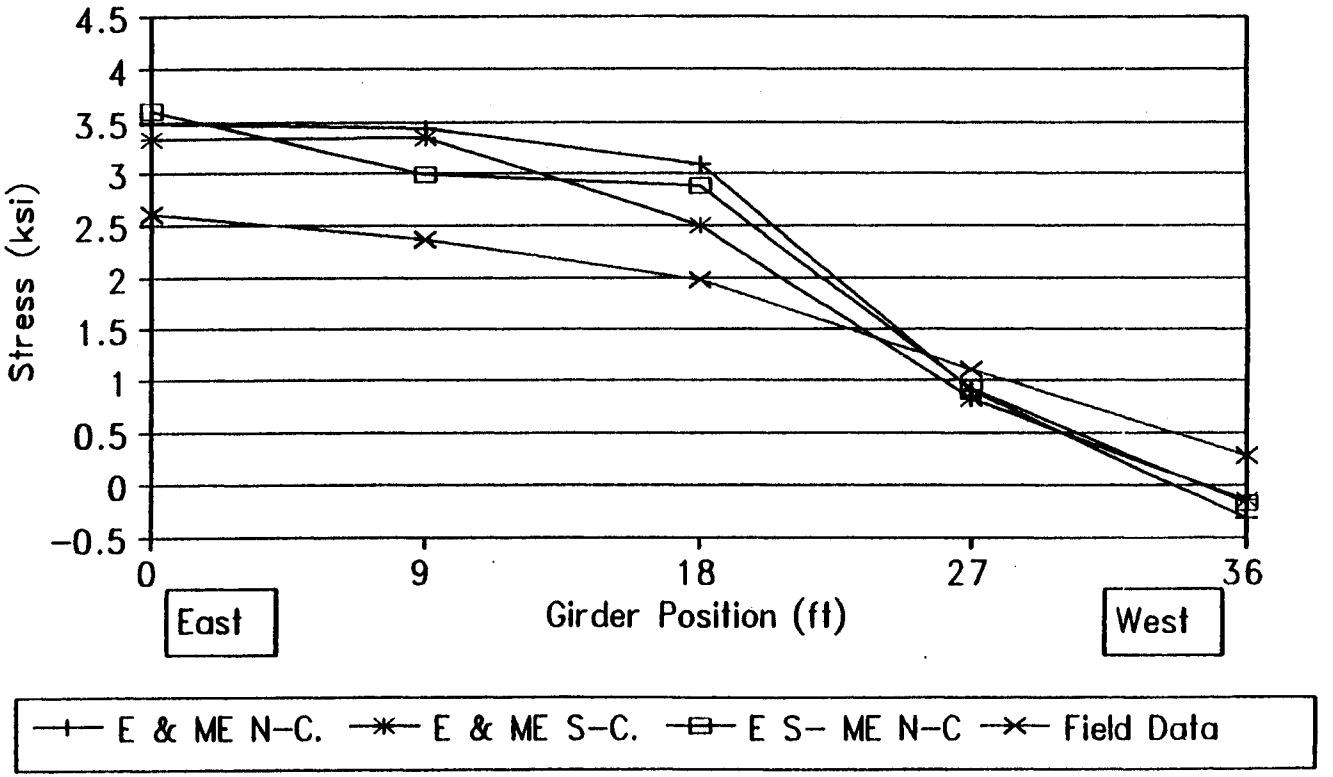

Figure 3.18 Middle girder stress distribution comparing the best three analytical models (east 2 lanes loaded)

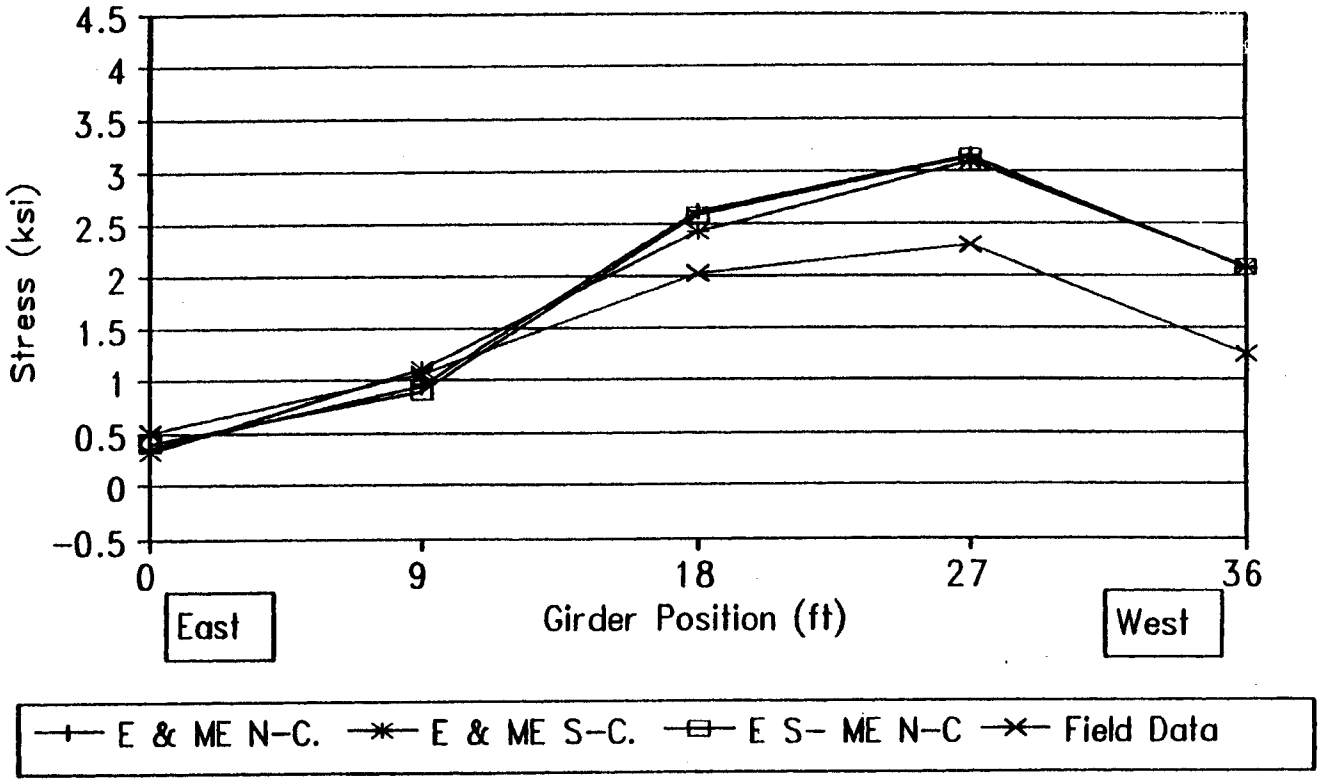

Figure 3.19 Middle girder stress distribution comparing the best three analytical models (west 2 lanes loaded)

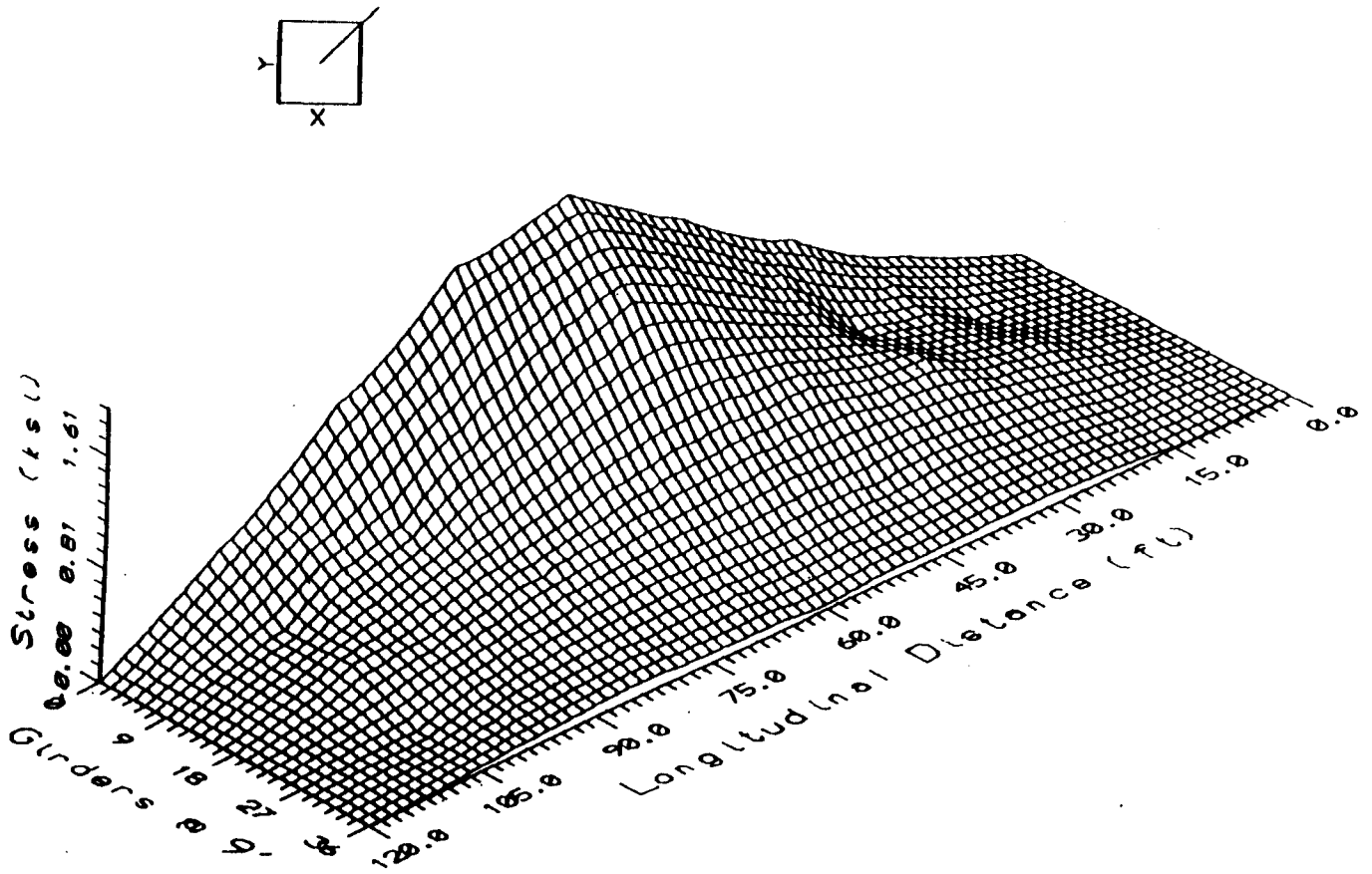

Figure 3.20 Influence surface of field stresses viewed north to south (east lane loaded)

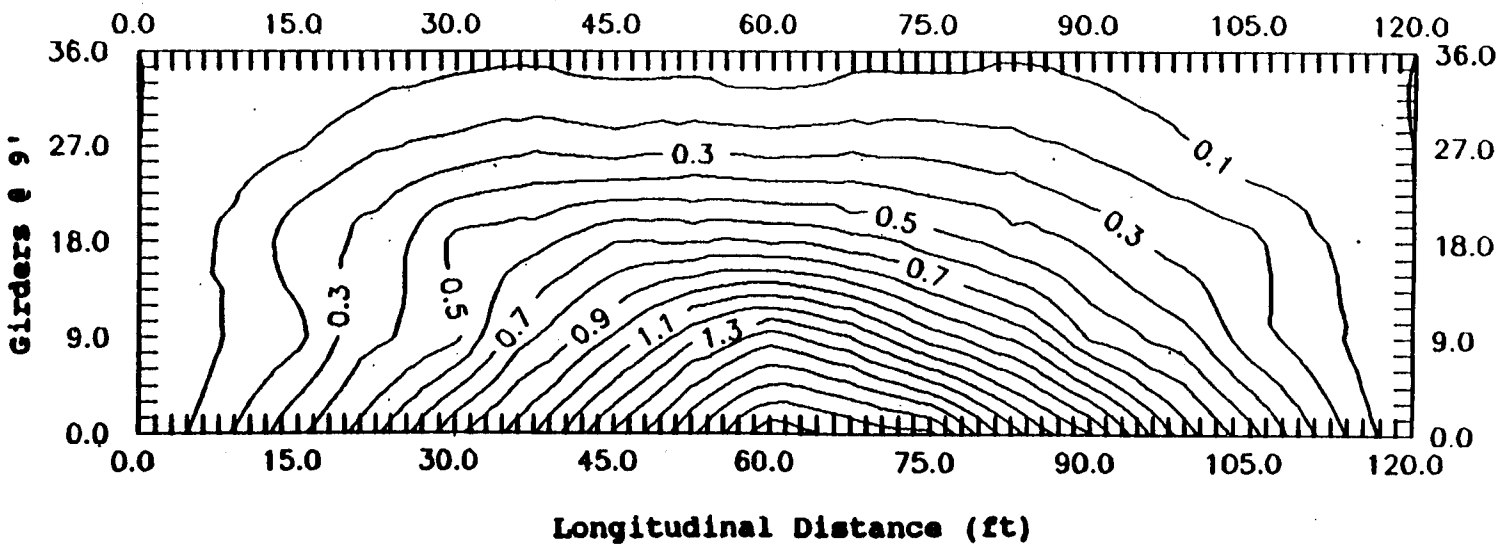

Figure 3.21 Topographic view of field stress influence surface

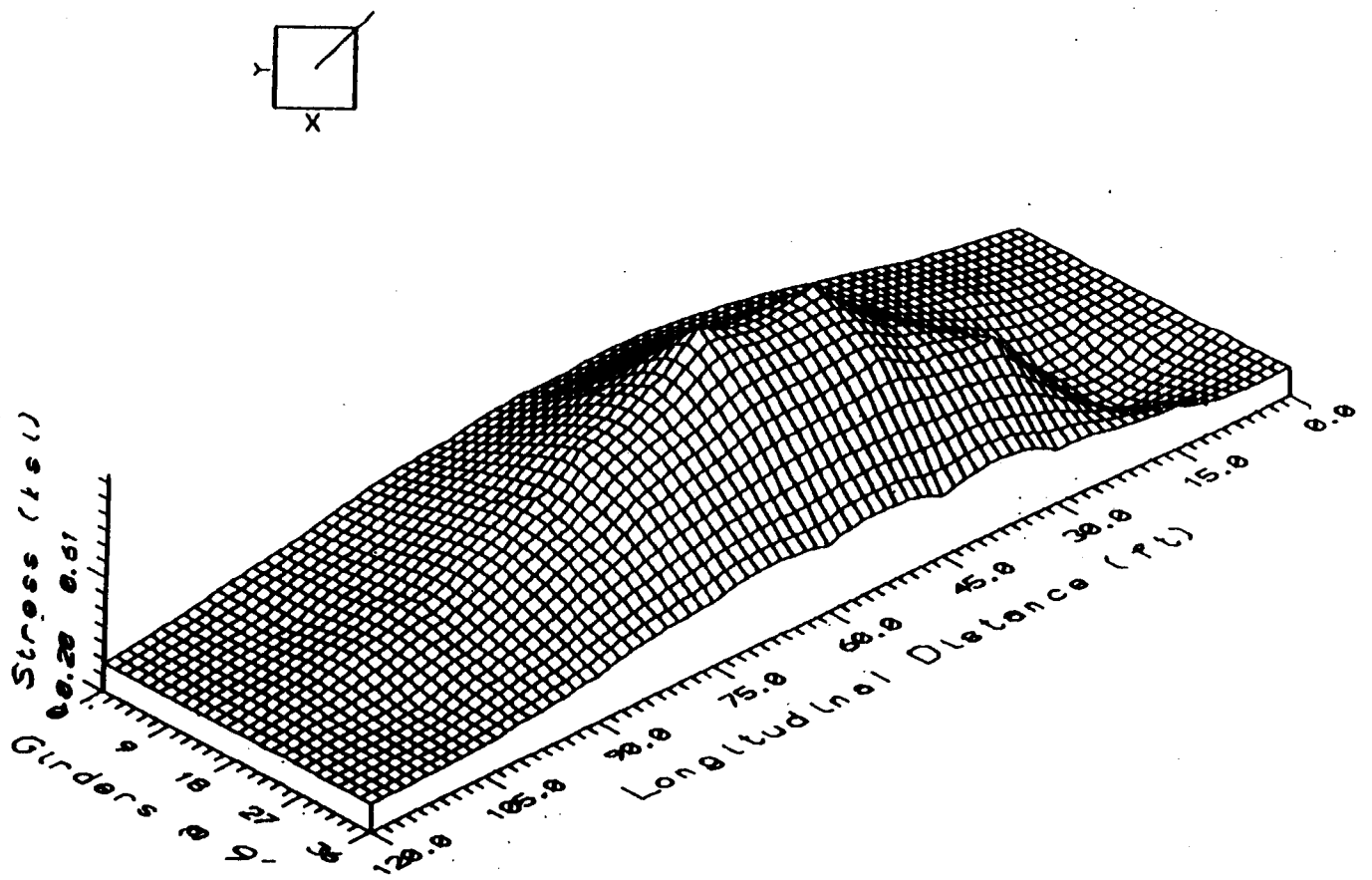

Figure 3.22 Influence surface of field stresses viewed north to south (middle lane loaded)

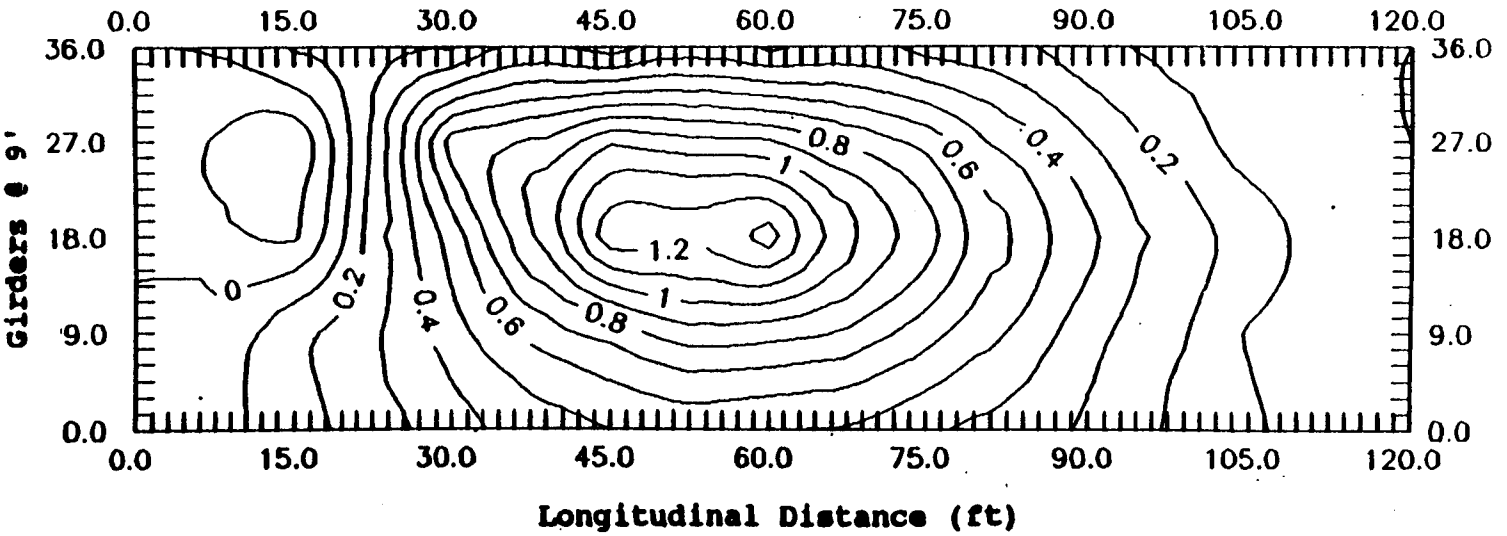

Figure 3.23 Topographic view of field stress influence surface

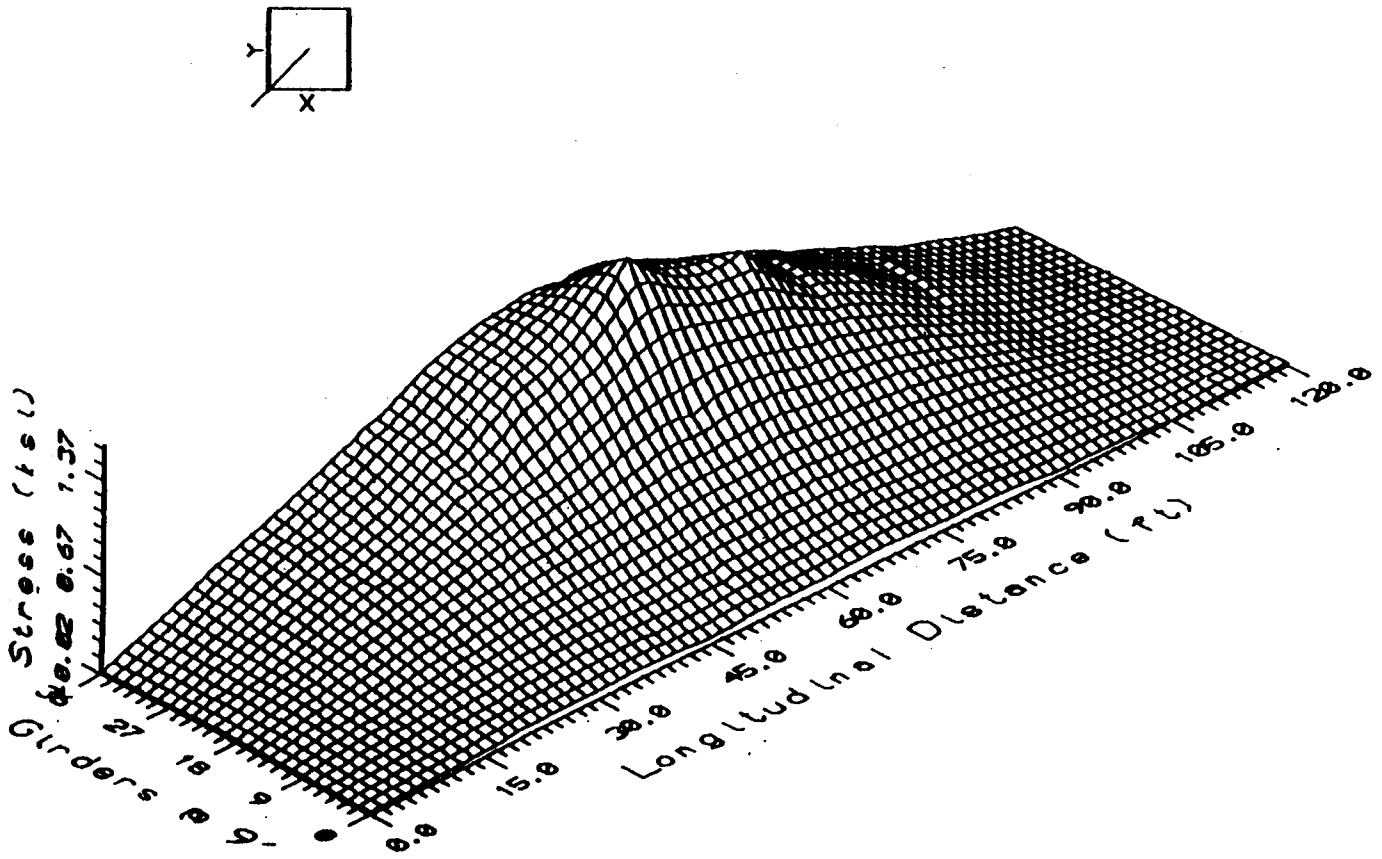

Figure 3.24 Influence surface of field stresses viewed south to north (west lane loaded)

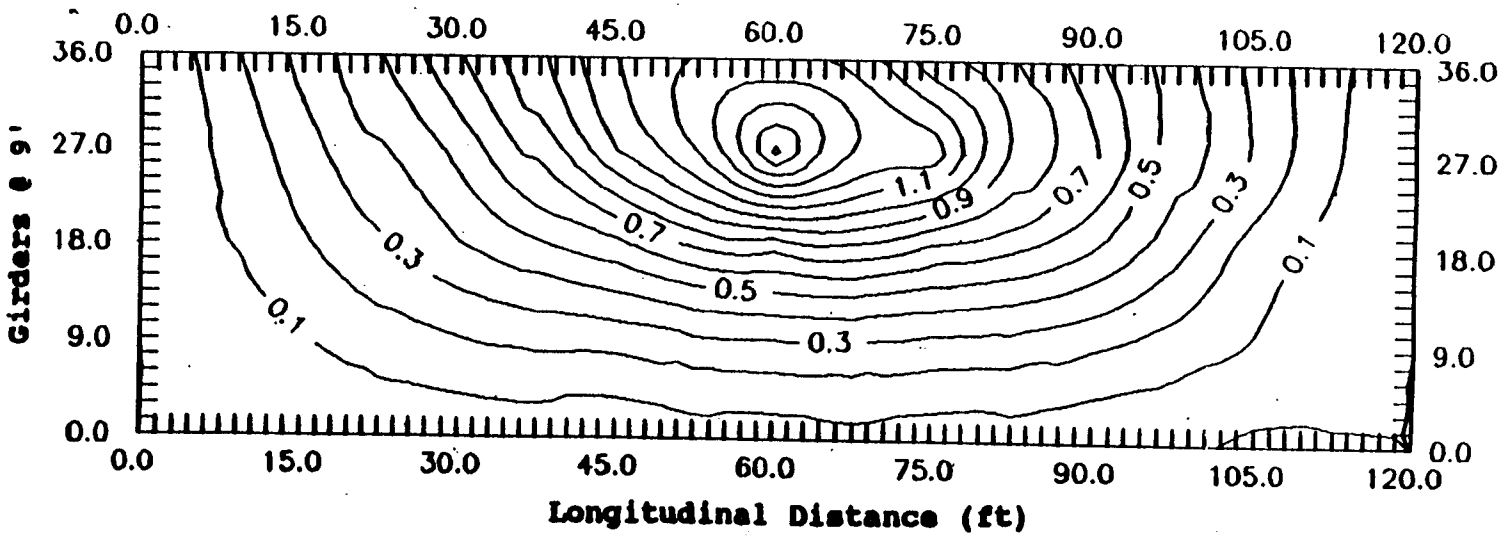

Figure 3.25 Topographic view of field stress influence surface

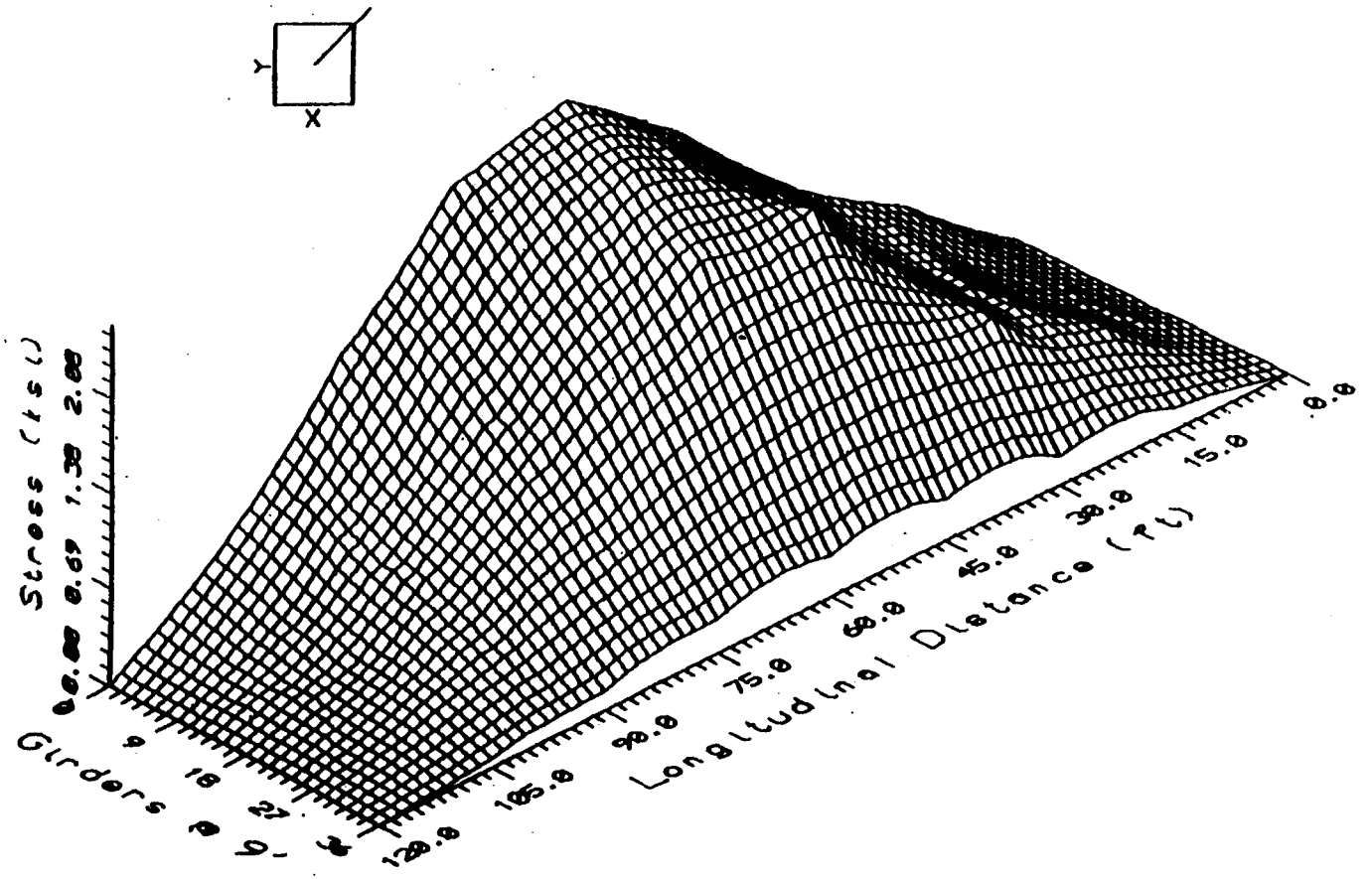

Figure 3.26 Influence surface of field stresses viewed north to south (east 2 lanes loaded)

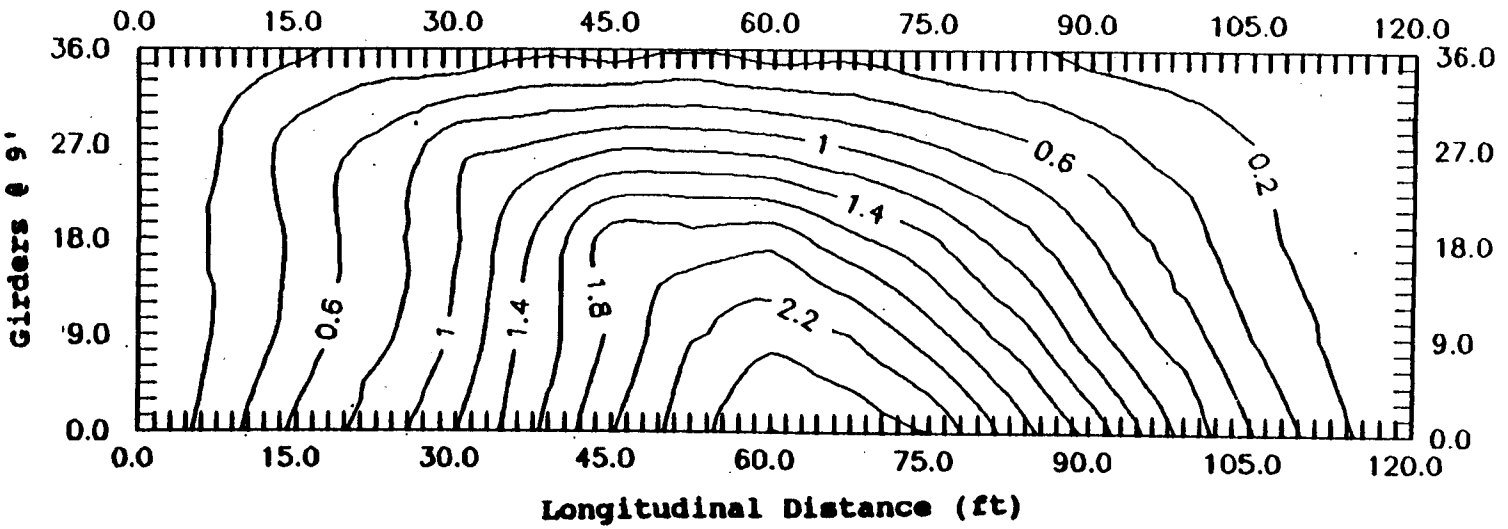

Figure 3.27 Topographic view of field stress influence surface

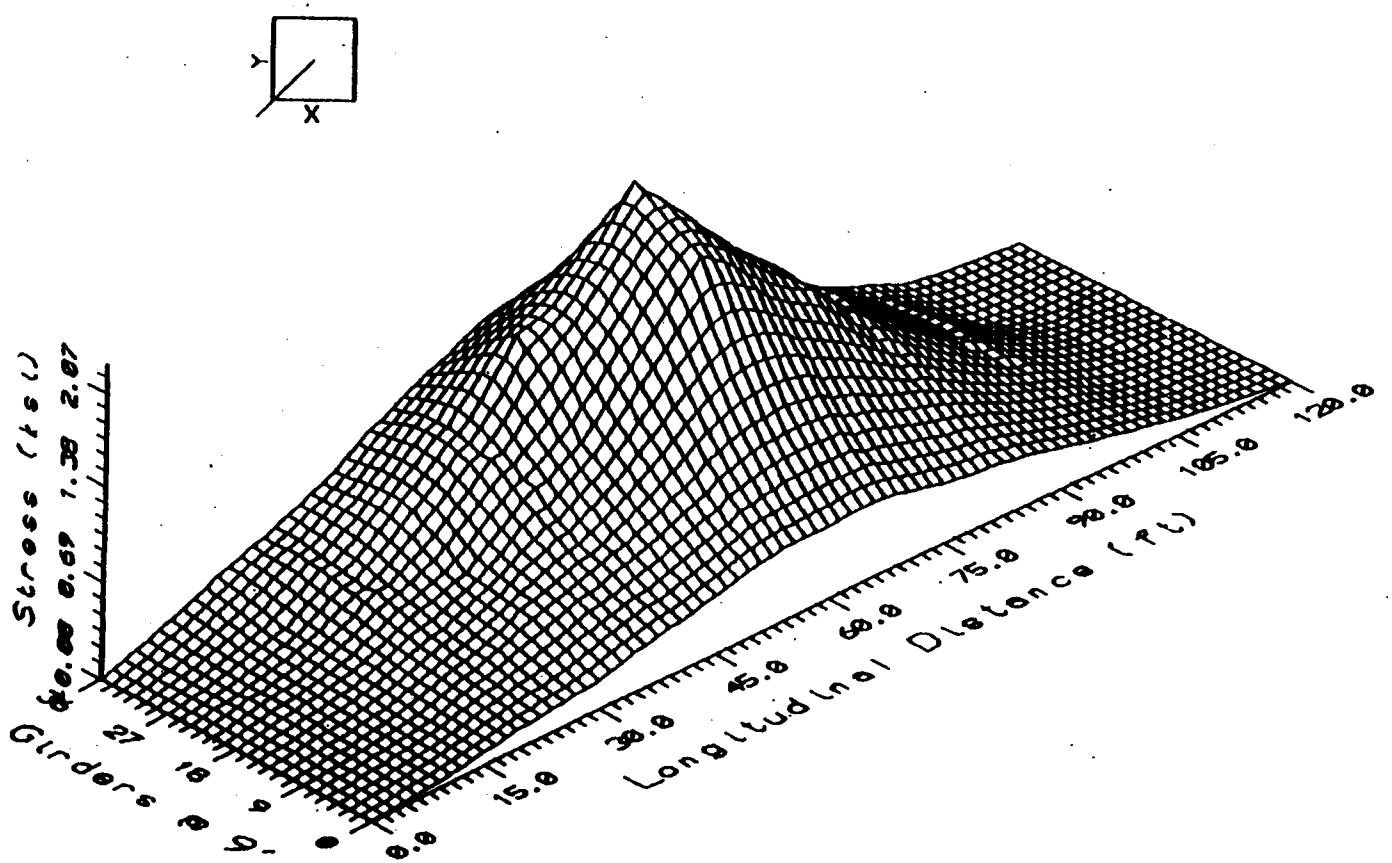

Figure 3.28 Influence surface of field stresses viewed south to north (west 2 lanes loaded)

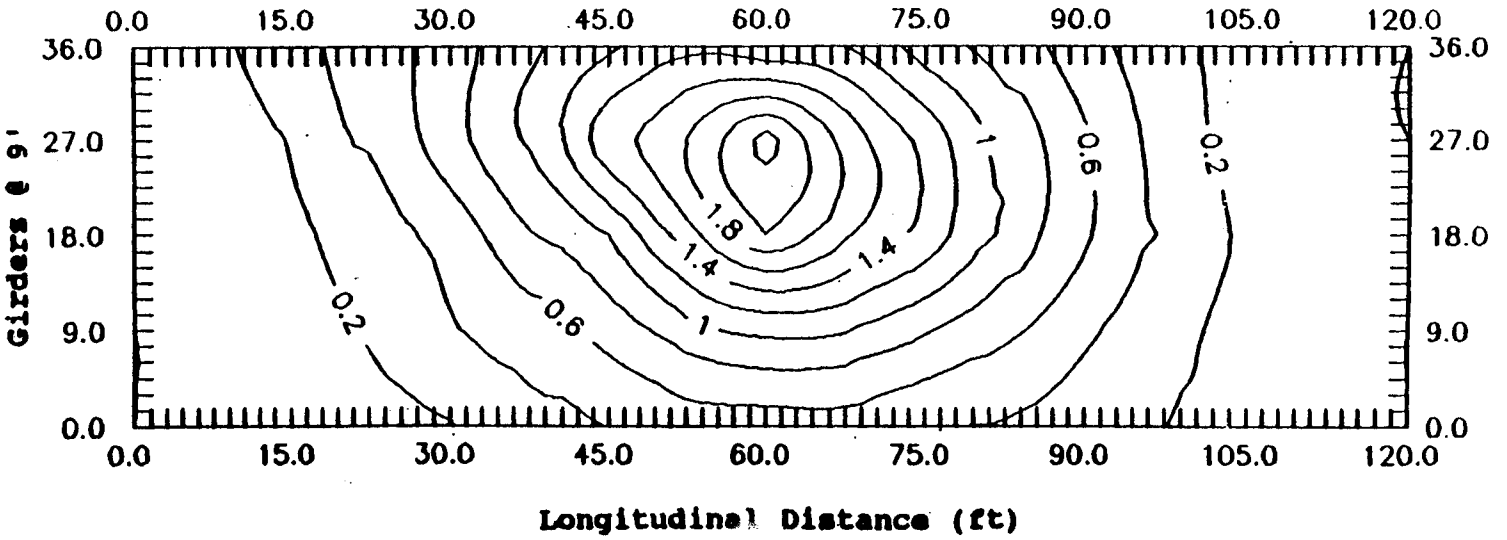

Figure 3.29 Topographic view of field stress influence surface

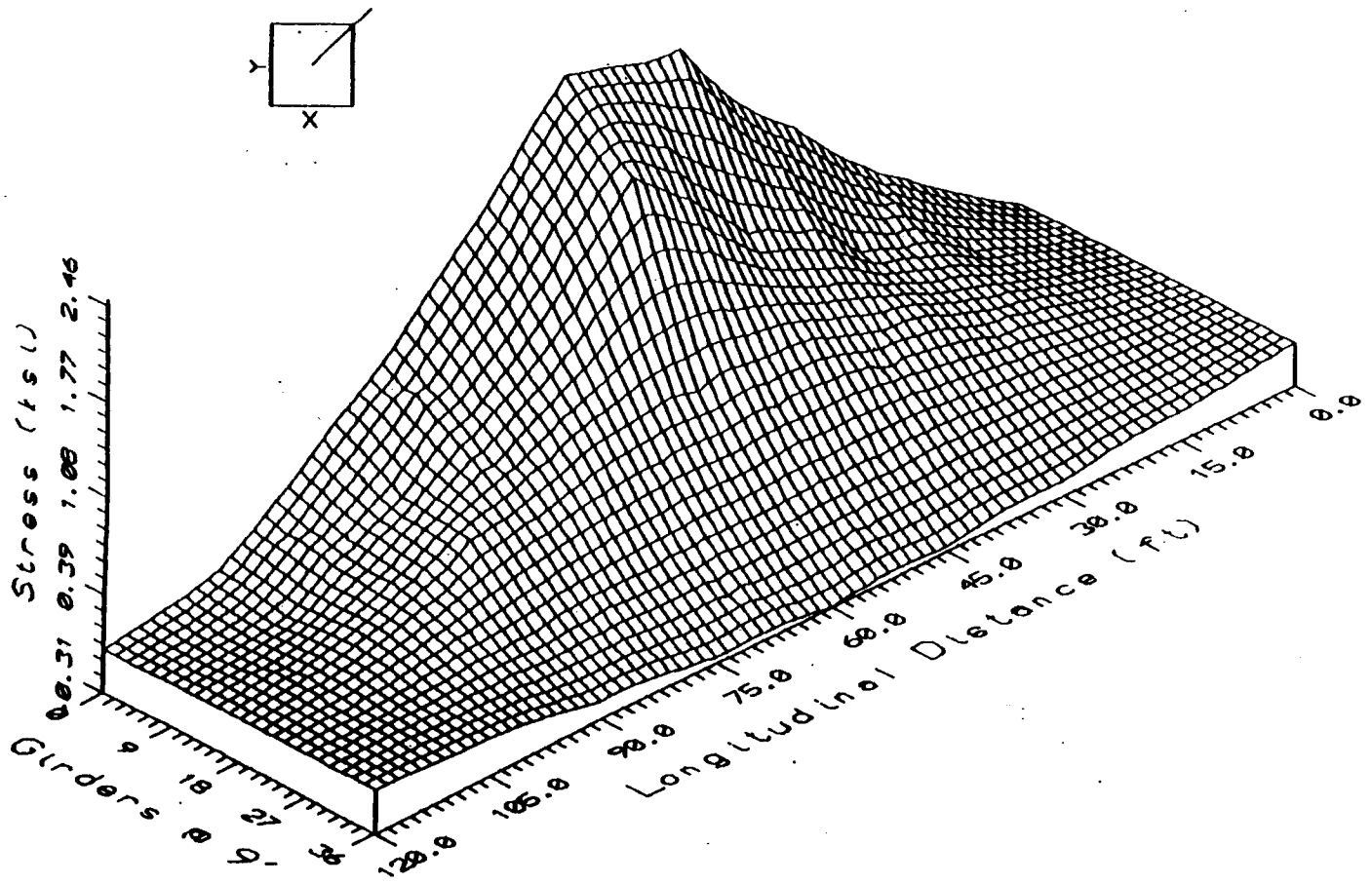

Figure 3.30 Influence surface of analytical stresses viewed north to south (east lane loaded)

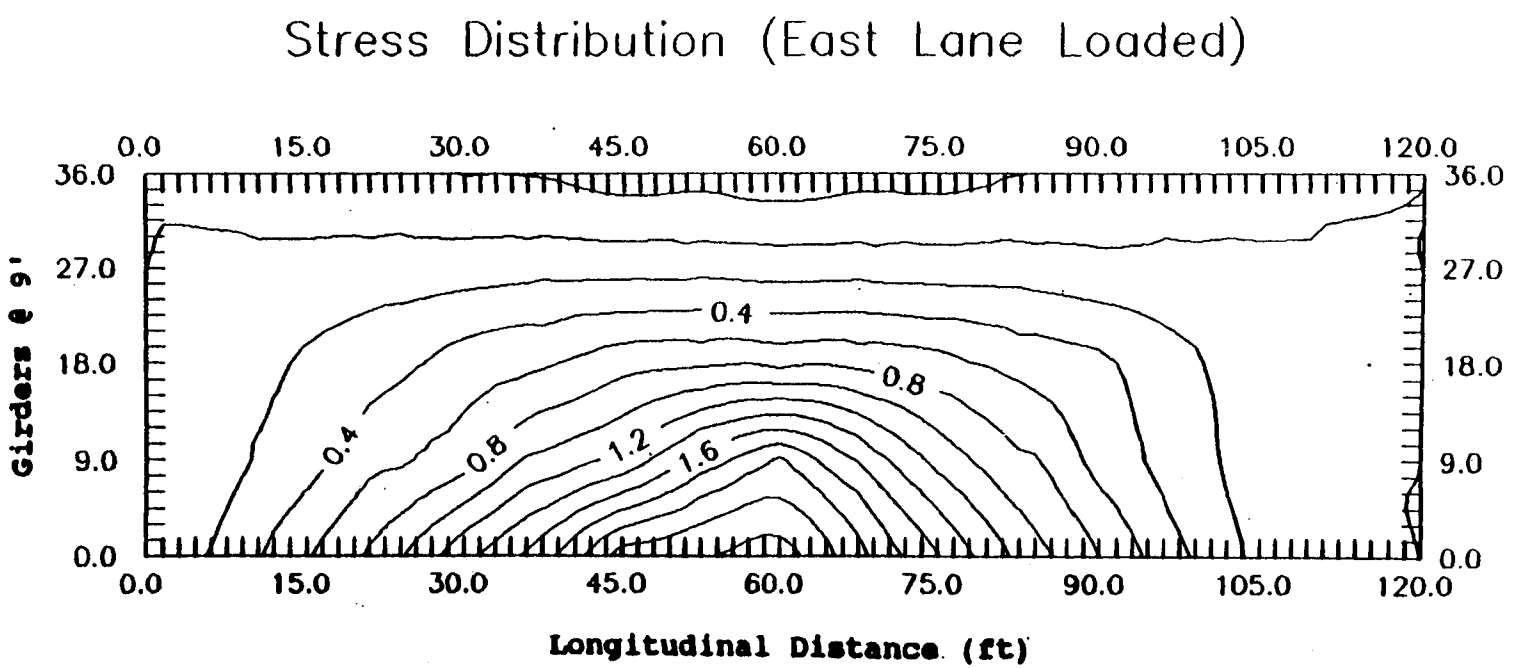

Figure 3.31 Topographic view of field stress influence surface

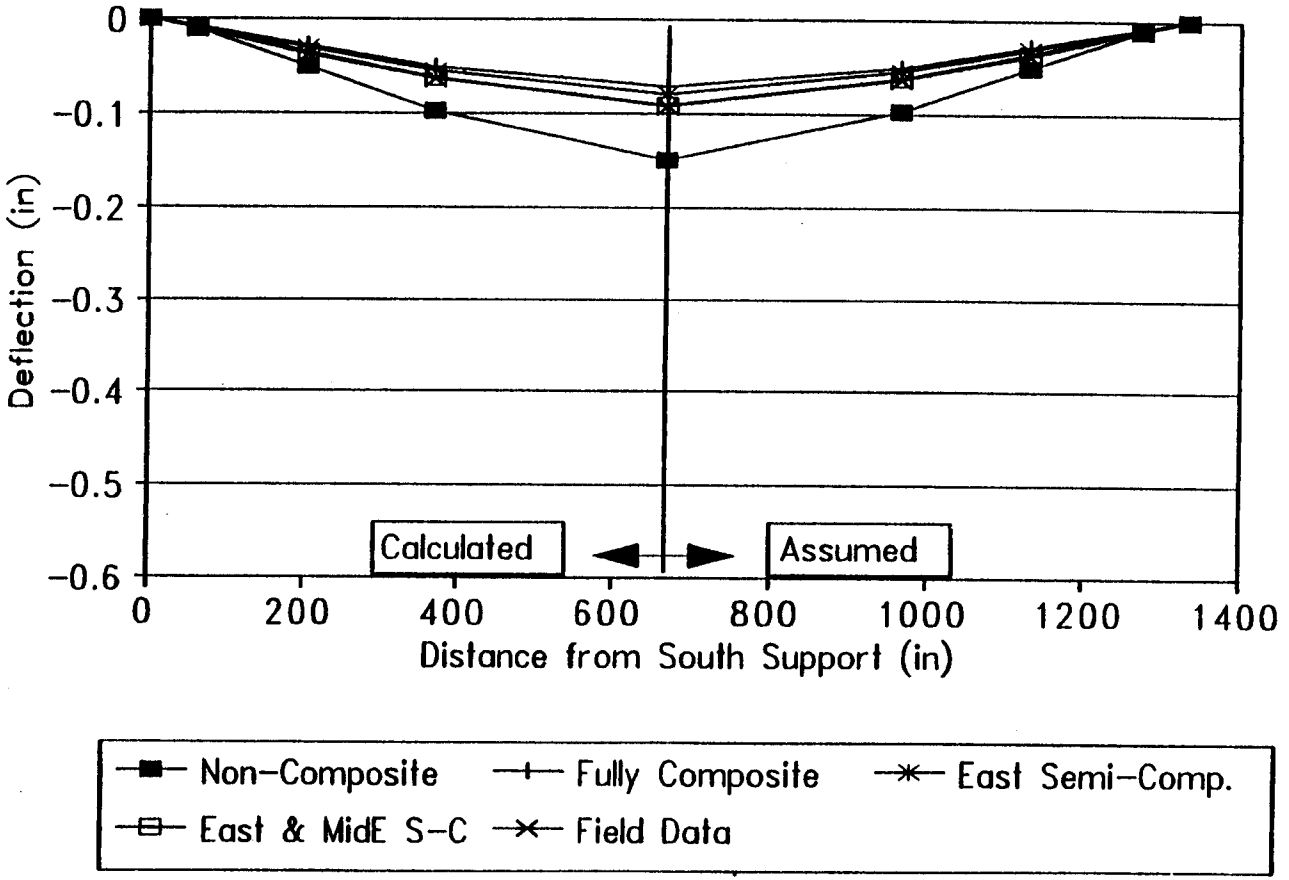

Figure 3.32 Middle girder deflection curves comparing the best three analytical models (east lane loaded)

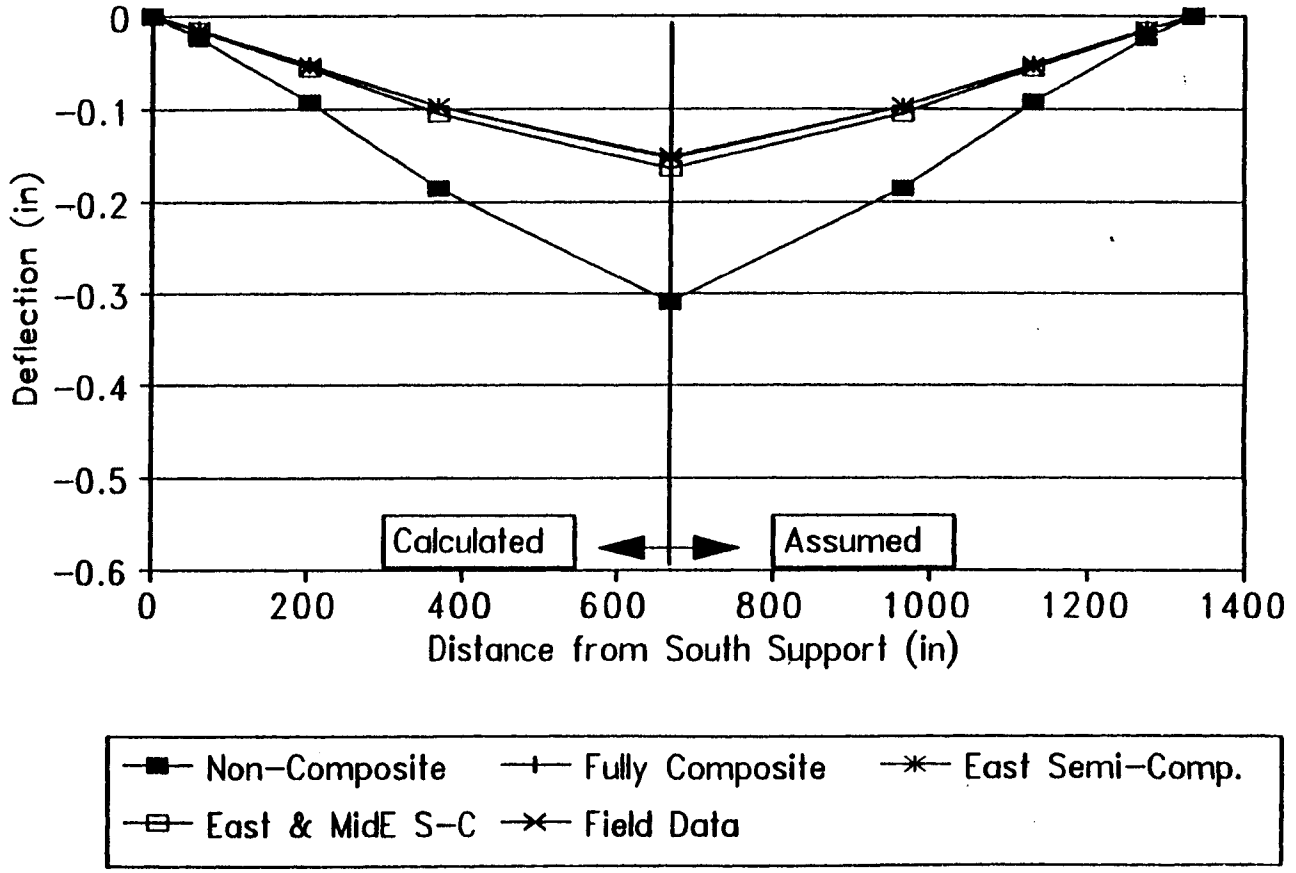

Figure 3.33 Middle girder deflection curves comparing the best three analytical models (middle lane loaded)

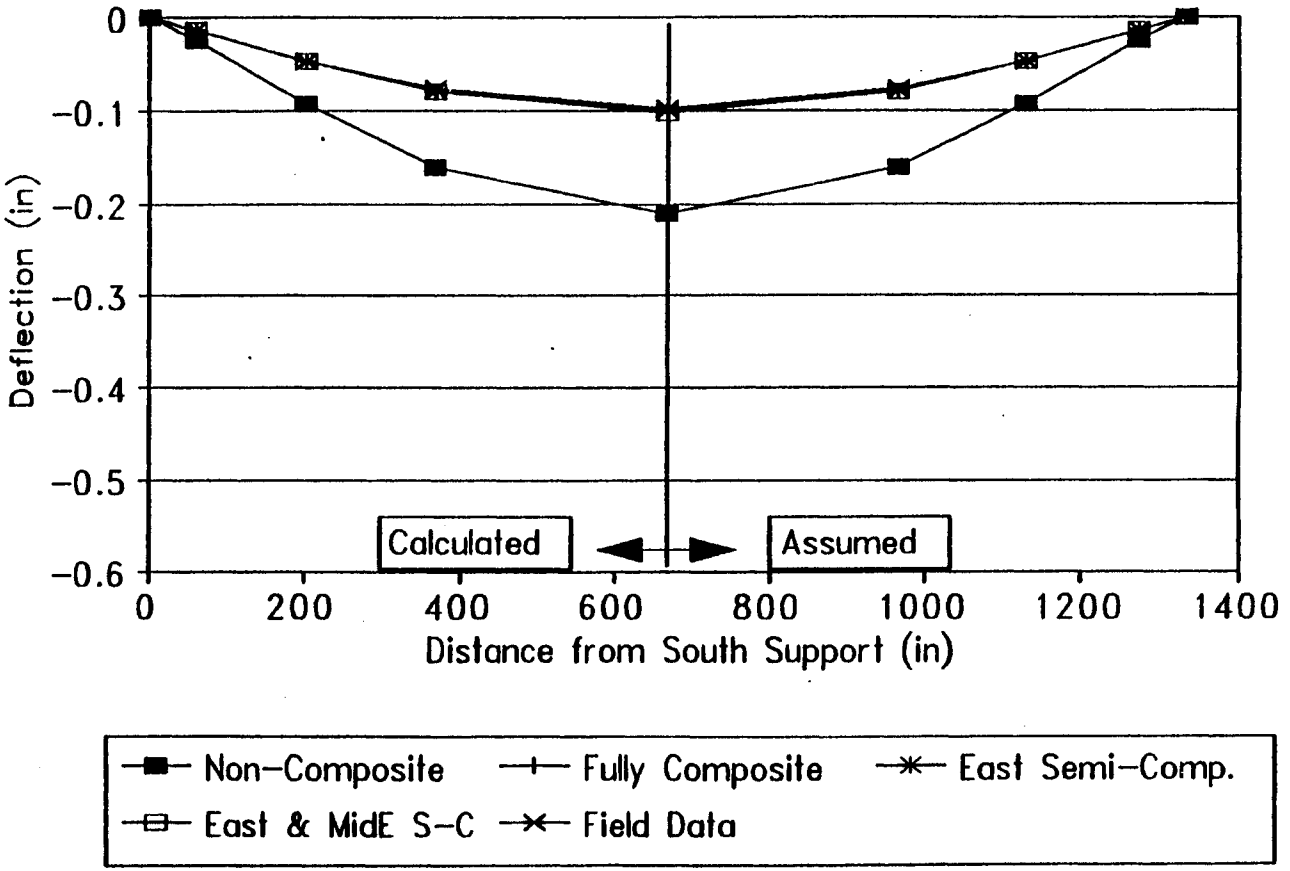

Figure 3.34 Middle girder deflection curves comparing the best three analytical models (west lane loaded)

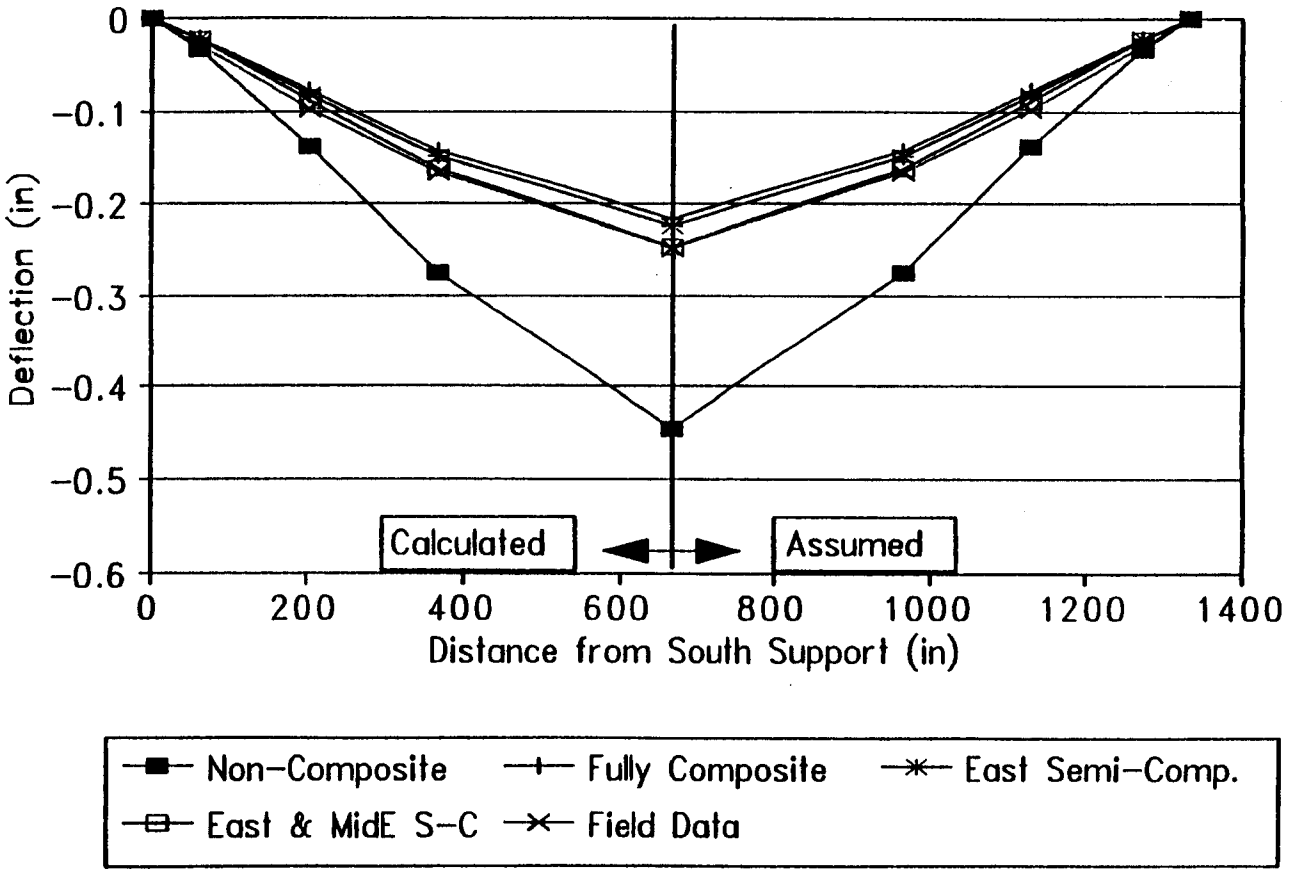

Figure 3.35 Middle girder deflection curves comparing the best three analytical models (east 2 lanes loaded)

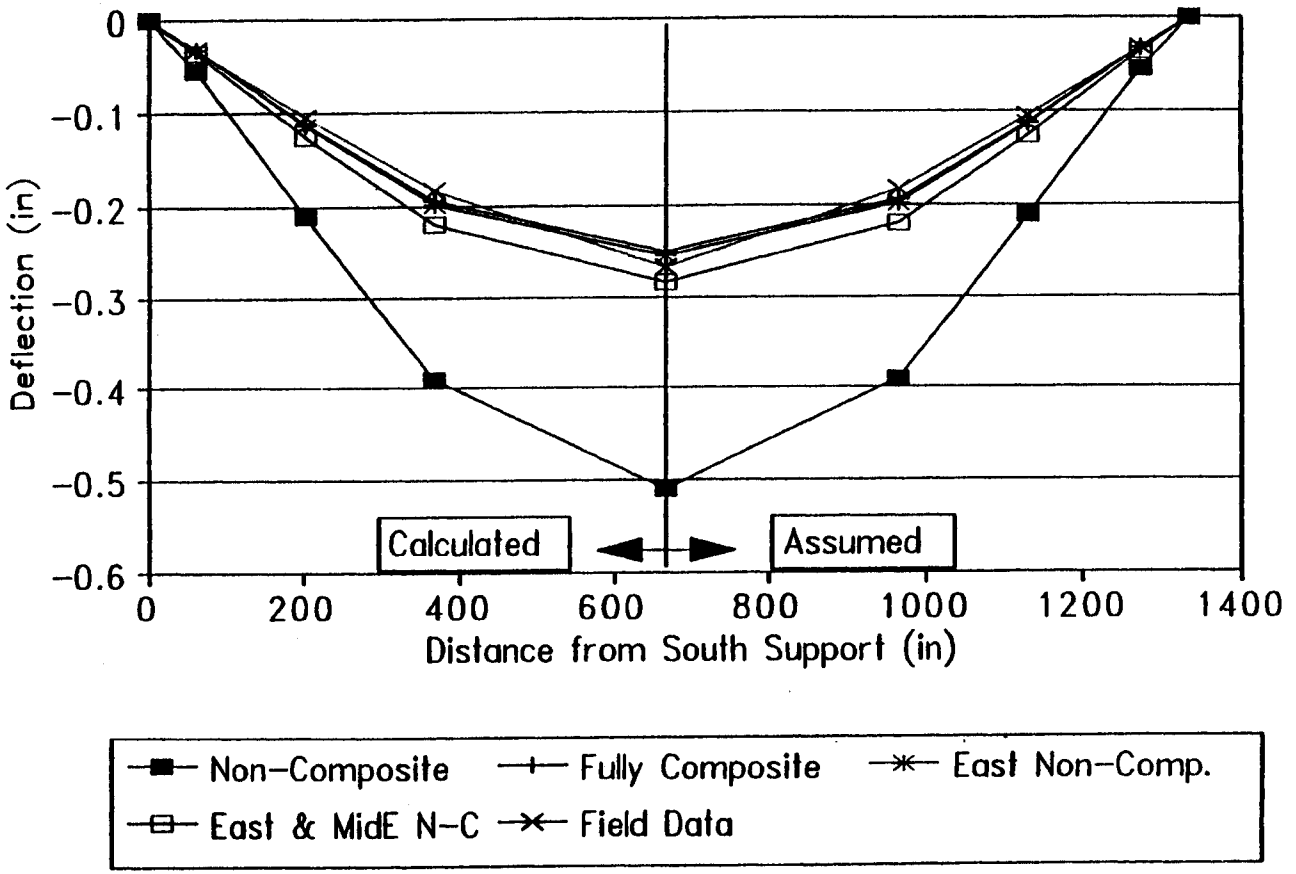

Figure 3.36 Middle girder deflection curves comparing the best three analytical models (west 2 lanes loaded)

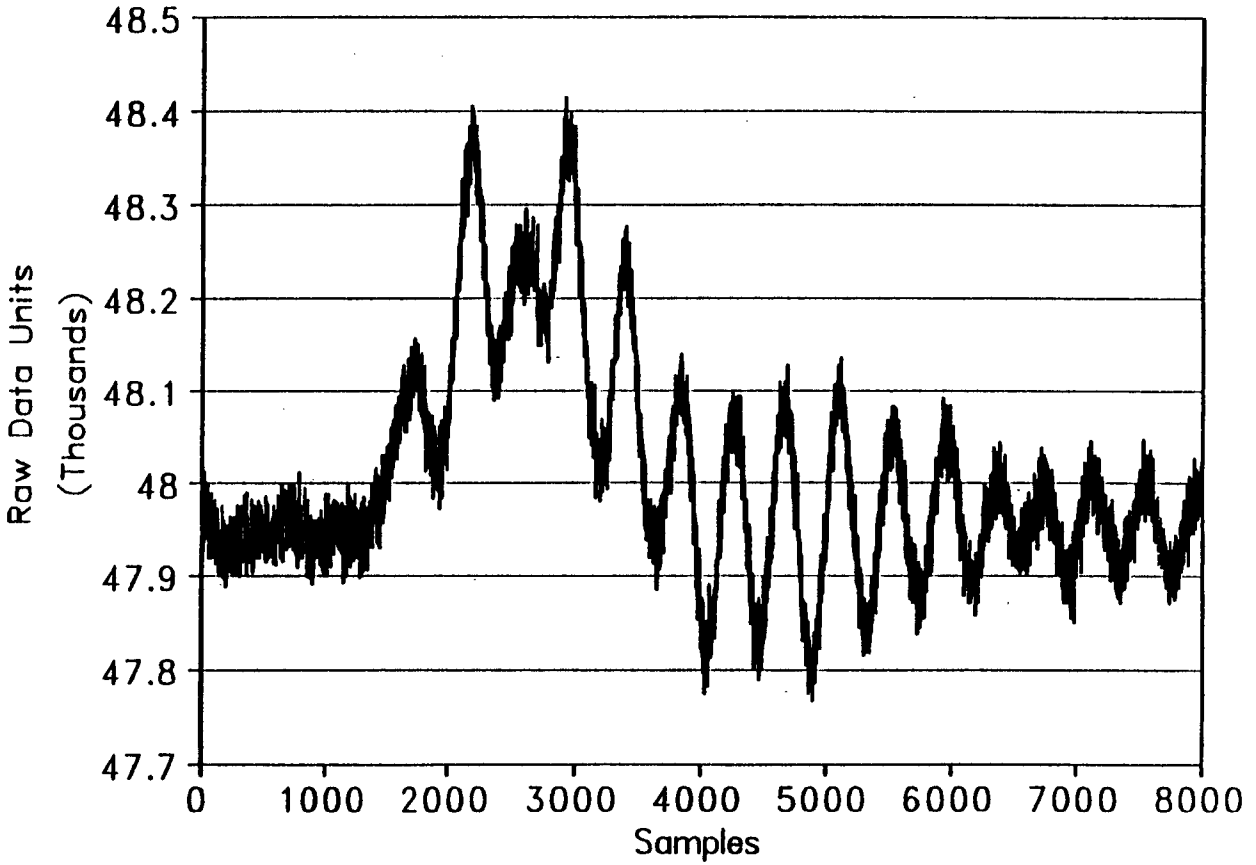

Figure 3.37 Dynamic response at midspan of east girder when west 2 lanes are loaded

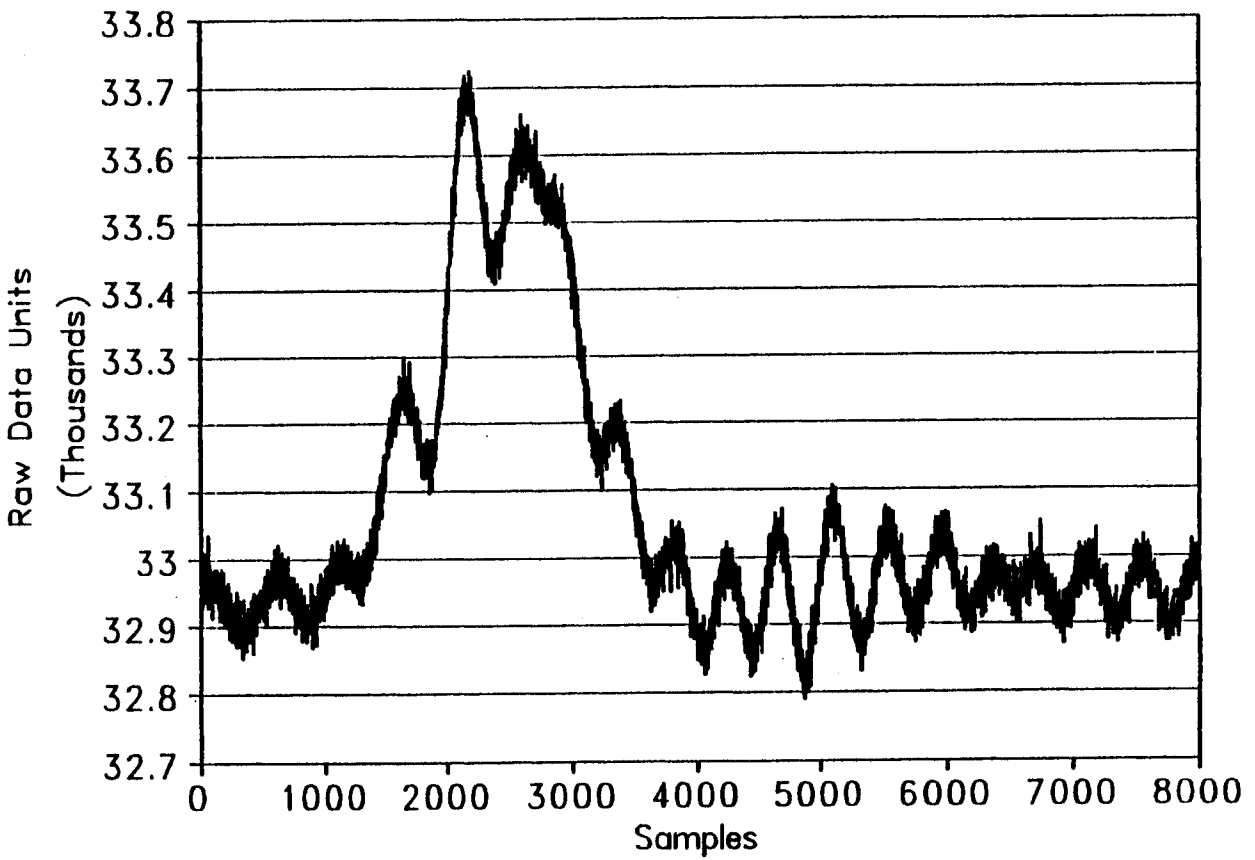

Figure 3.38 Dynamic response at midspan of middle east girder when west 2 lanes are loaded

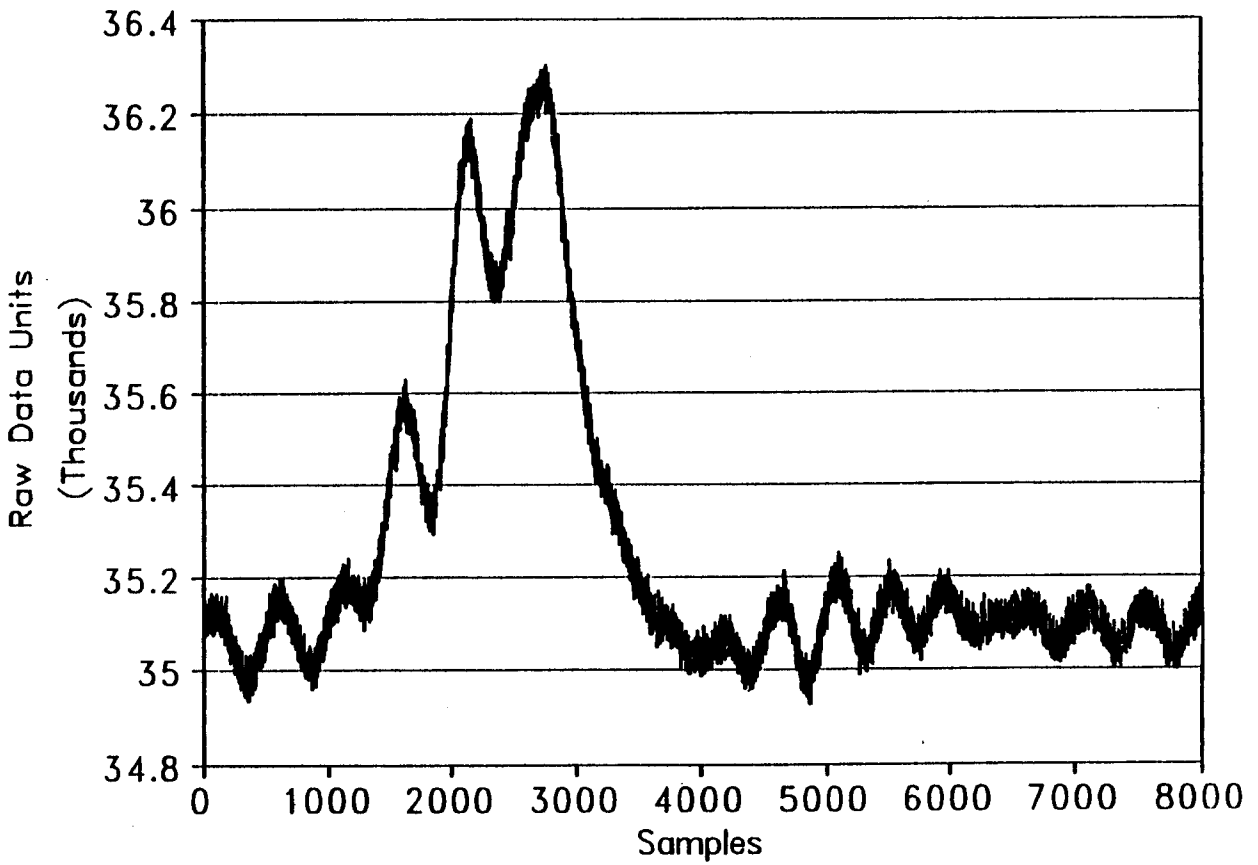

Figure 3.39 Dynamic response at midspan of middle girder when west 2 lanes are loaded

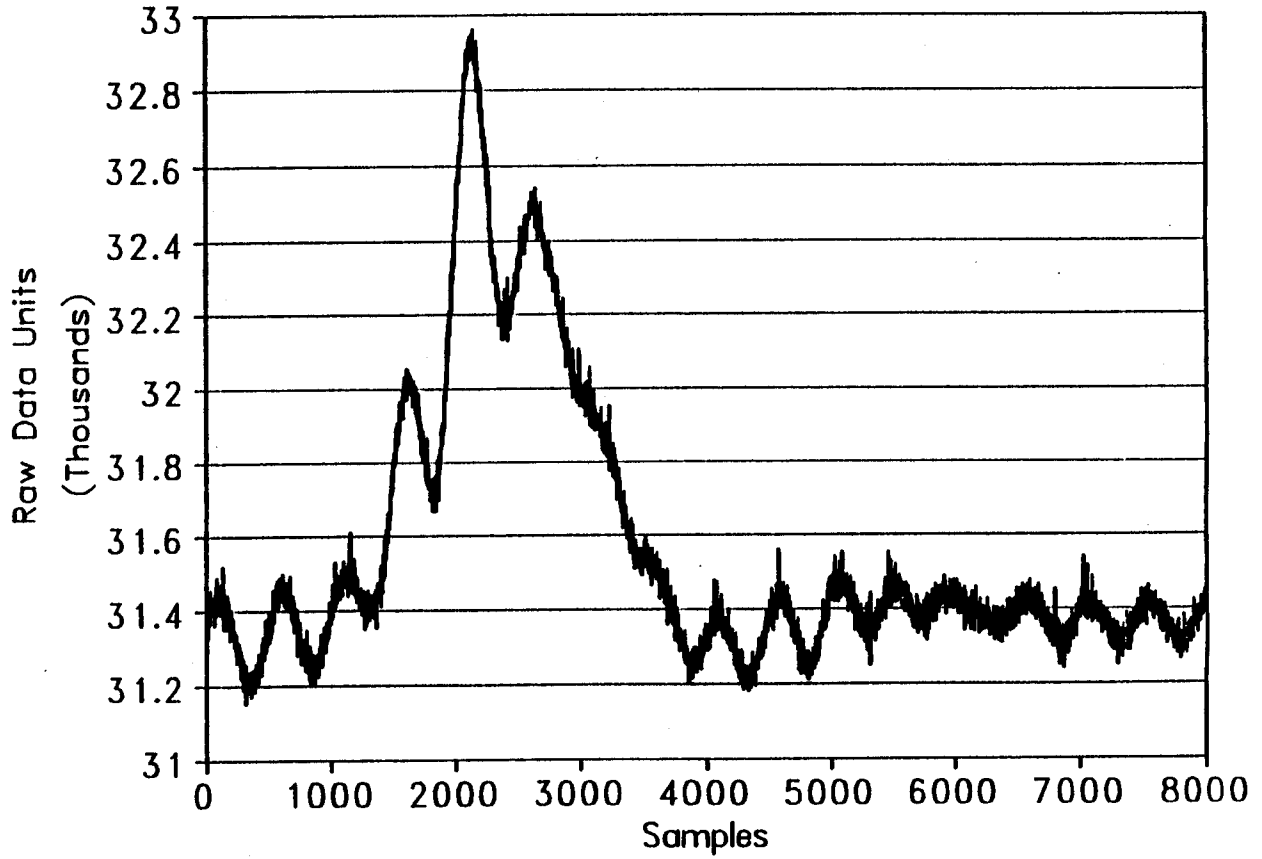

Figure 3.40 Dynamic response at midspan of middle west girder when west 2 lanes are loaded

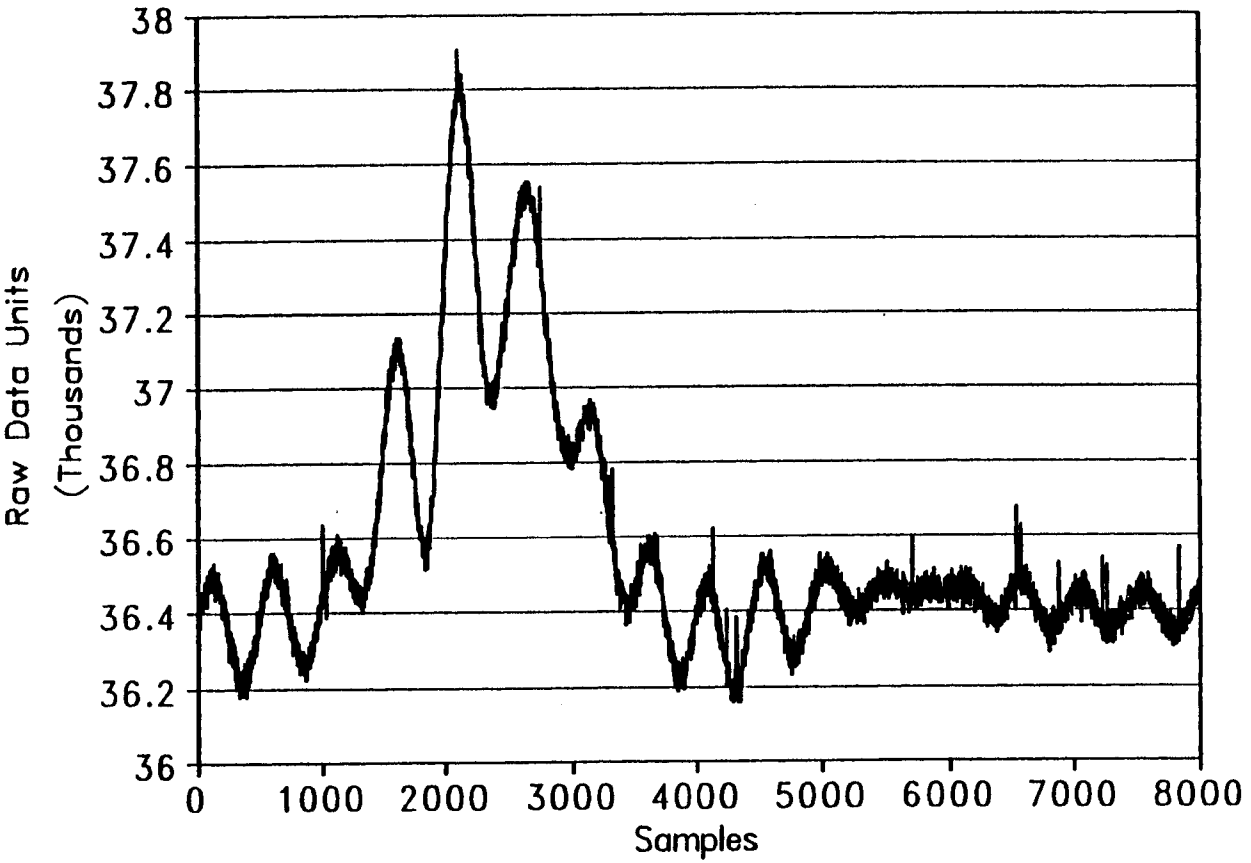

Figure 3.41 Dynamic response at midspan of west girder when west 2 lanes are loaded

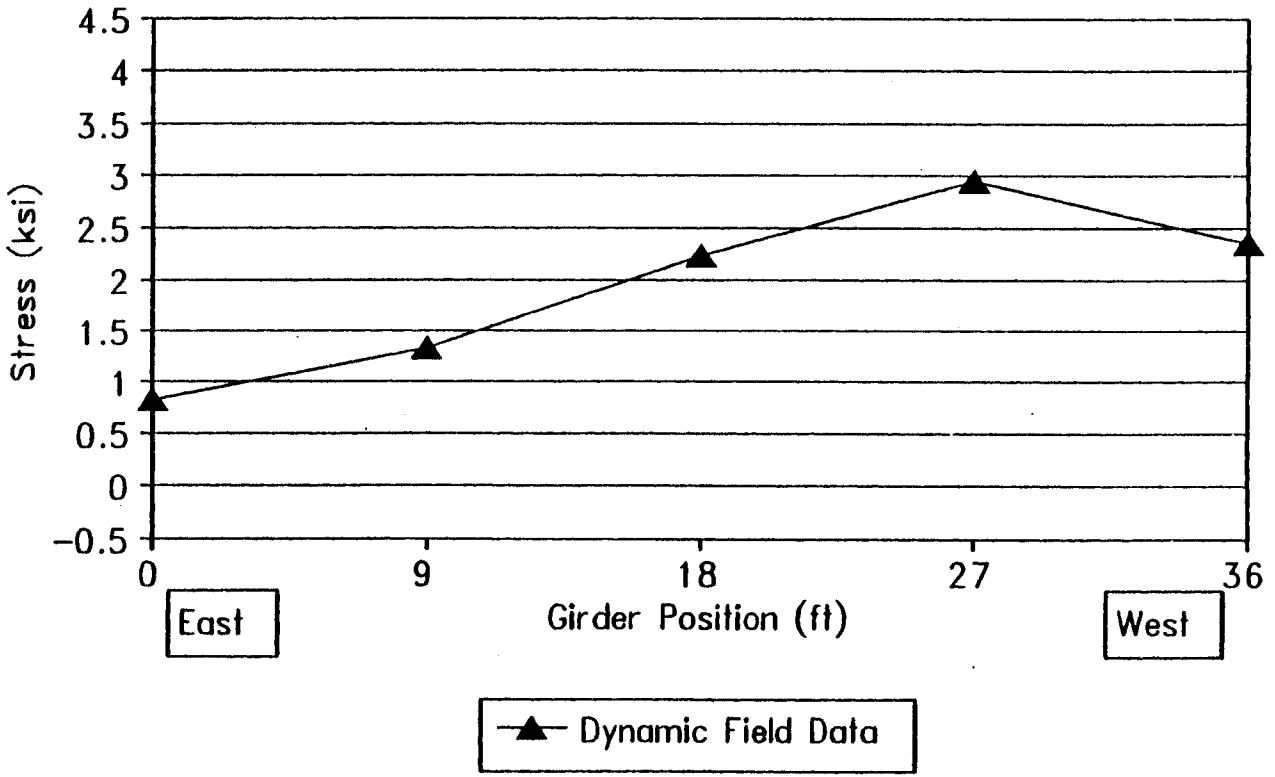

Figure 3.42 Transverse stress distribution of peak dynamic stresses for each girder with the west 2 lanes loaded

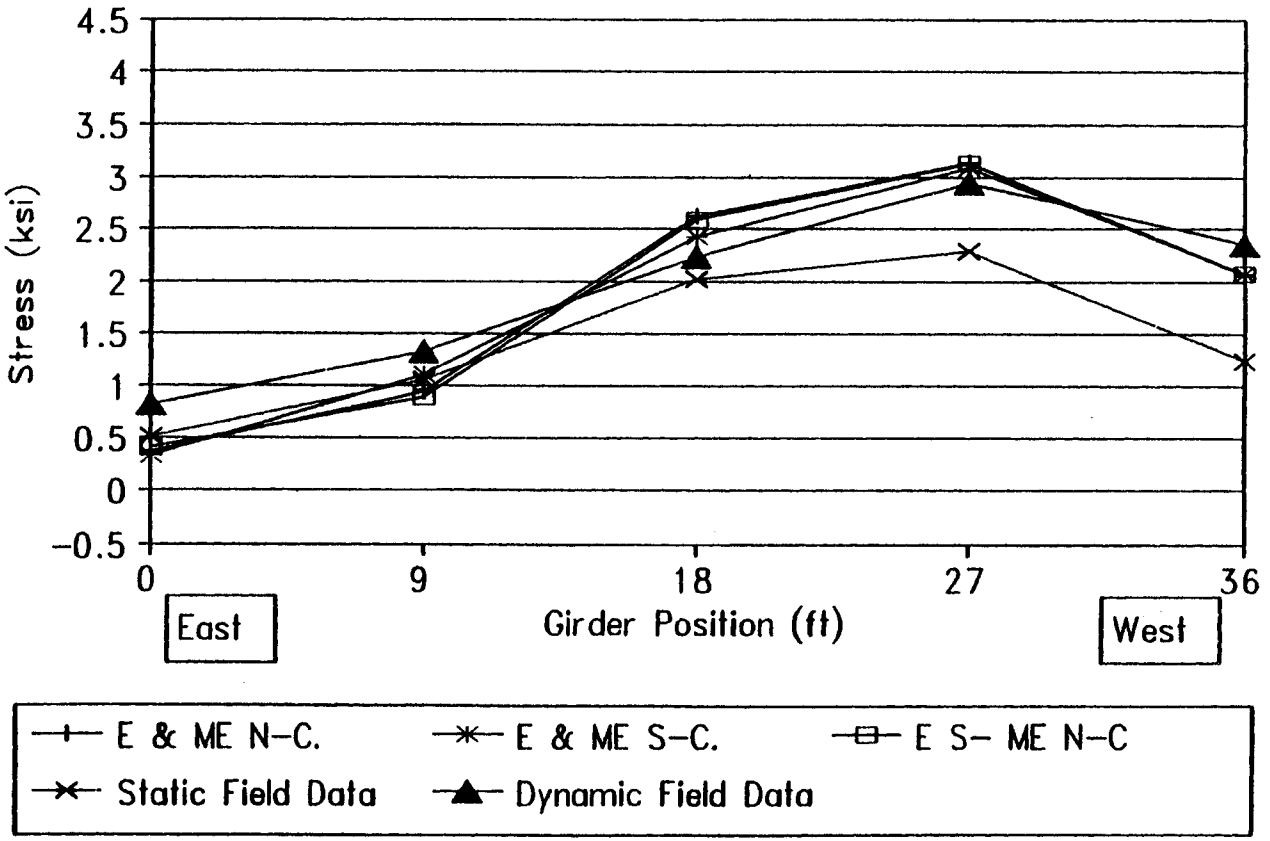

Figure 3.43 Transverse distribution comparing the best 3 models with the static and dynamic peak stresses (west 2 lanes loaded)

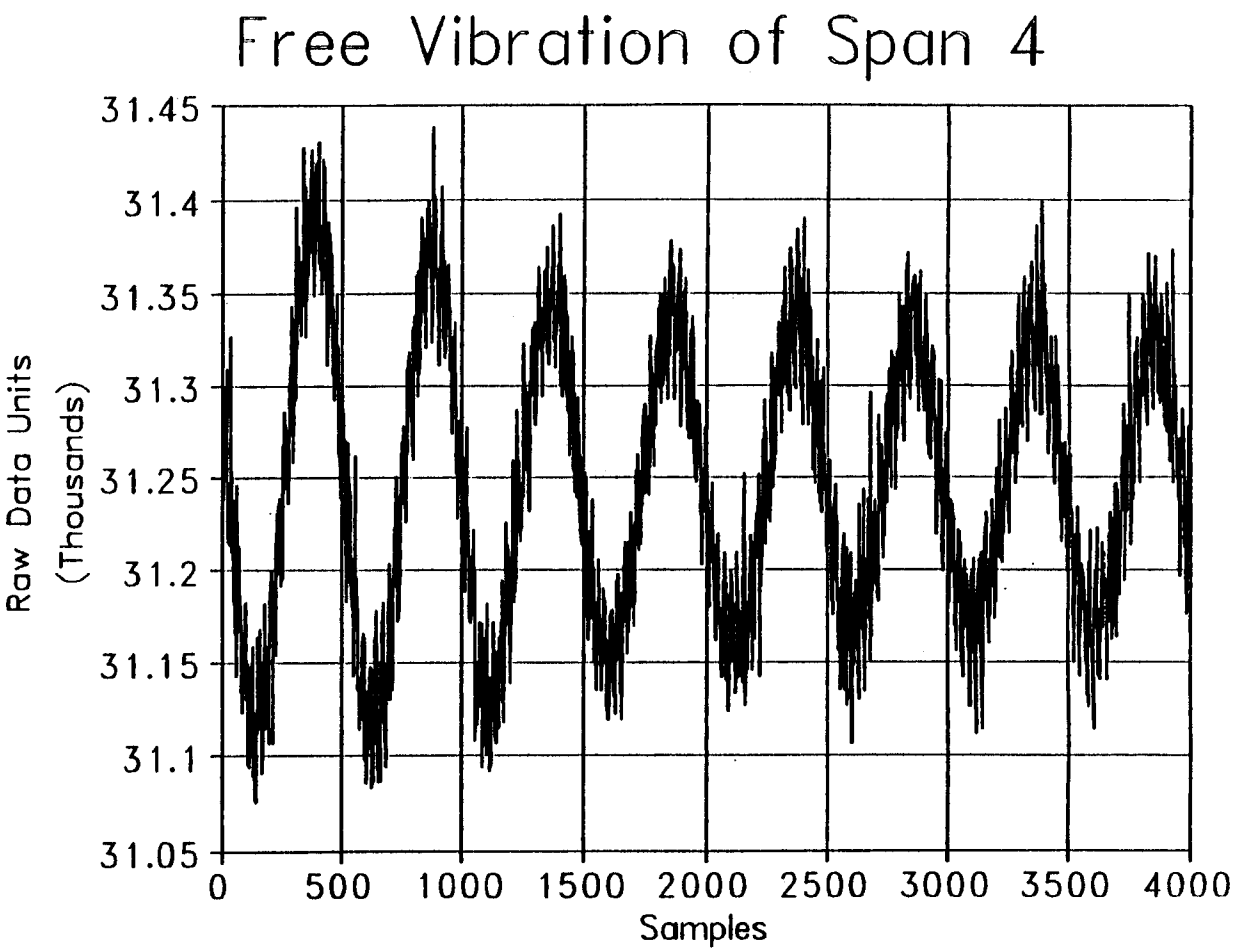

Figure 3.44 Free vibration of span 4 (middle girder)

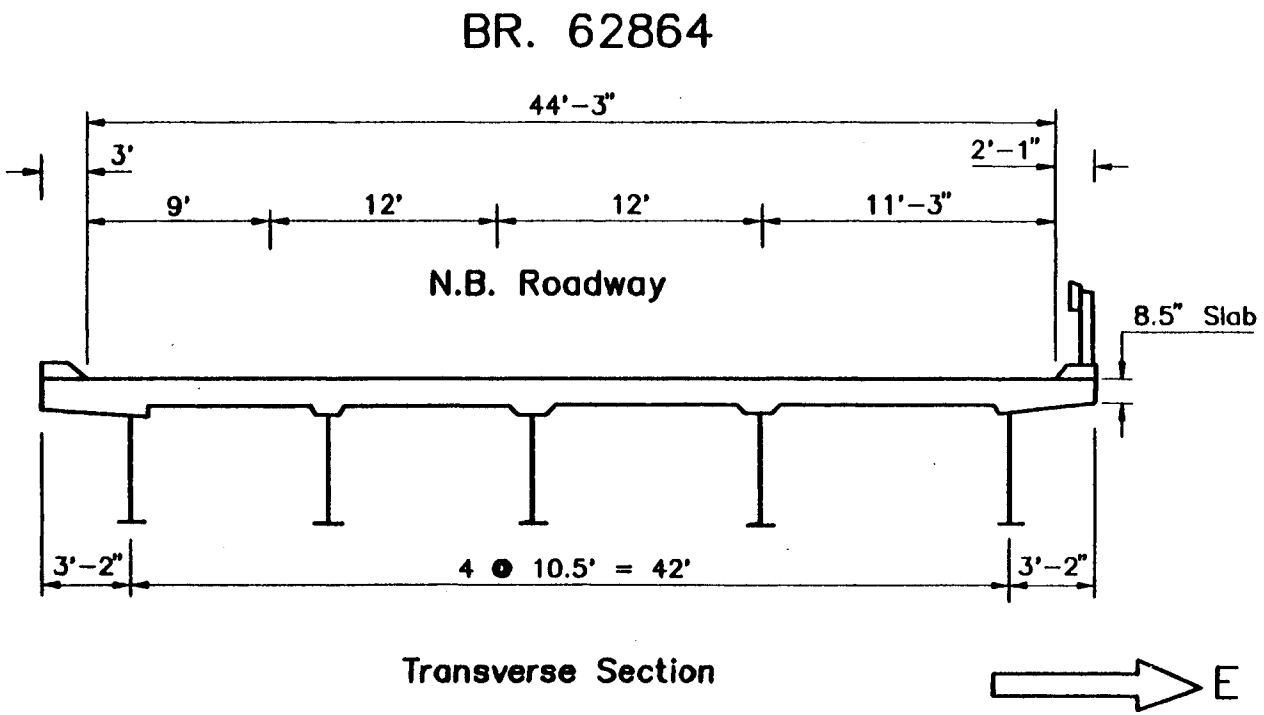

Figure 4.1 Cross section of bridge no. 62864

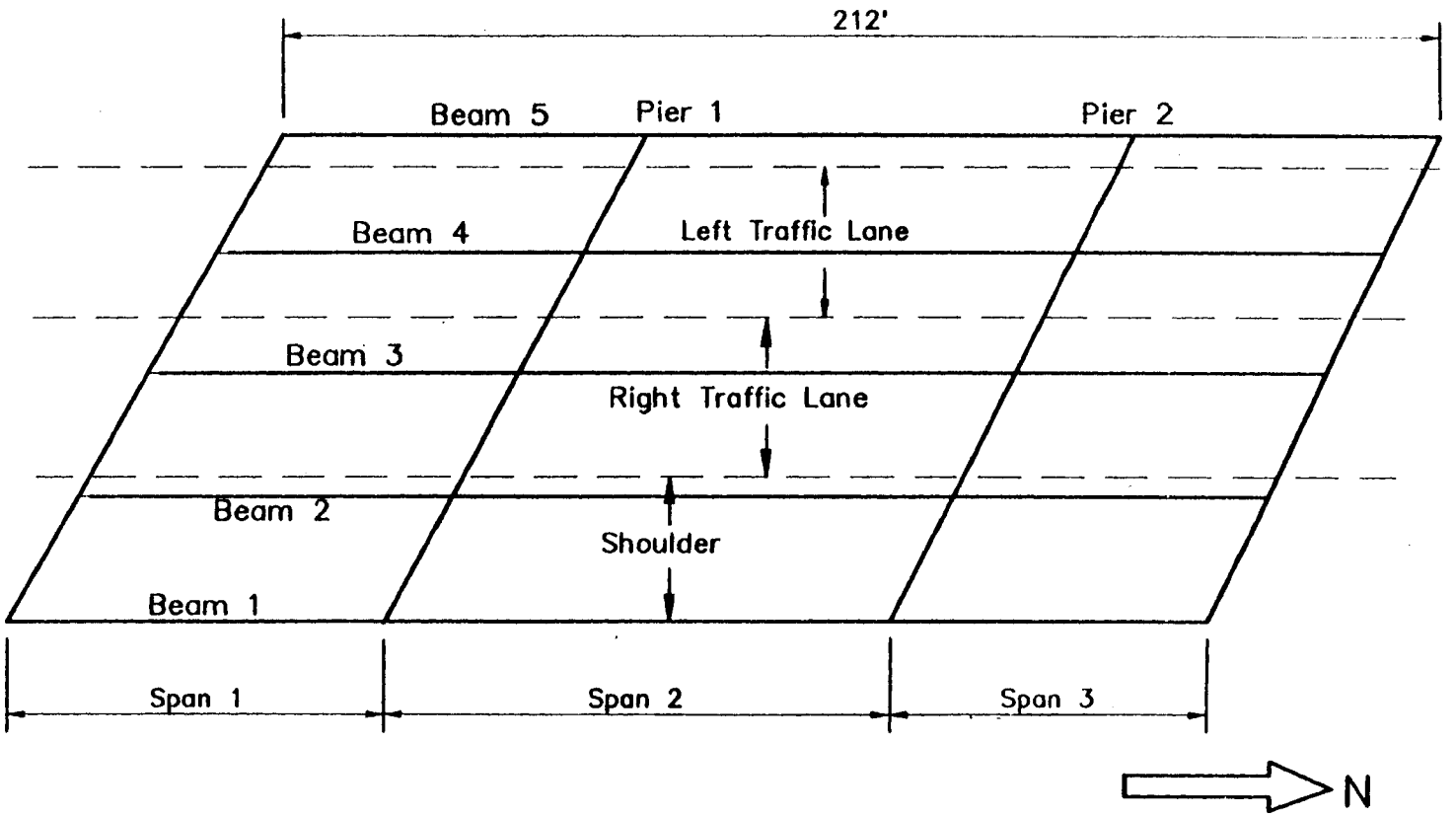

Figure 4.2 Plan view of bridge no. 62864

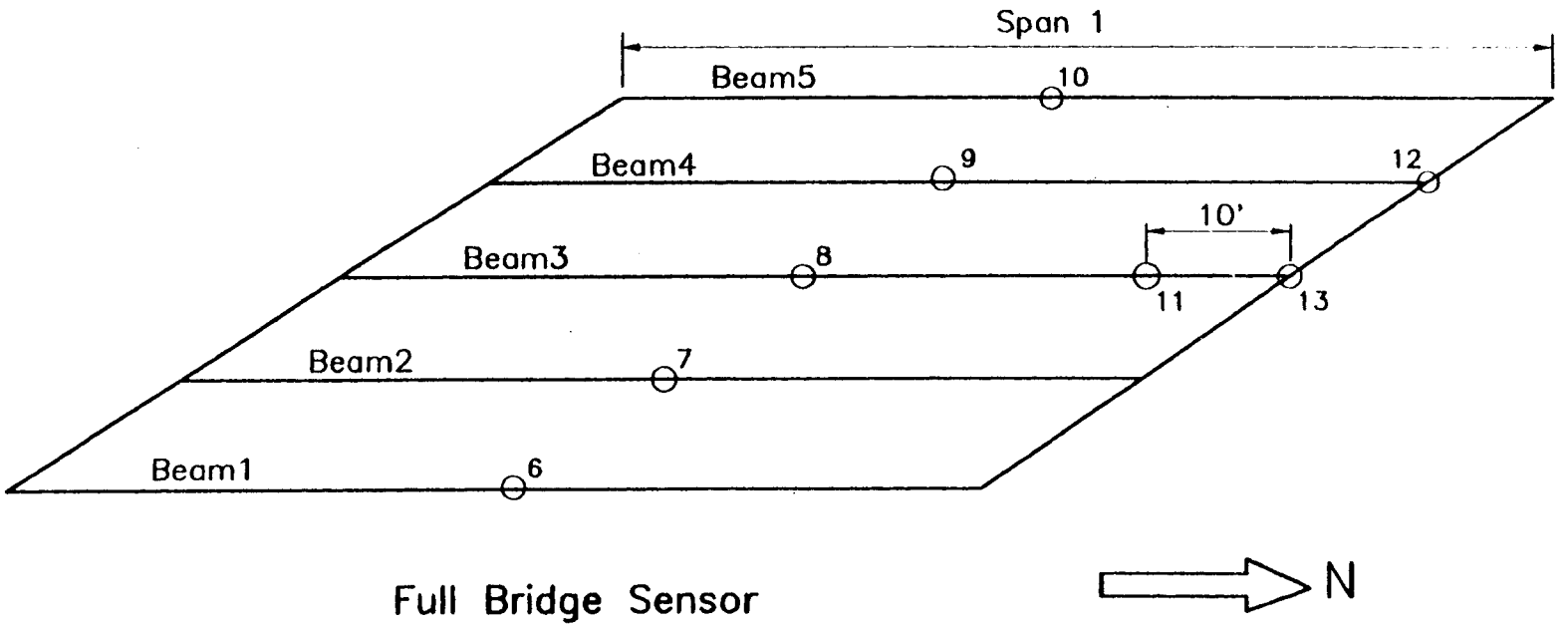

Figure 4.3 Location of strain sensors for bridge no. 62864

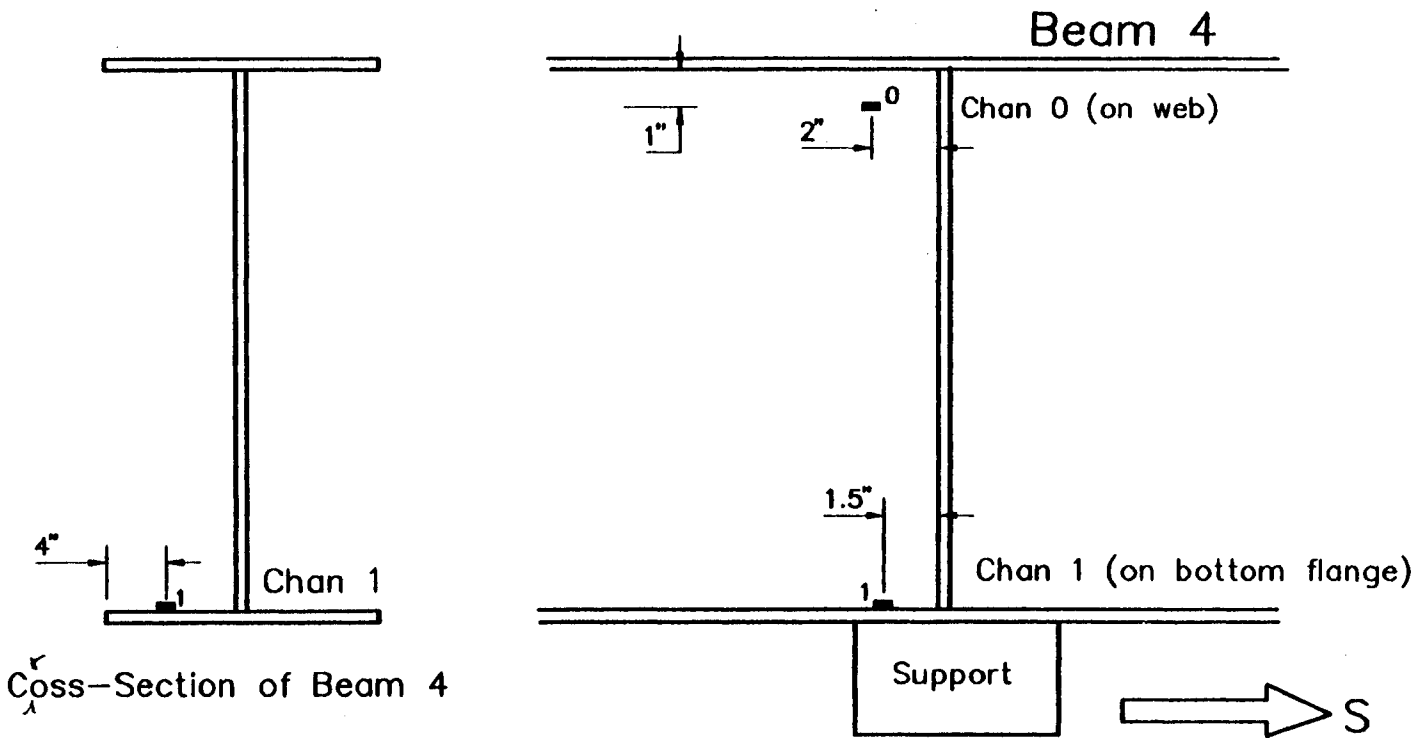

Figure 4.4 Location of strain gages for fatigue measurements

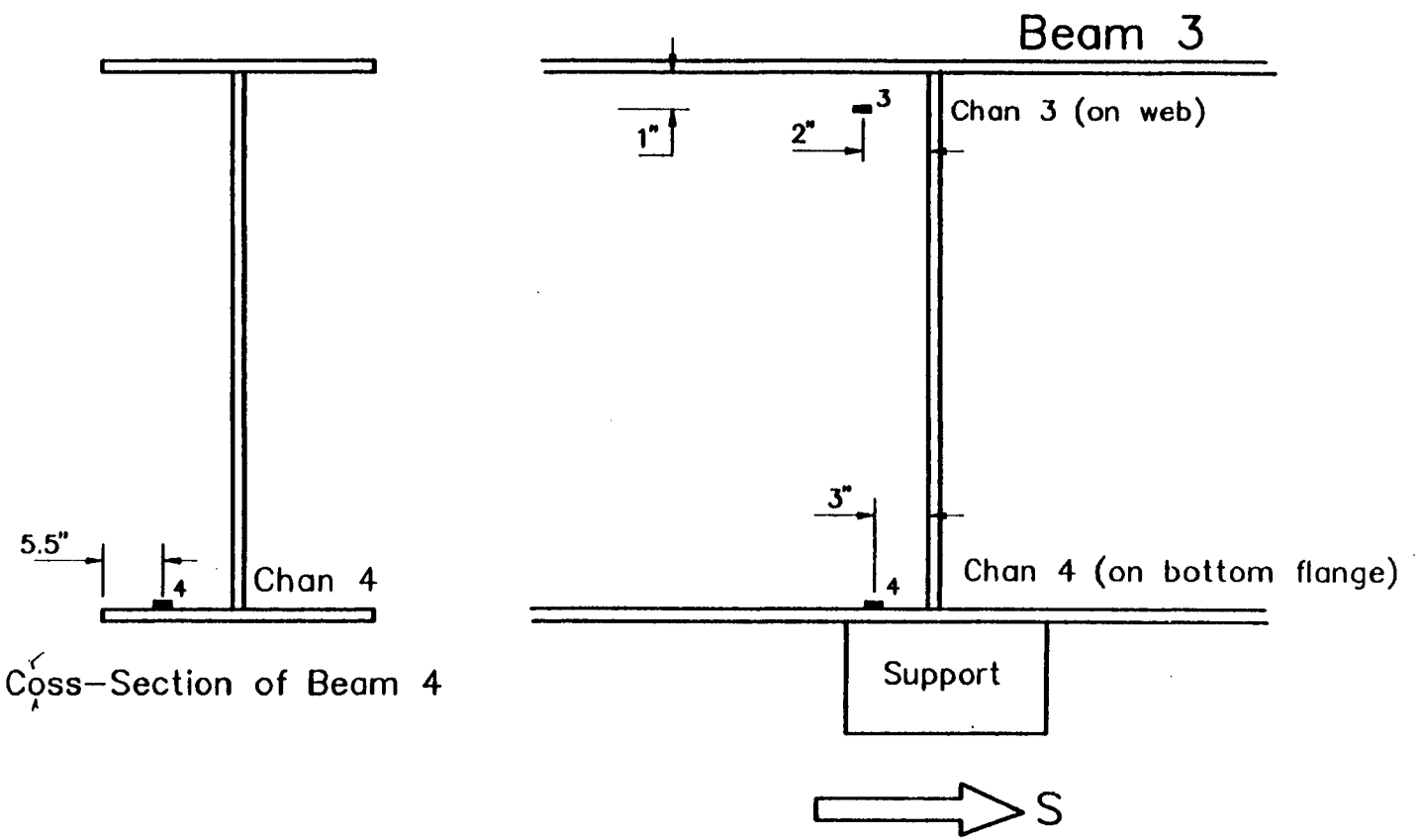

Figure 4.5 Location of strain gages for fatigue measurements

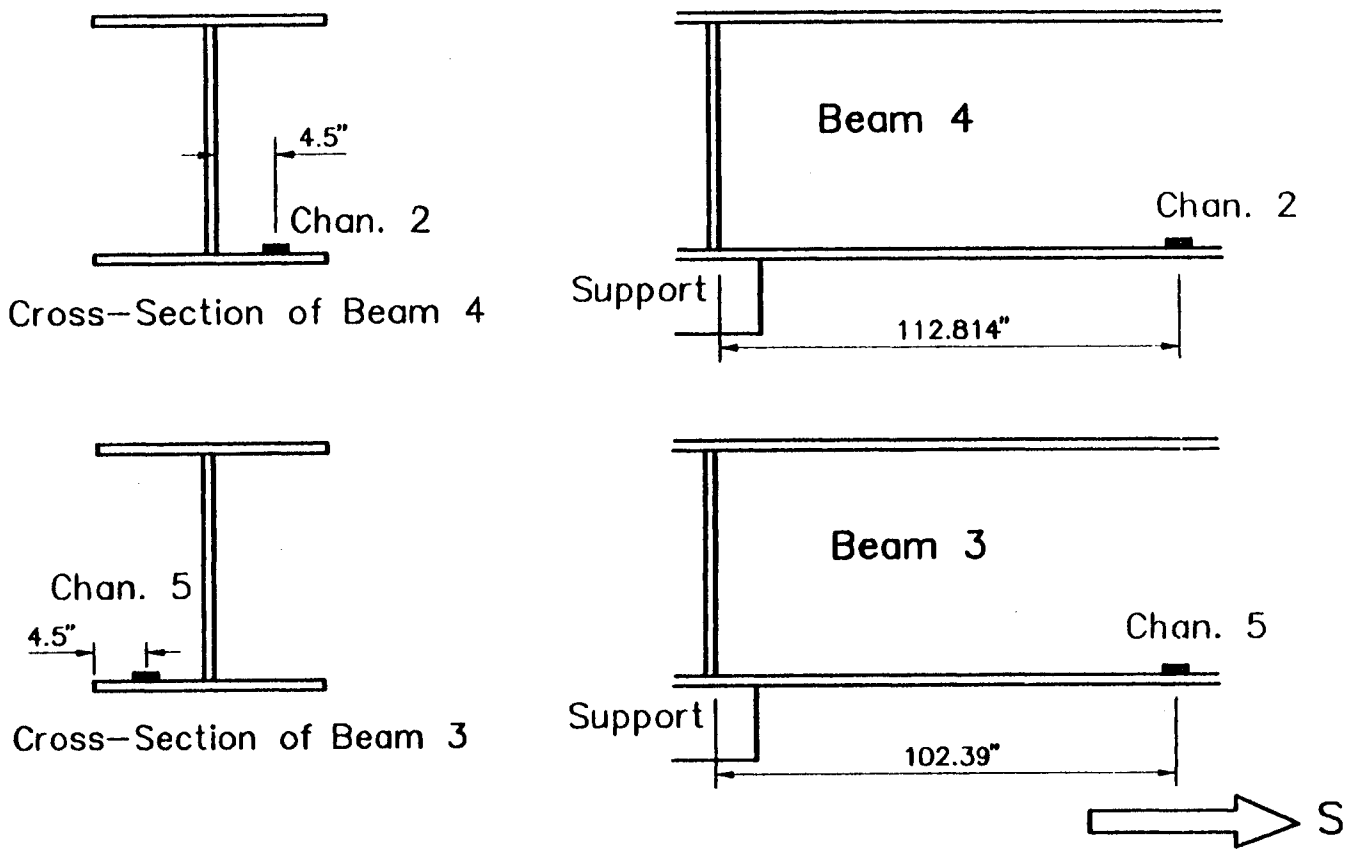

Figure 4.6 Location of strain gages for fatigue measurements

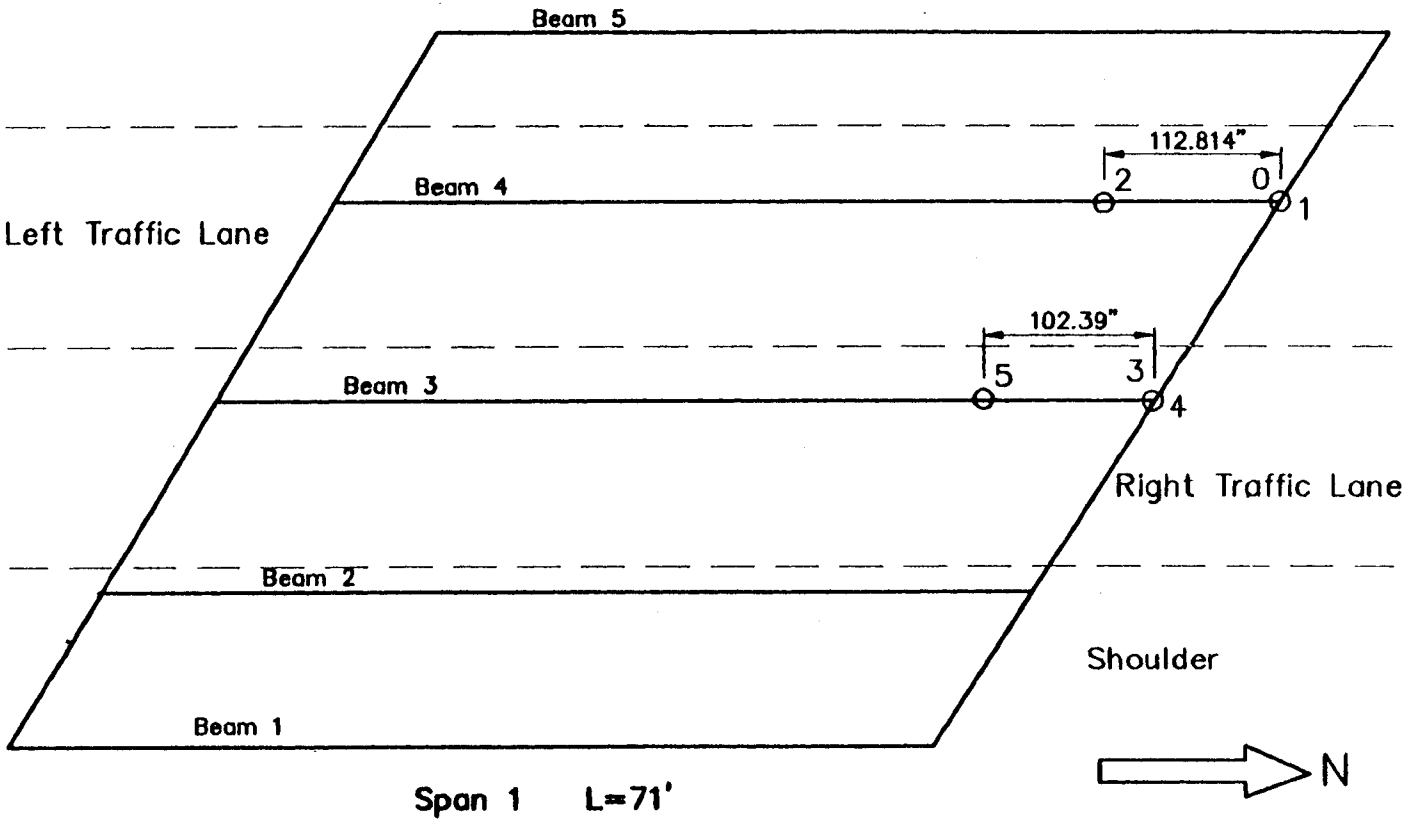

Figure 4.7 Location of strain gages for fatigue measurements

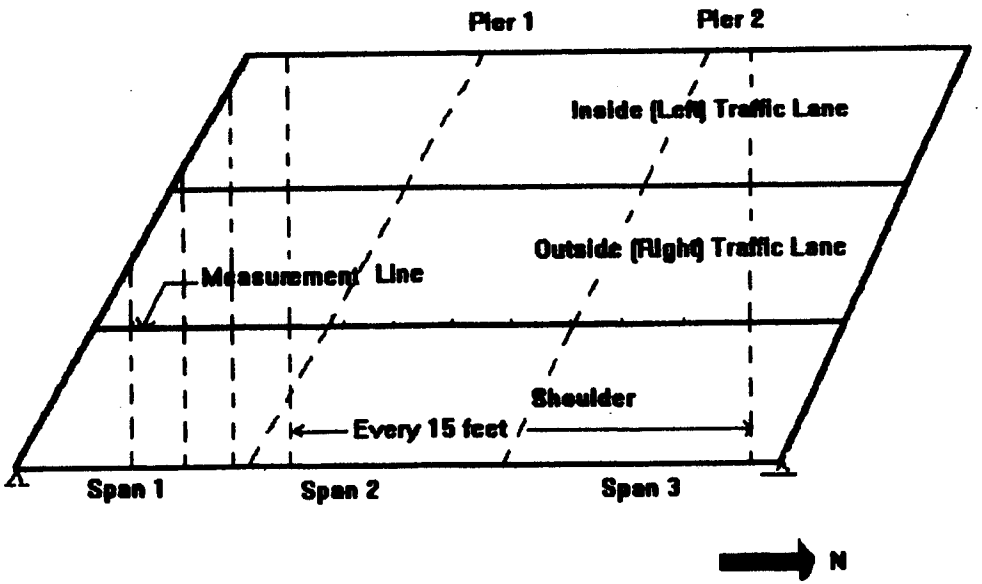

Figure 4.8 Lane definitions and the locations of the truck

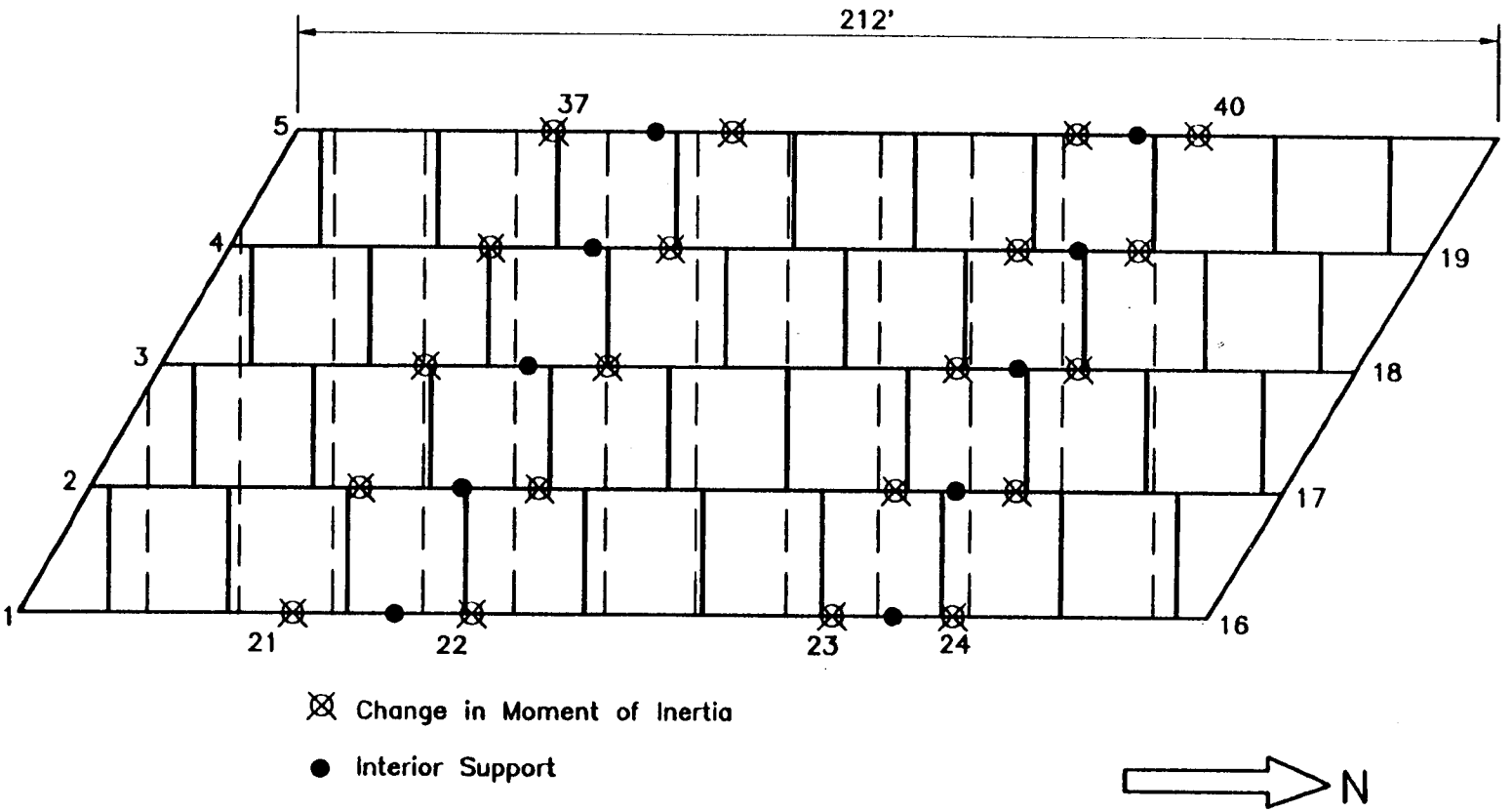

Figure 4.9 Nodemap for analytical model of bridge no. 62864

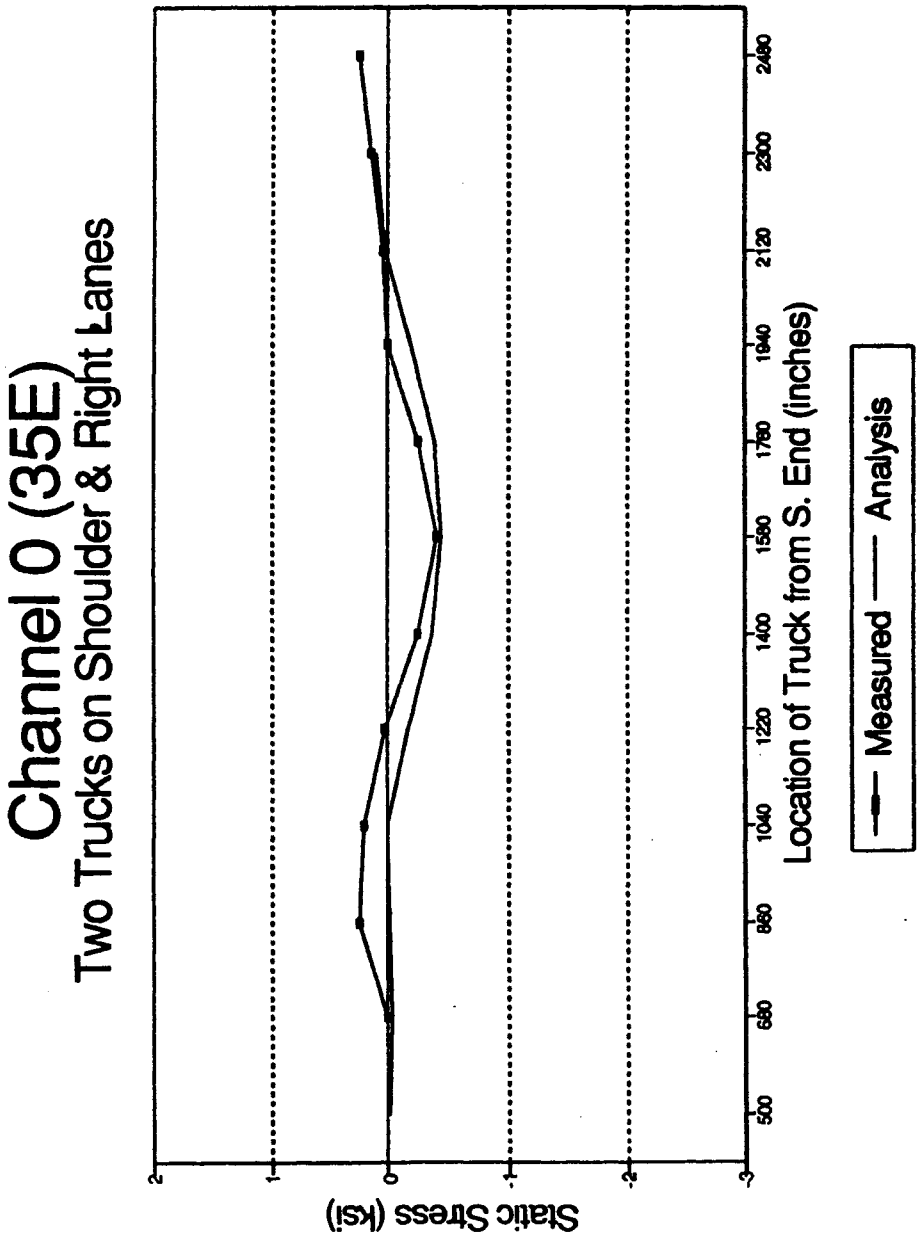

Figure 4.10 Stress distribution

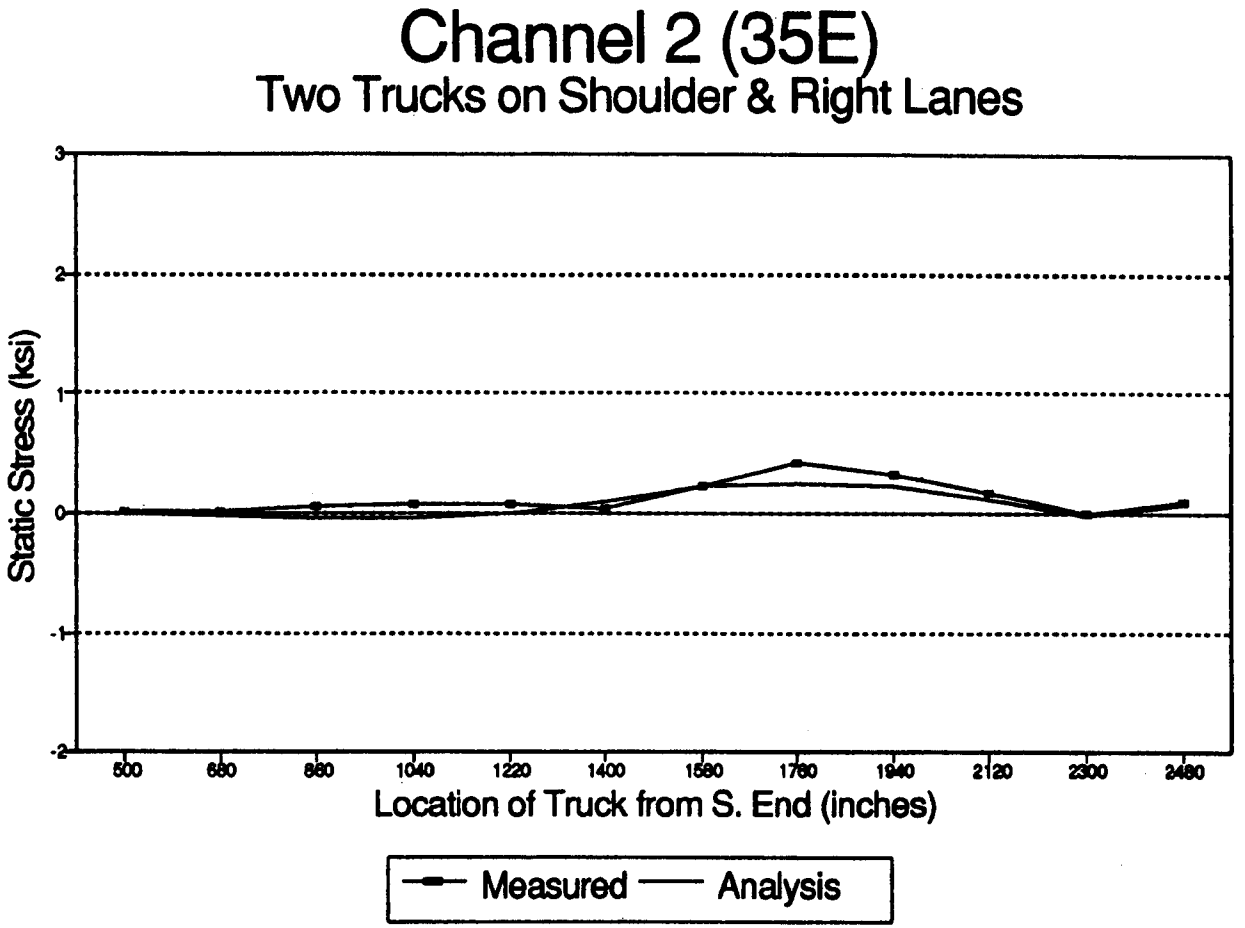

Figure 4.11 Stress distribution

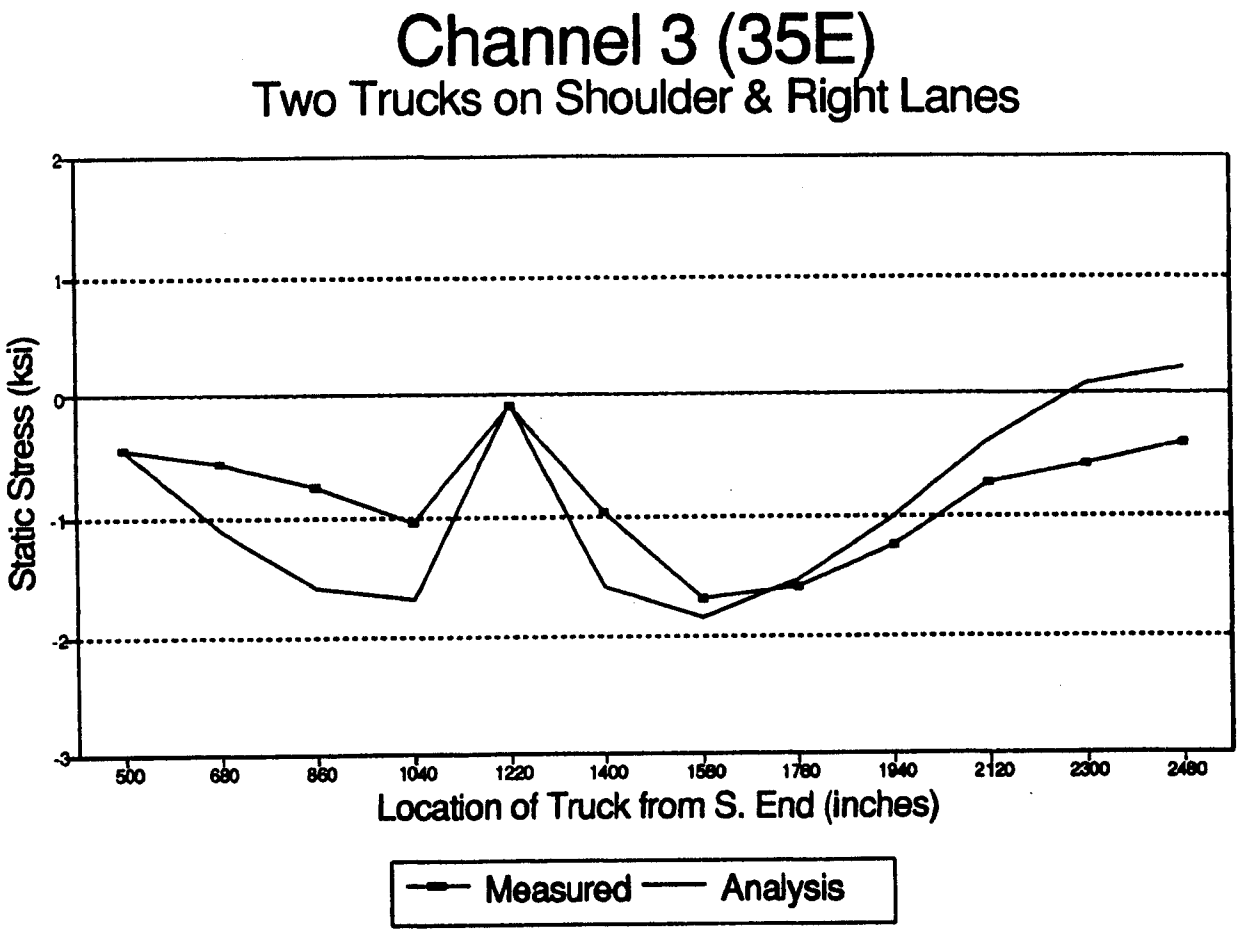

Figure 4.12 Stress distribution

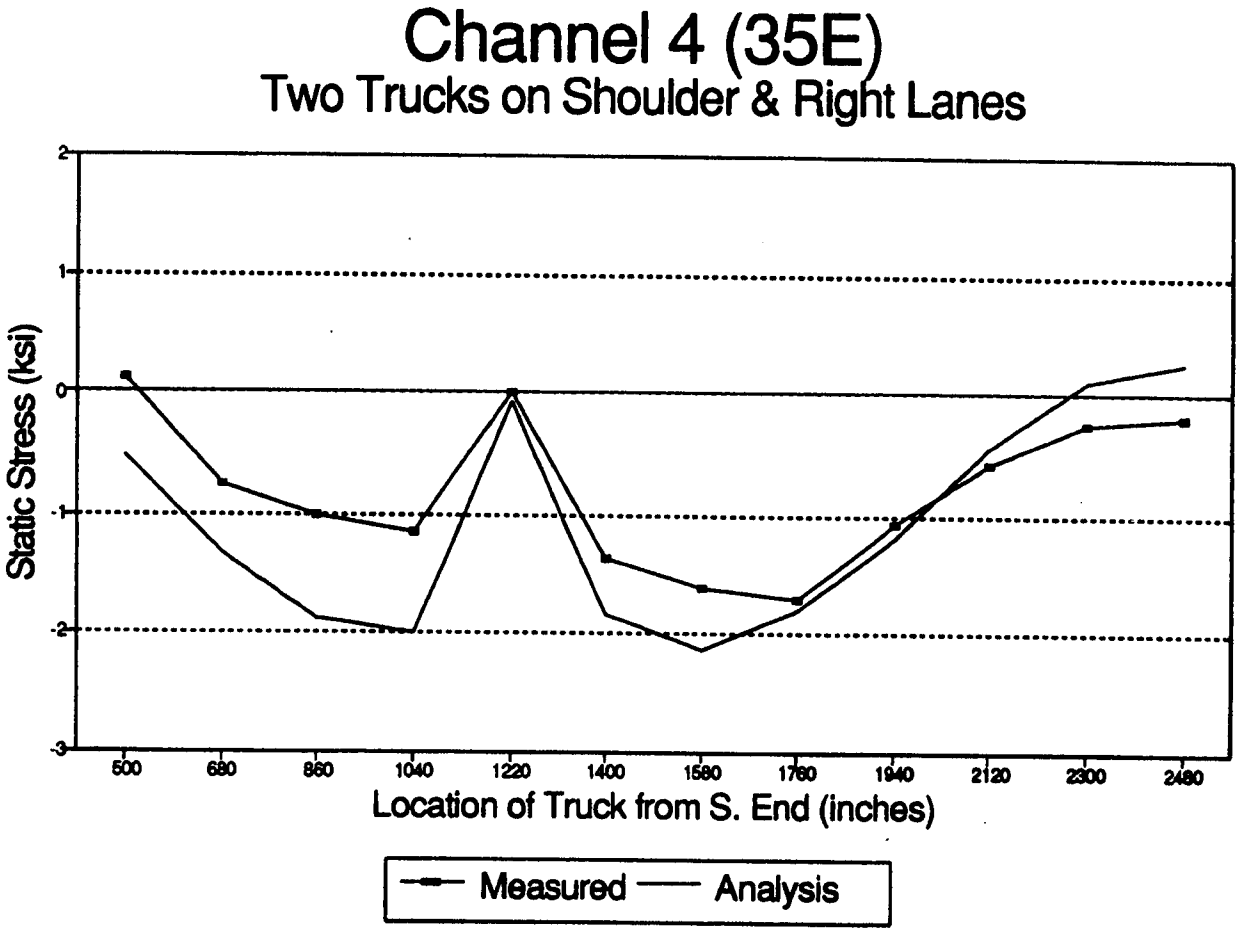

Figure 4.13 Stress distribution

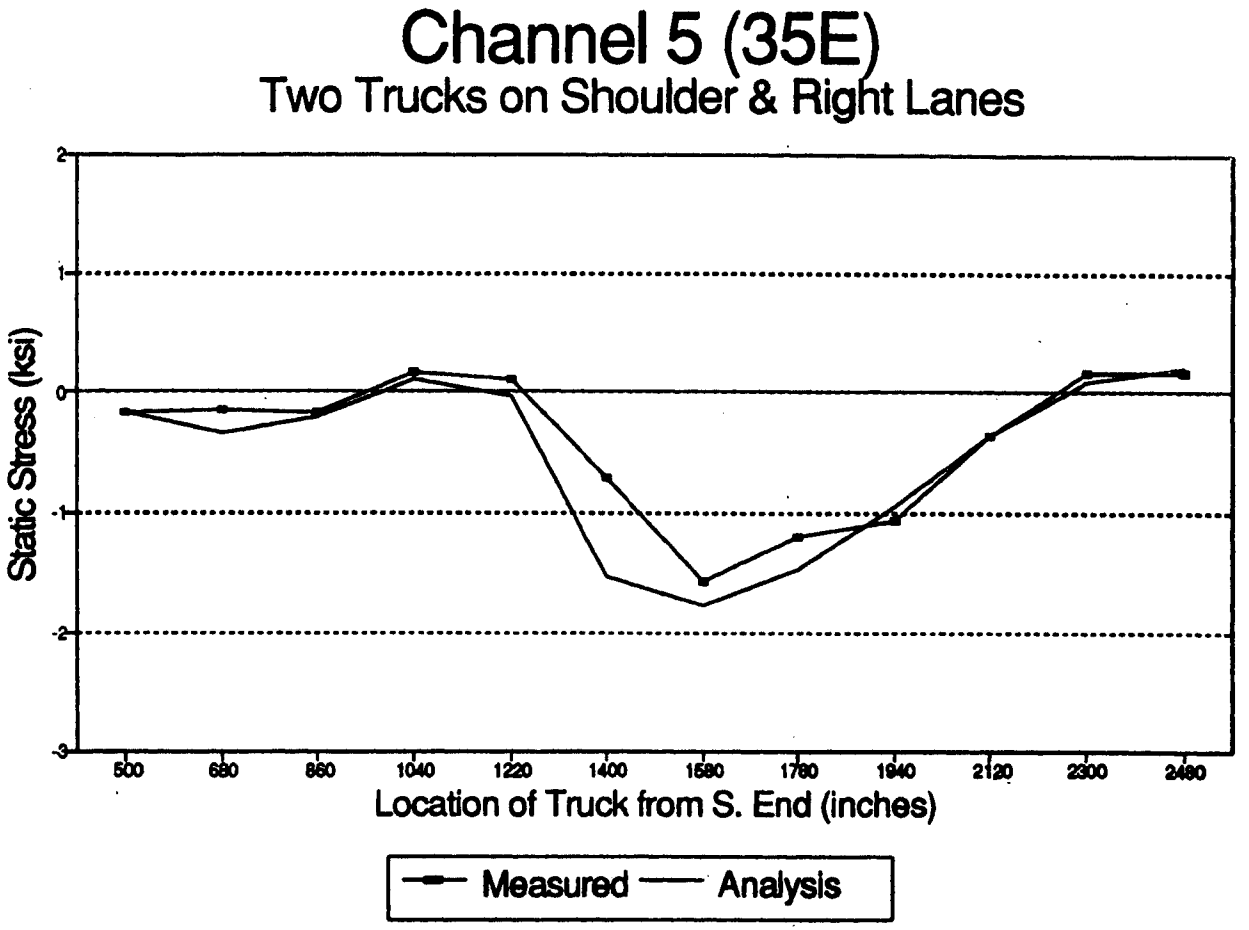

Figure 4.14 Stress distribution

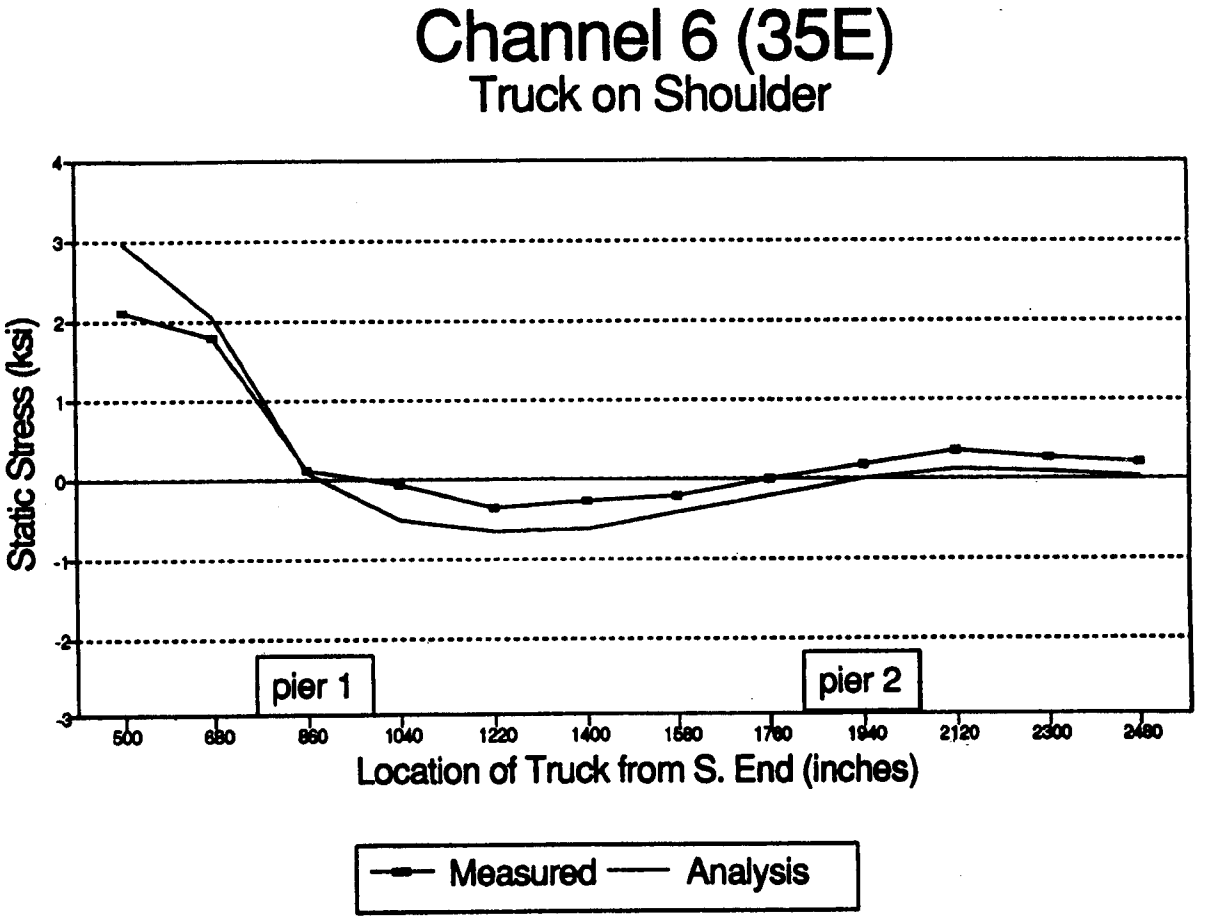

Figure 4.15 Stress distribution

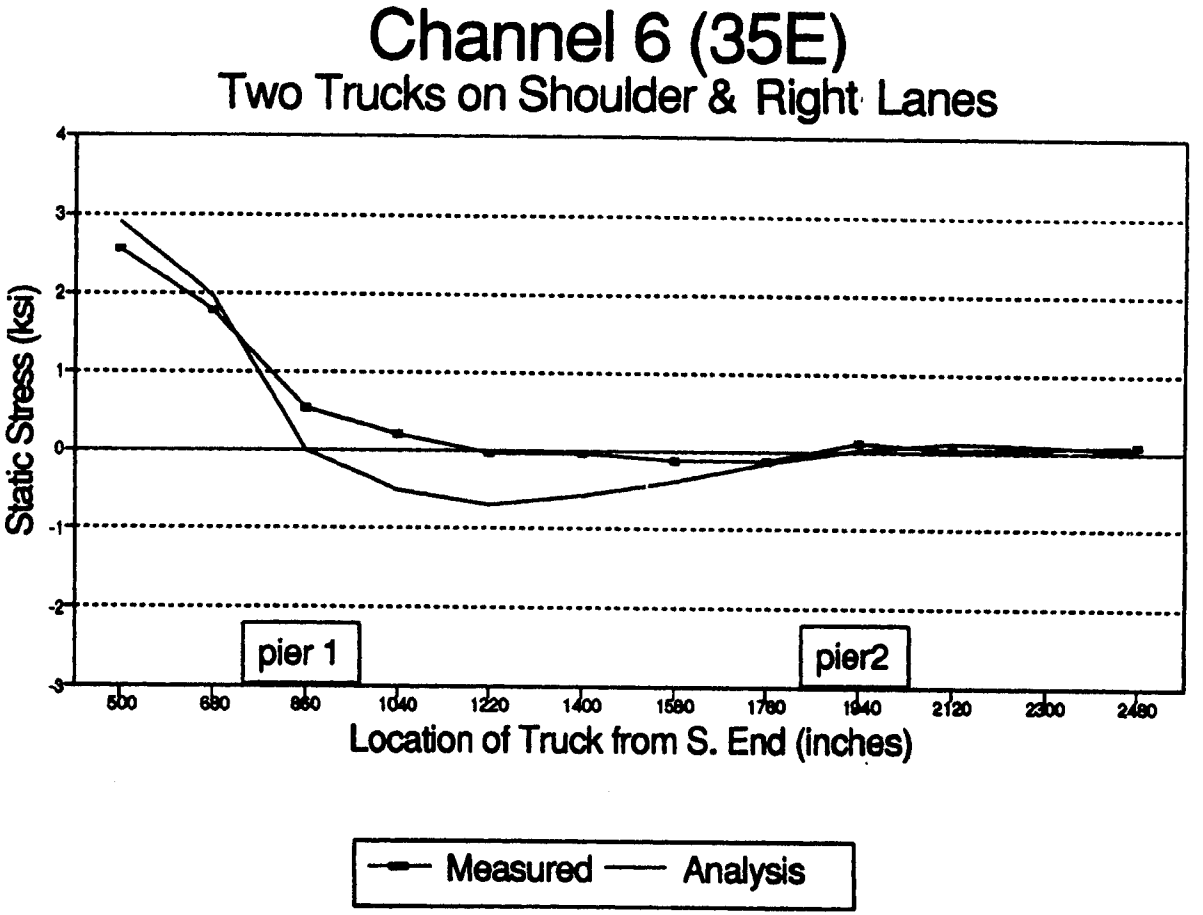

Figure 4.16 Stress distribution

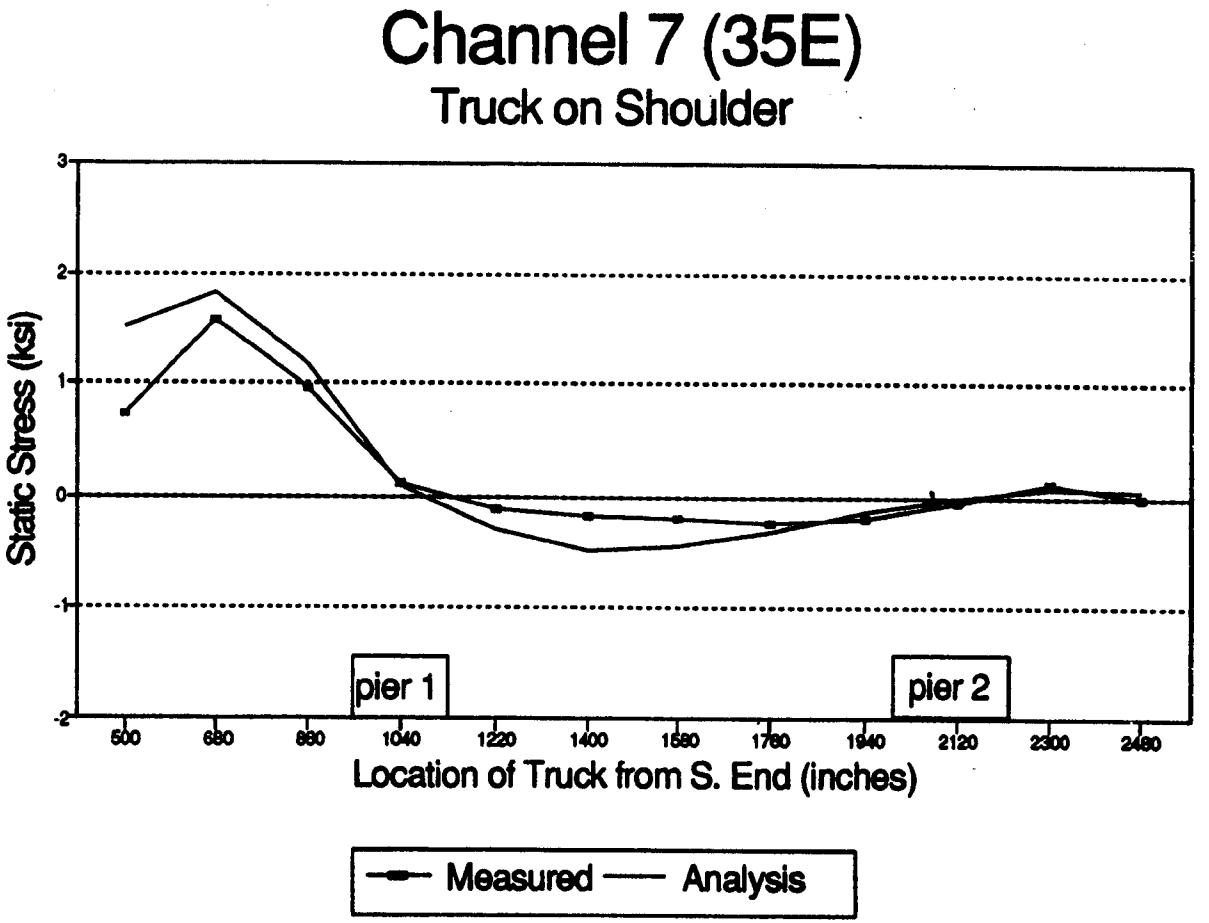

Figure 4.17 Stress distribution

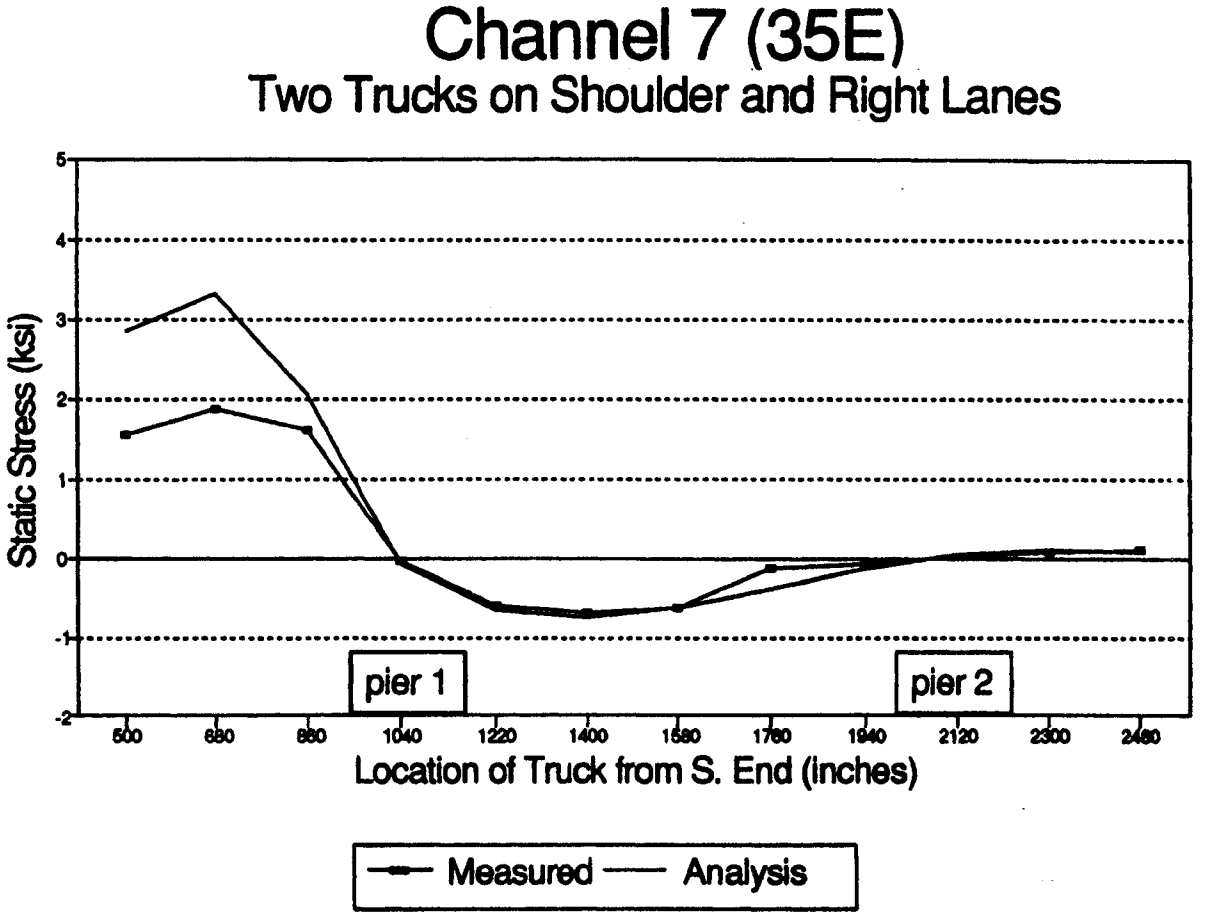

Figure 4.18 Stress distribution

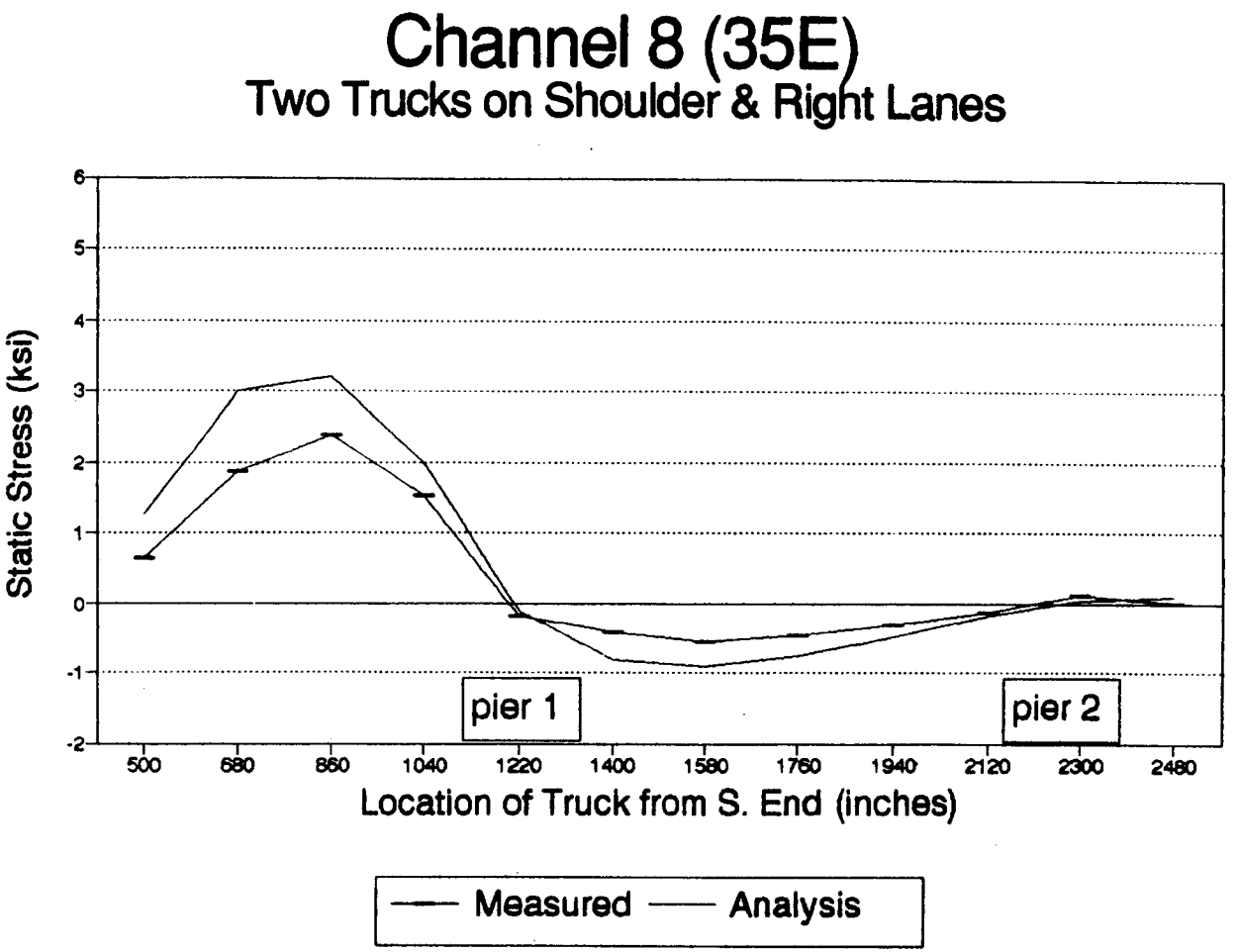

Figure 4.19 Stress distribution

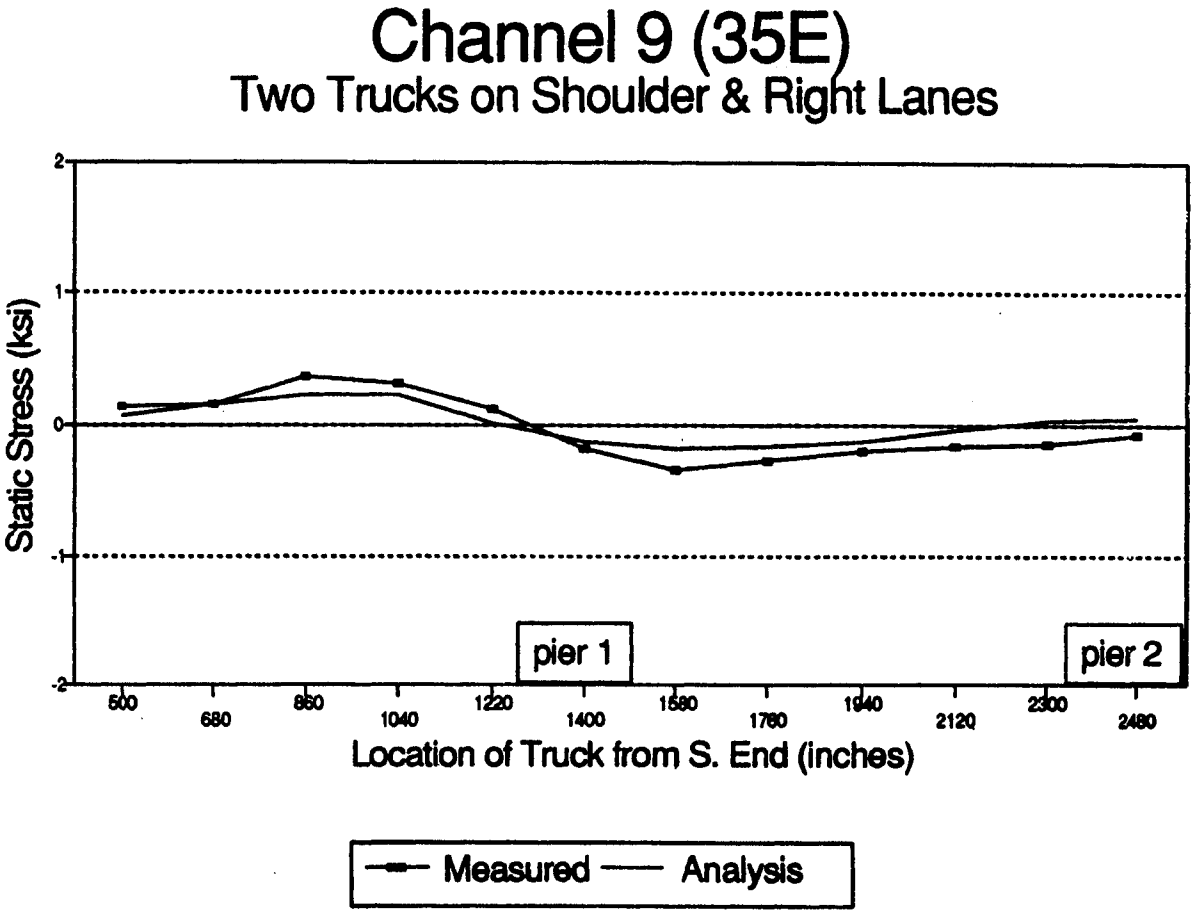

Figure 4.20 Stress distribution

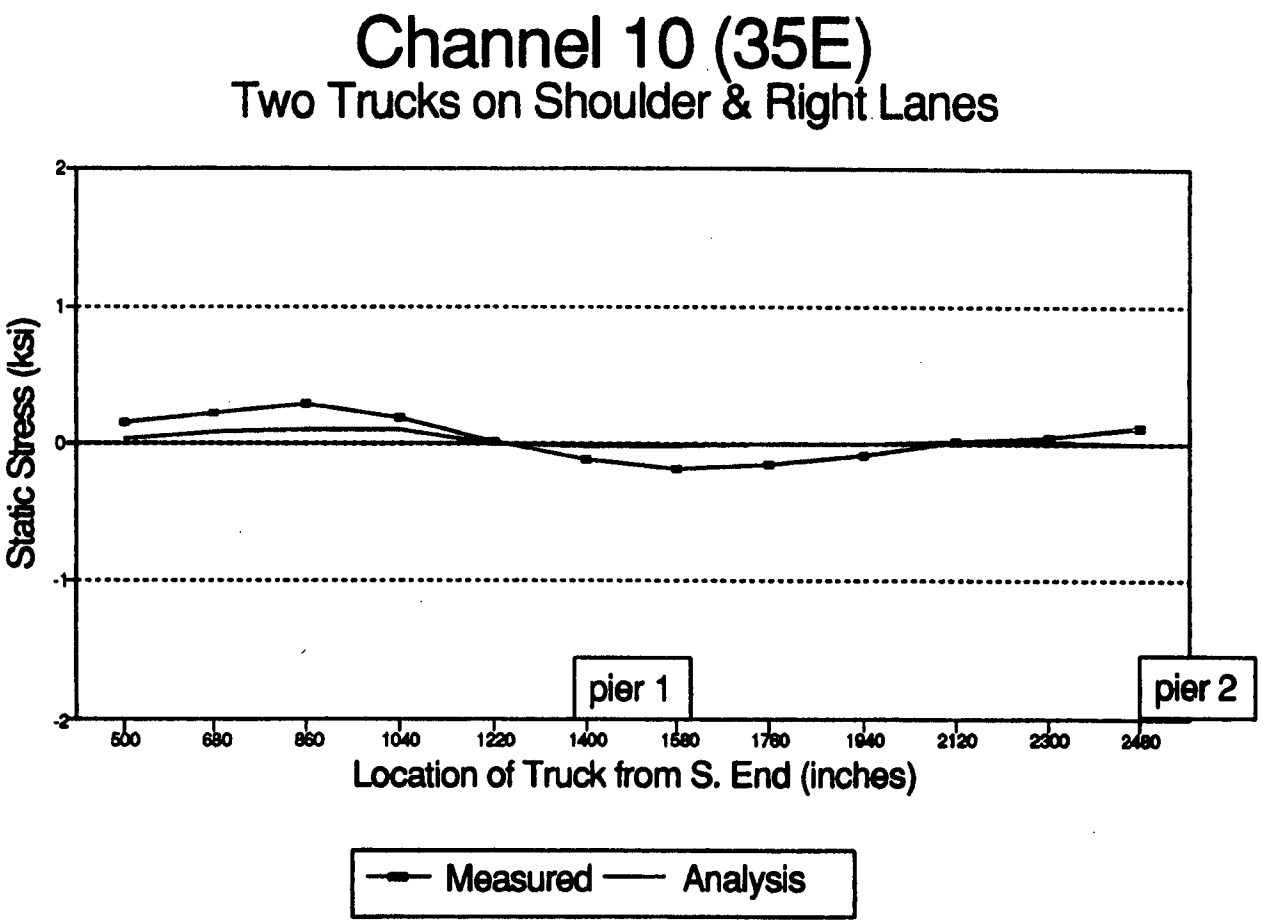

Figure 4.21 Stress distribution

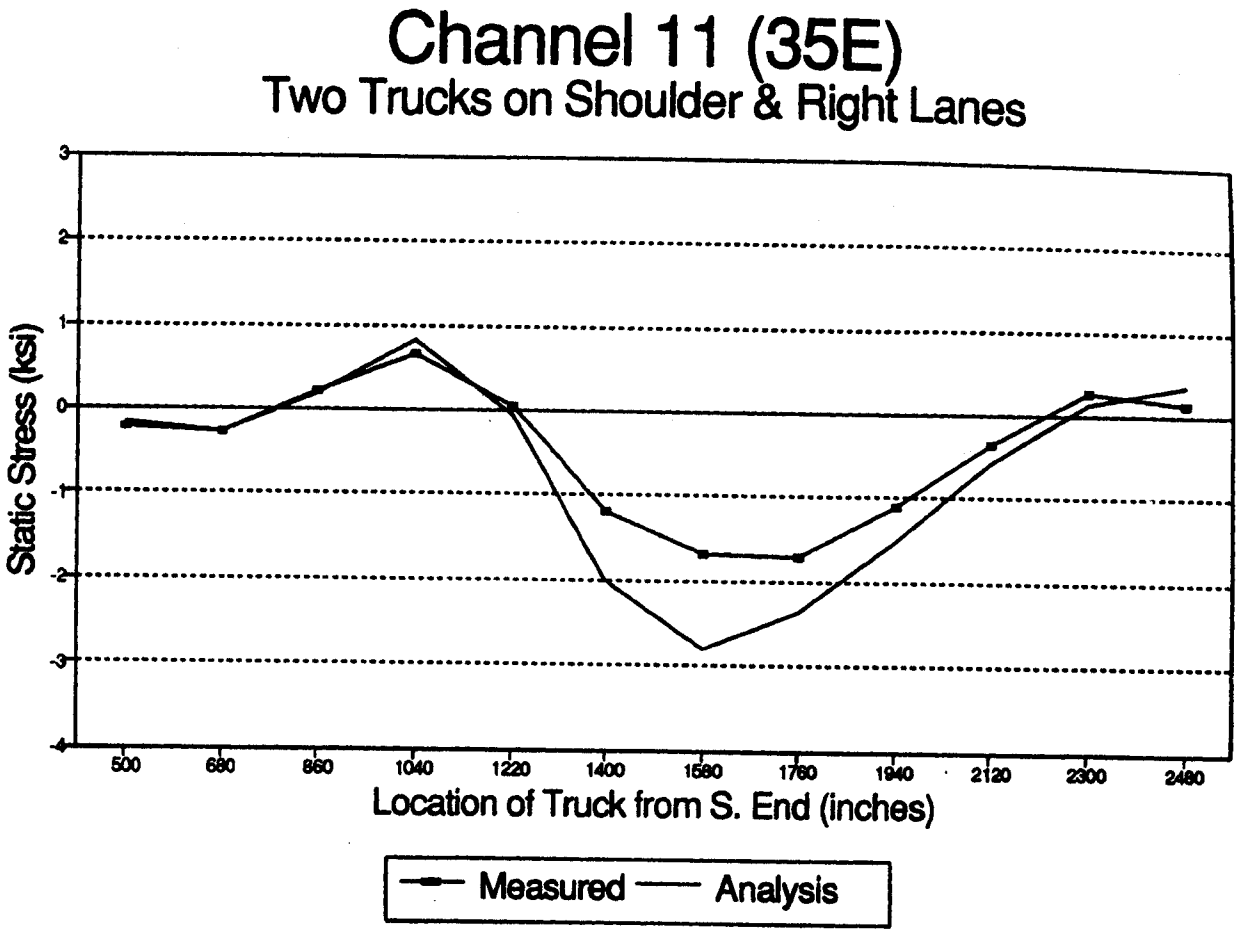

Figure 4.22 Stress distribution

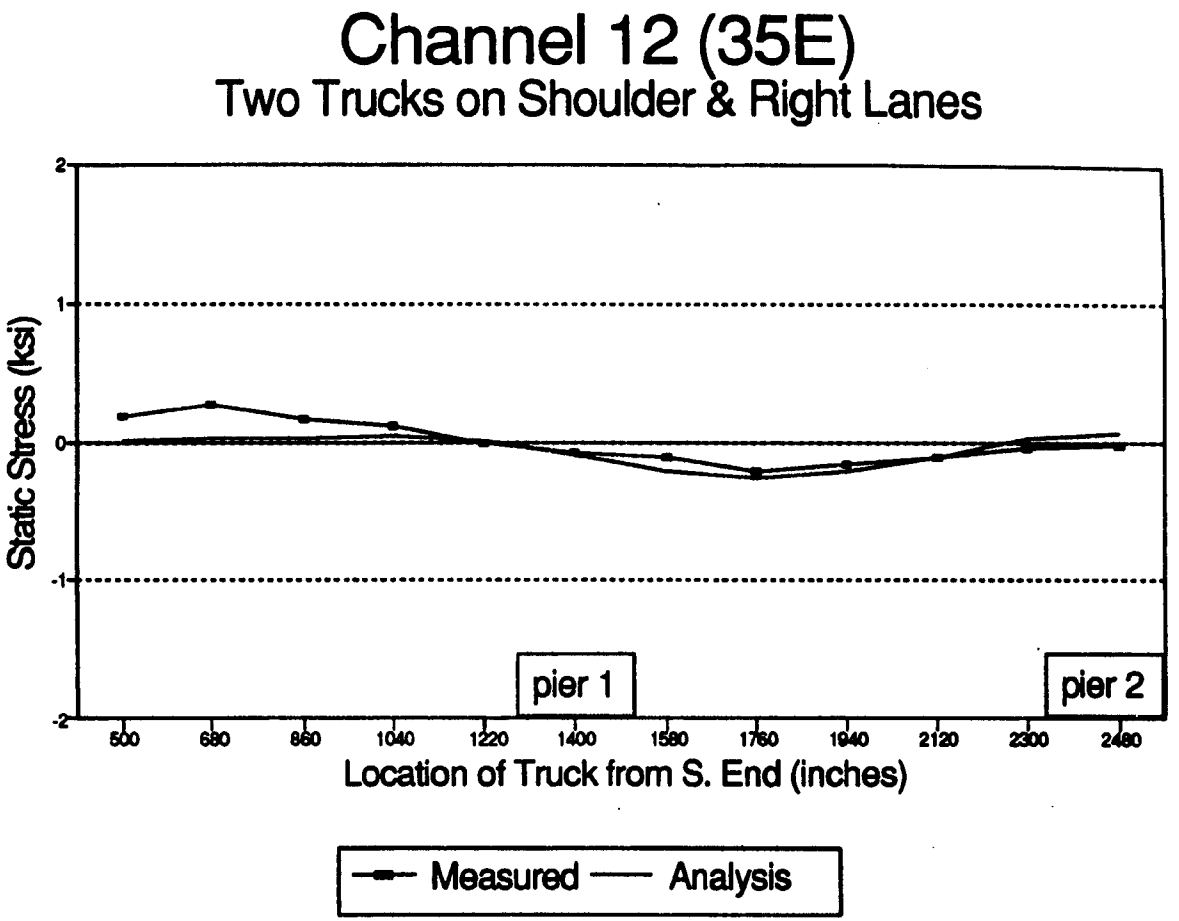

Figure 4.23 Stress distribution

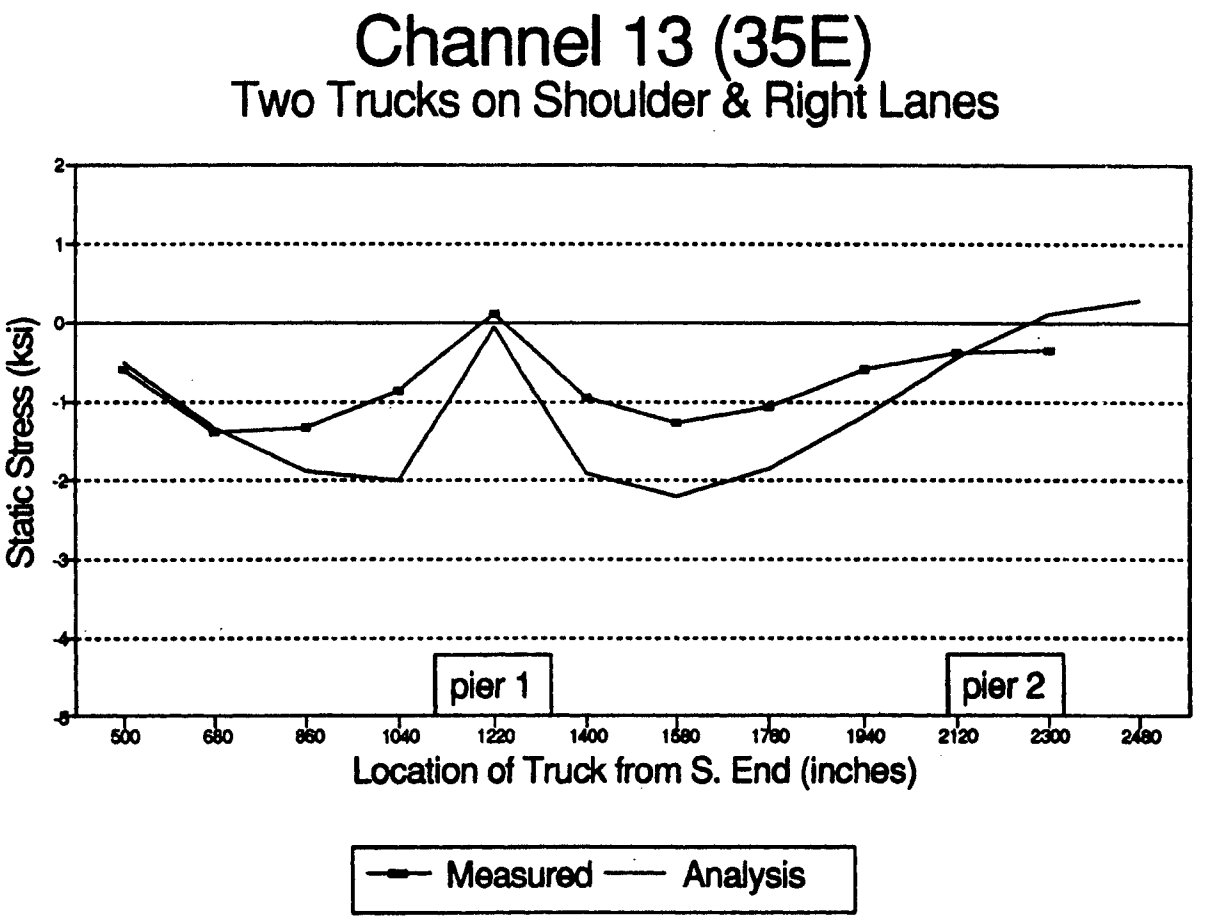

Figure 4.24 Stress distribution

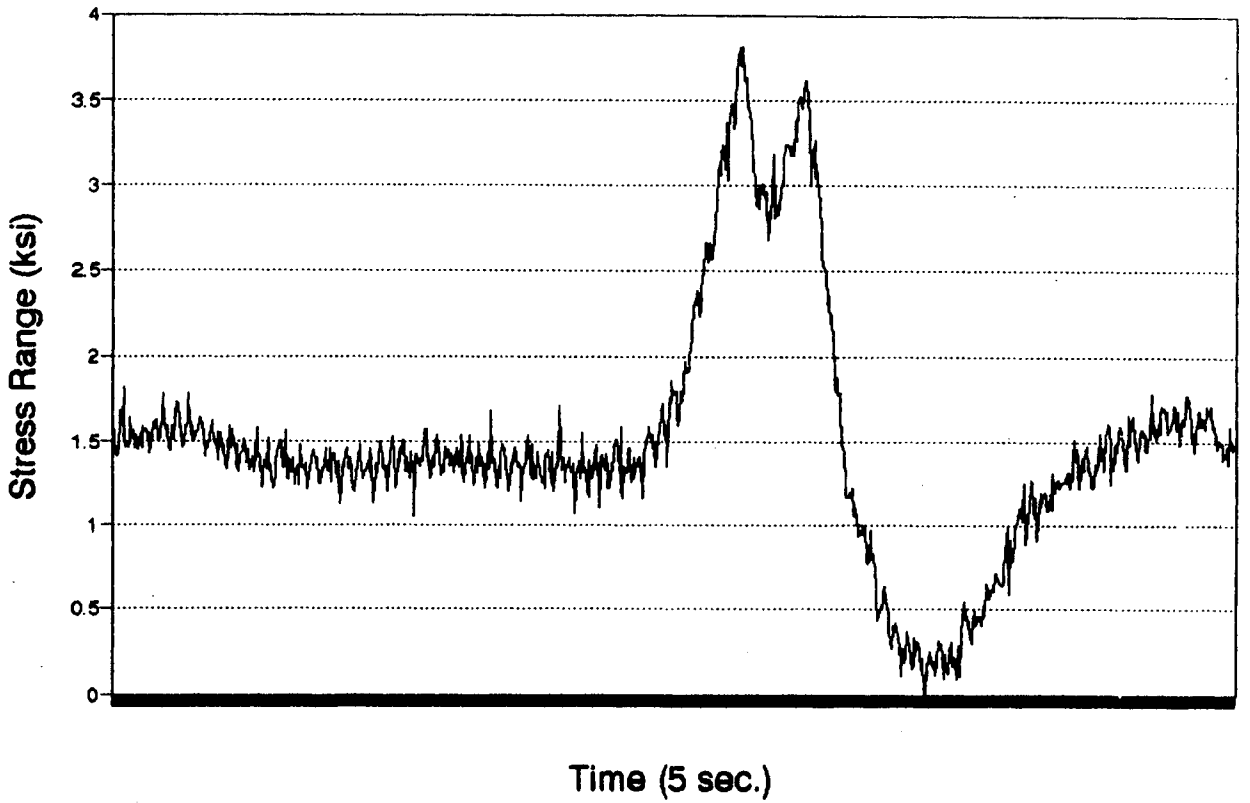

Figure 4.25 Stress vs. time for channel 12

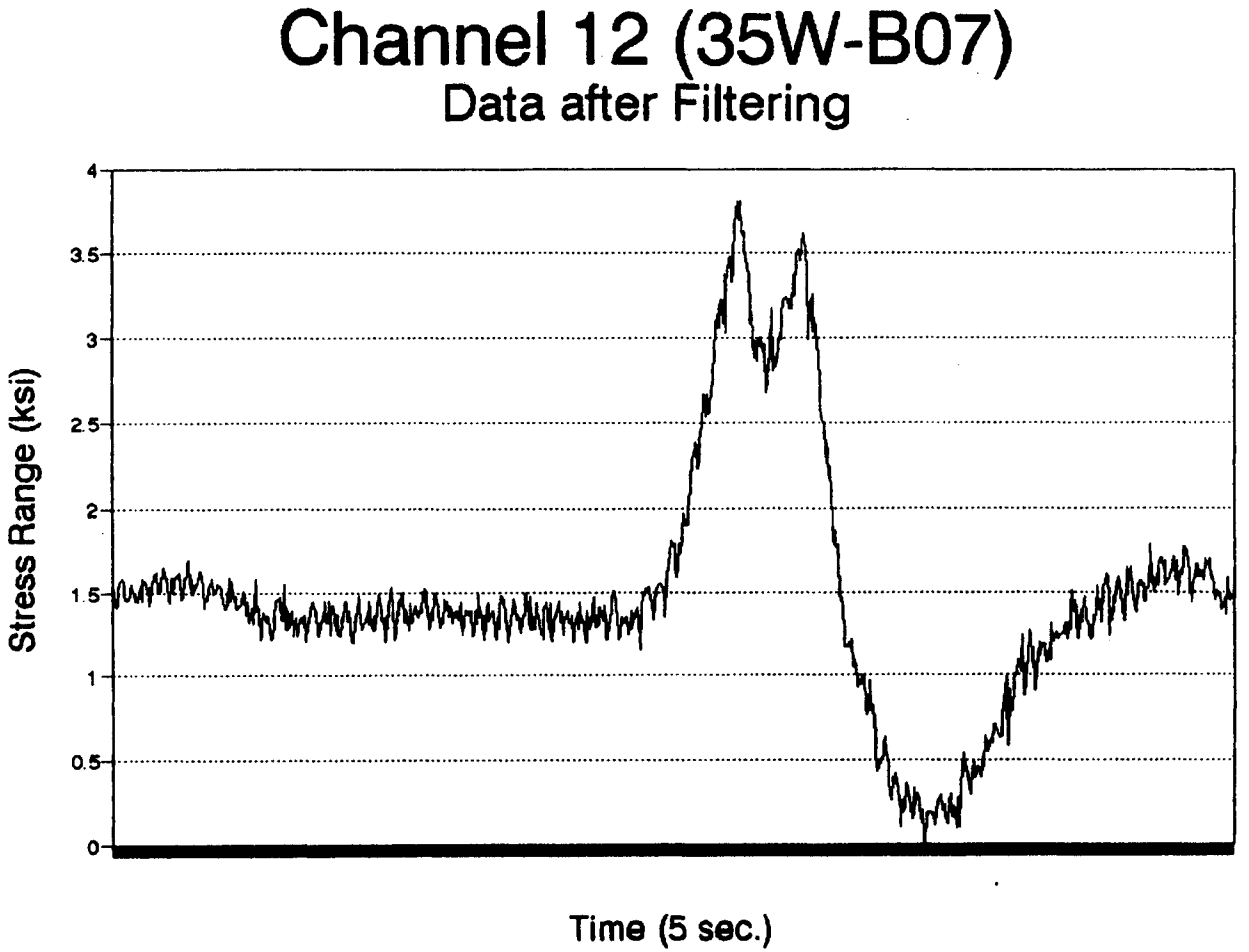

Figure 4.26 Filtered data for channel 12

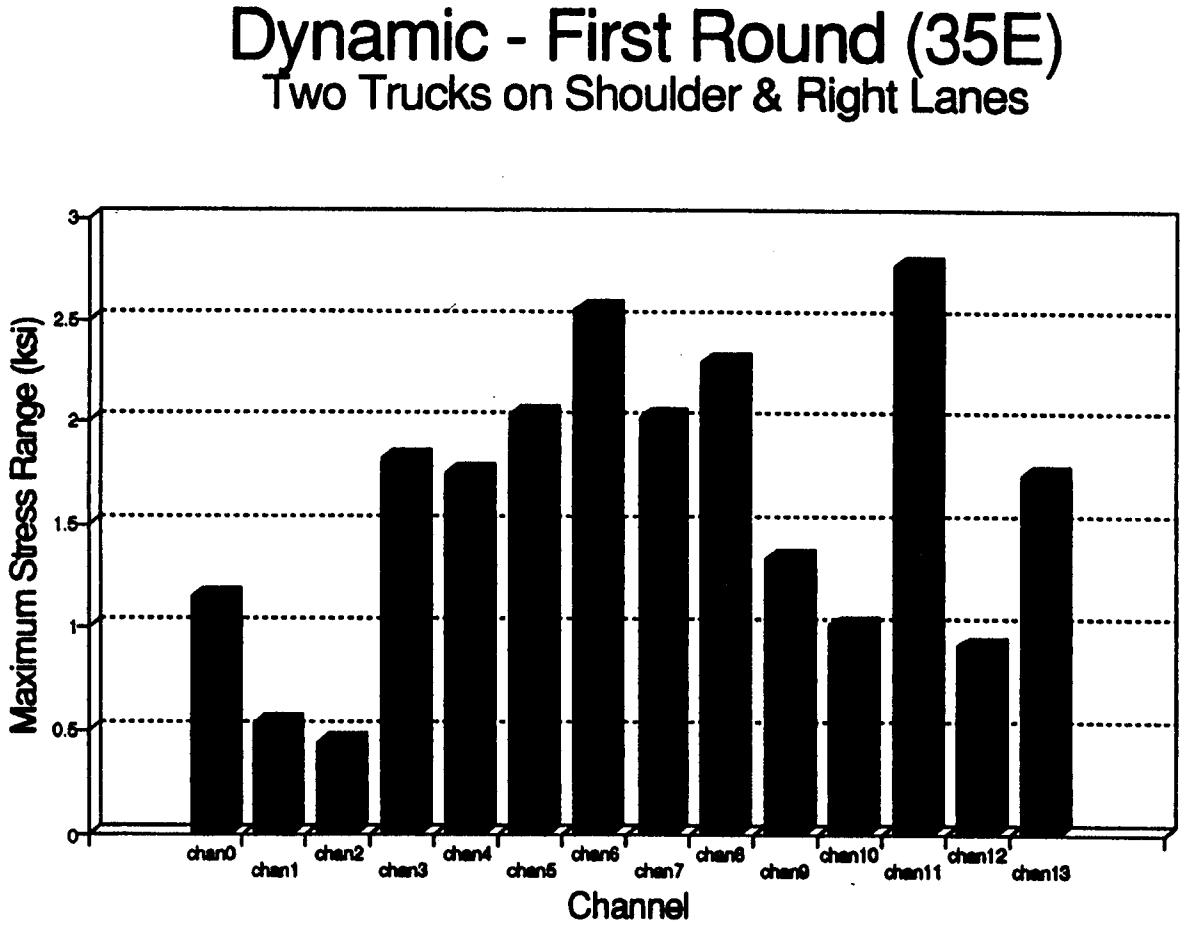

Figure 4.27 Maximum stress ranges (raw data)

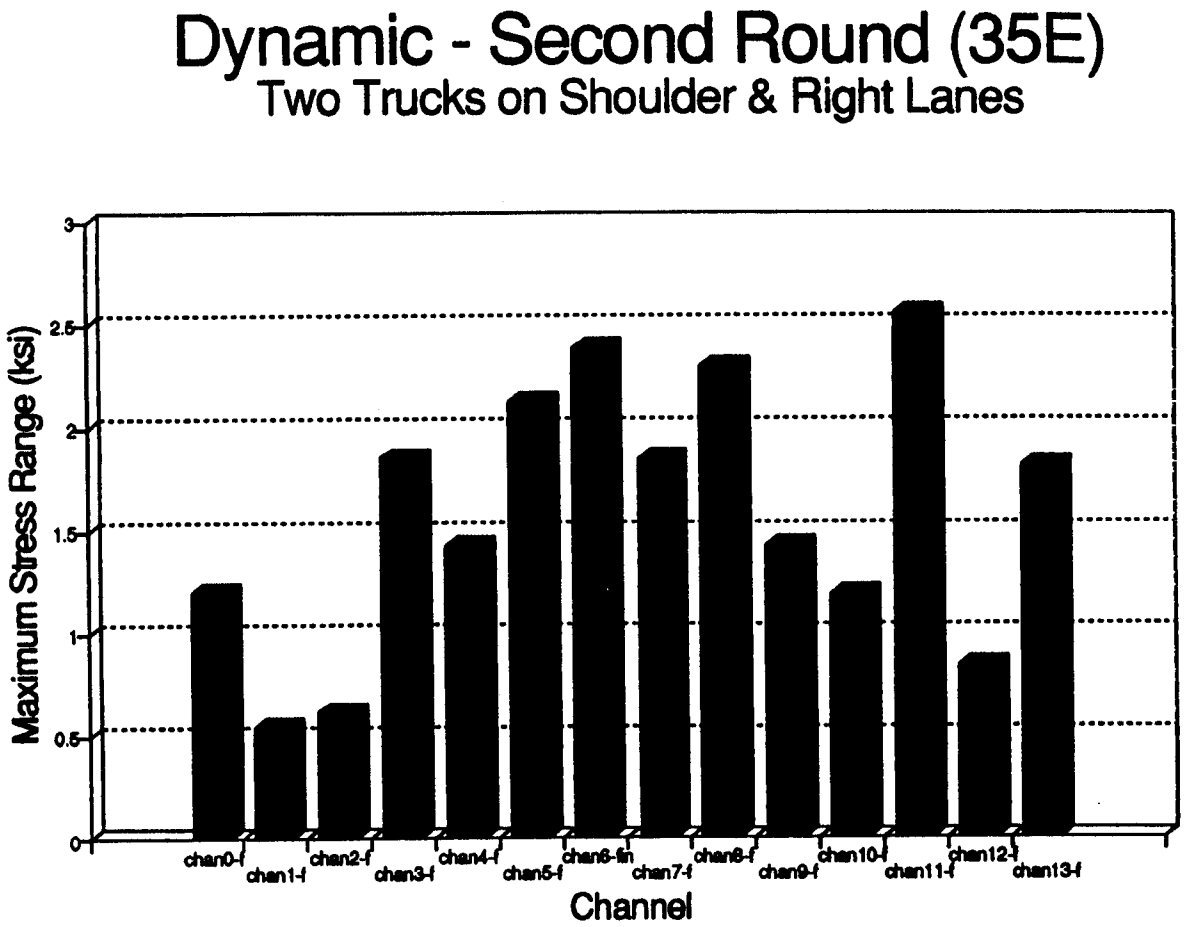

Figure 4.28 Maximum stress ranges (filtered data)

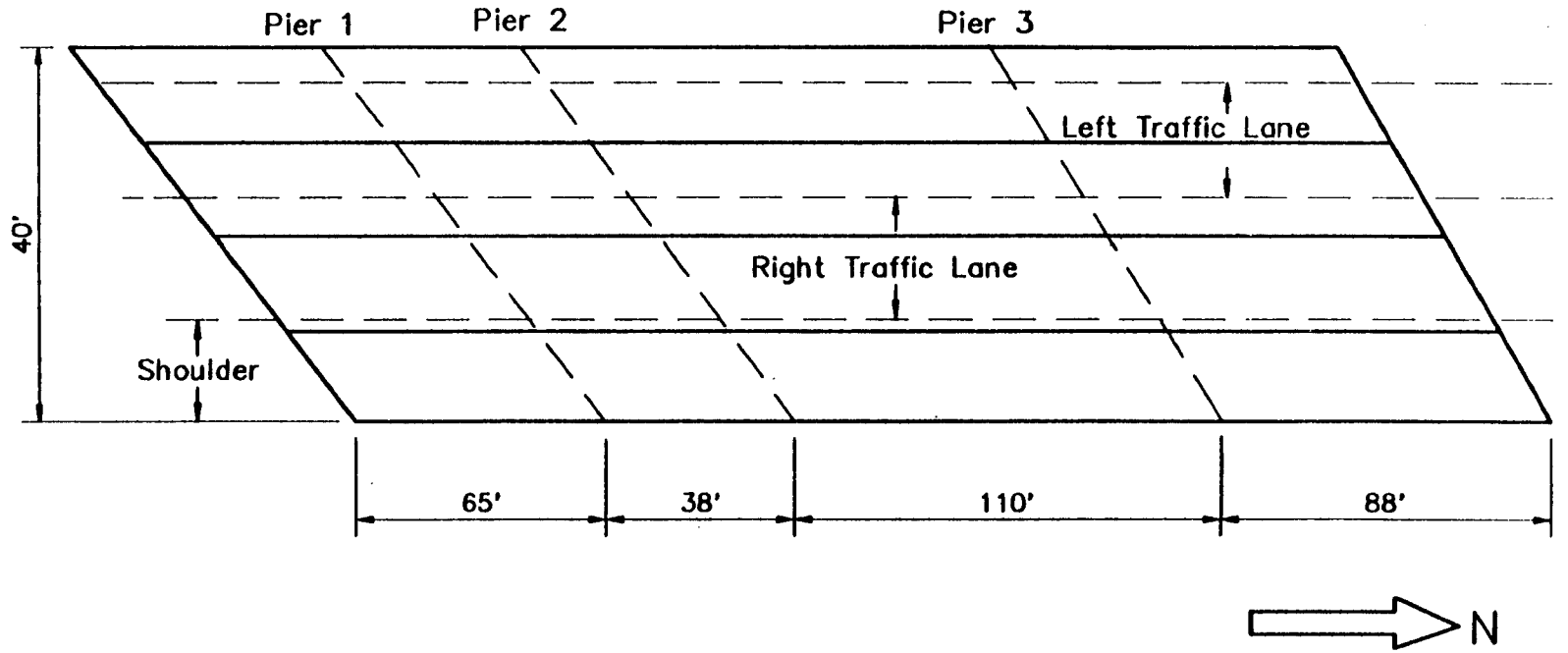

Figure 5.1 Plan view of bridge no. 9613

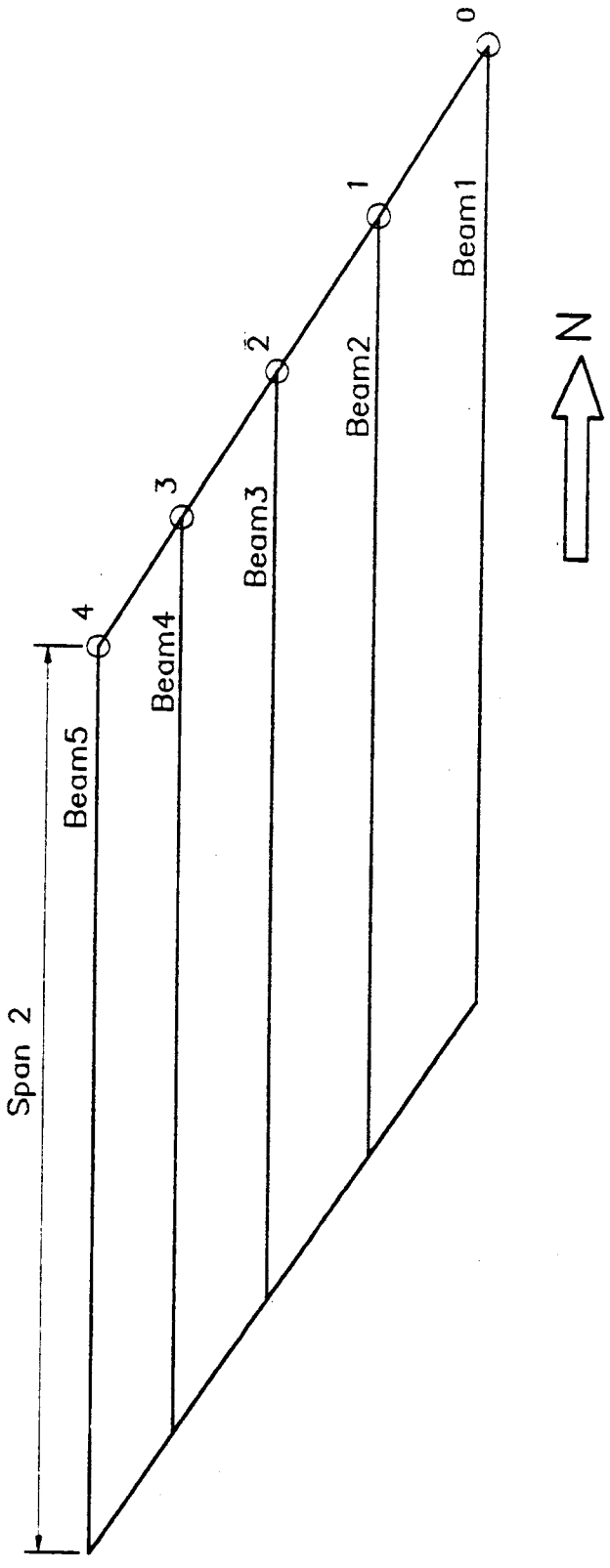

Figure 5.2 Location of strain sensors for bridge no. 9613

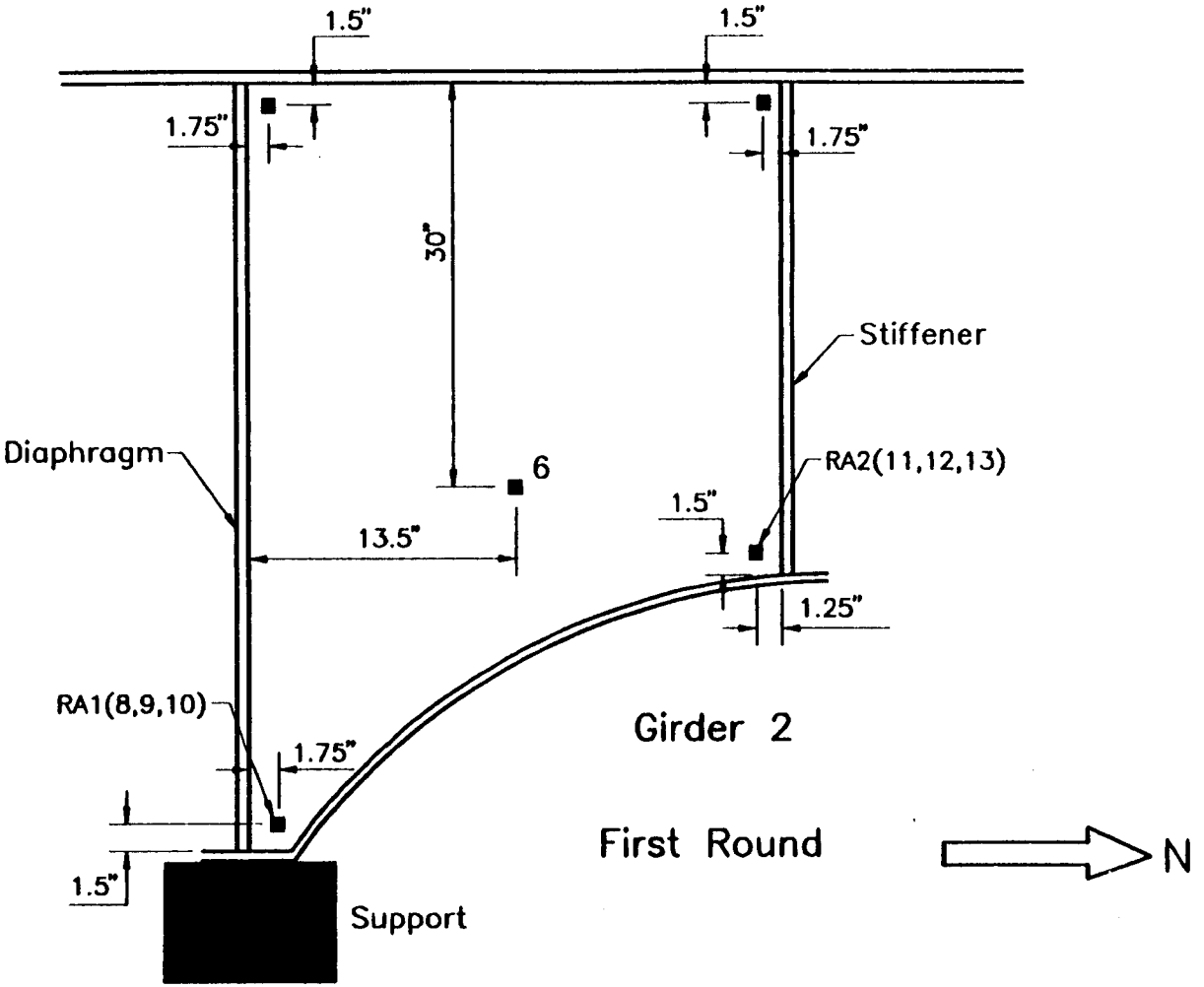

Figure 5.3 Location of strain gages for fatigue measurements

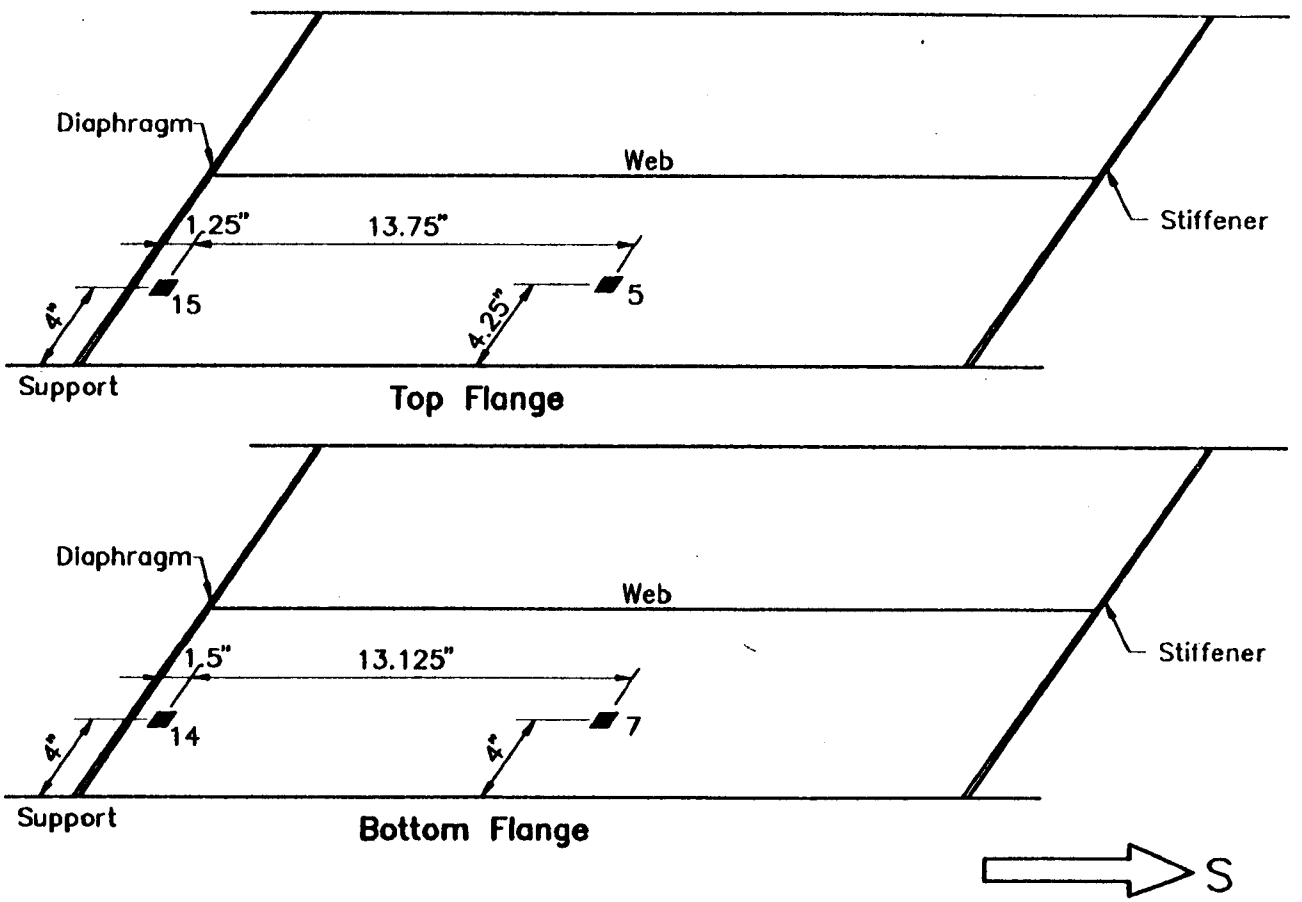

Figure 5.4 Location of strain gages for fatigue measurements

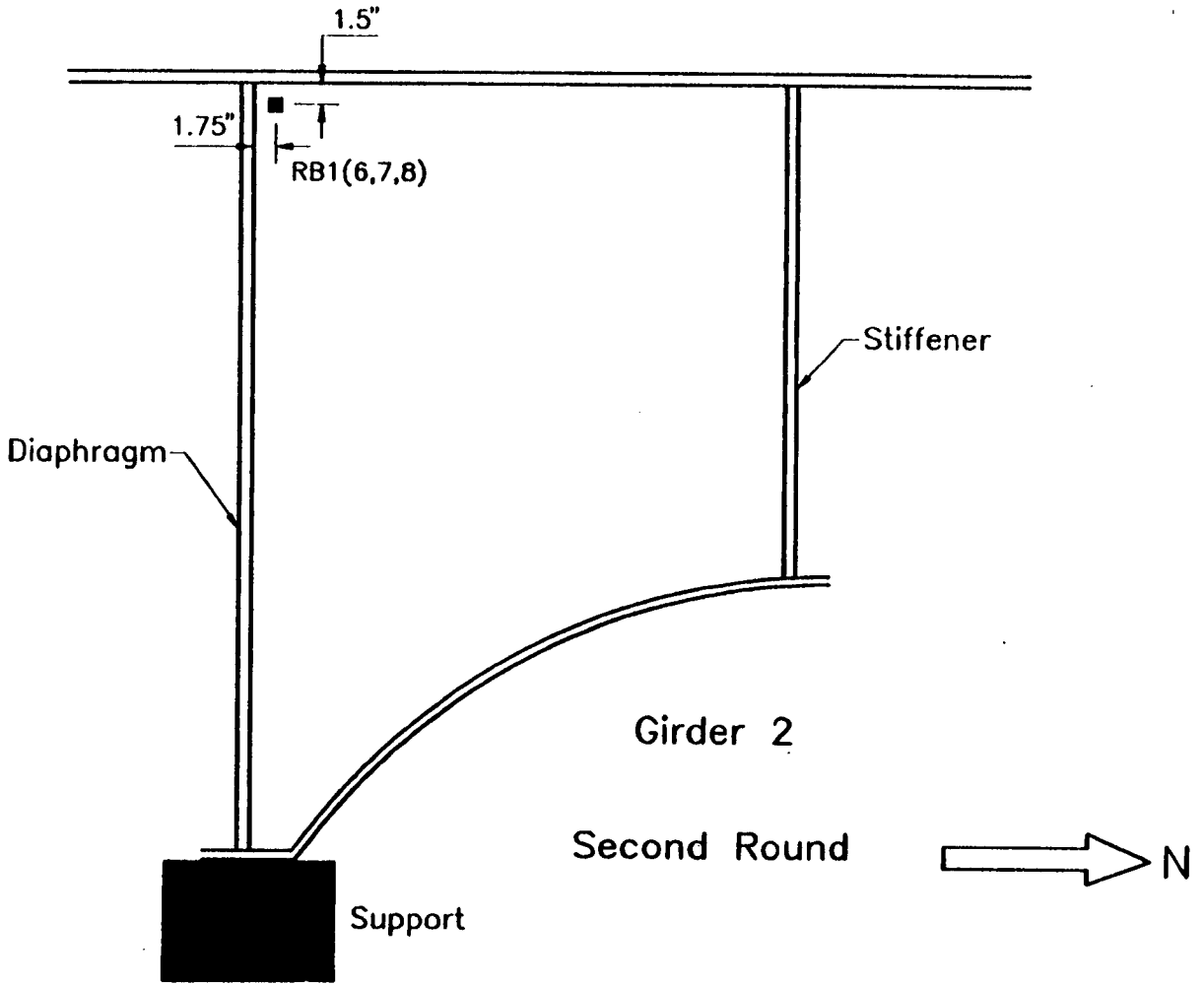

Figure 5.5 Location of strain gages for fatigue measurements

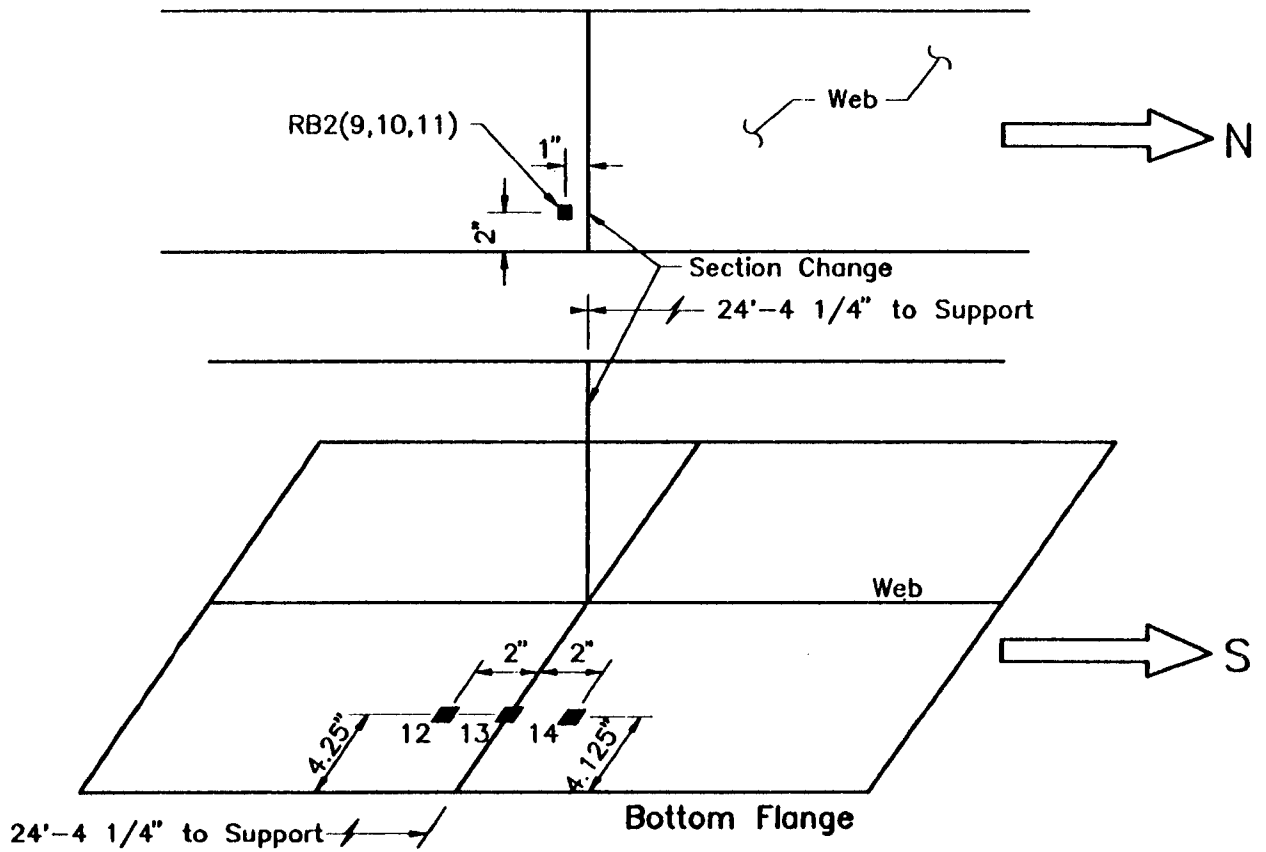

Figure 5.6 Location of strain gages for fatigue measurements

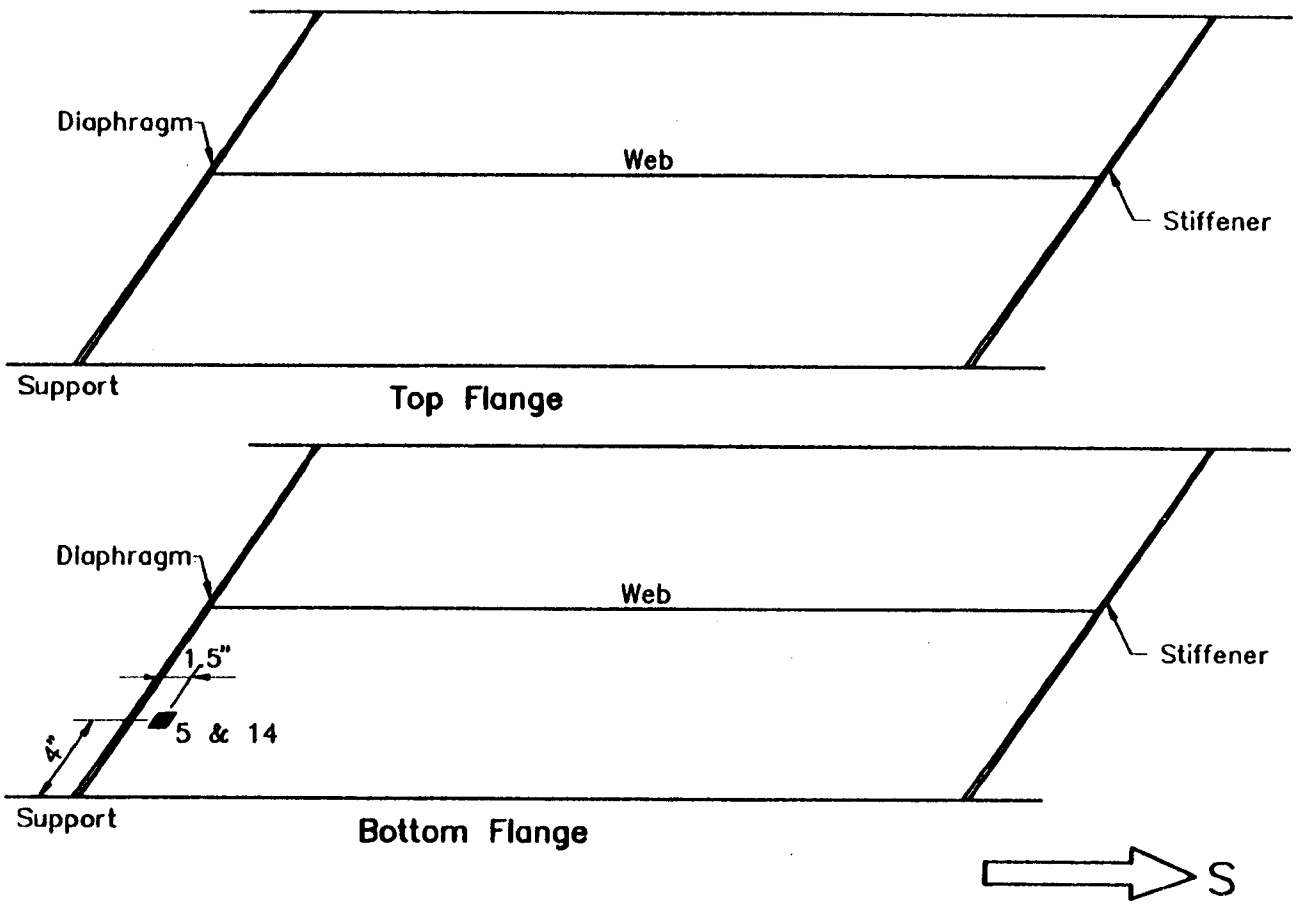

Figure 5.7 Location of strain gages for fatigue measurements

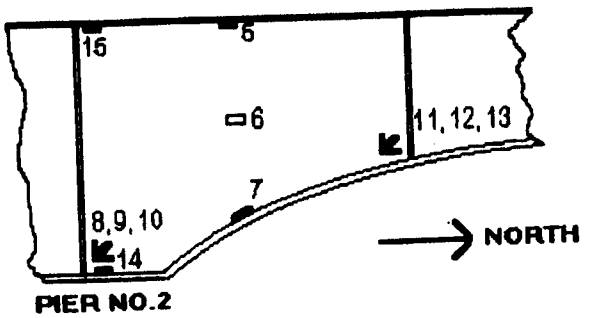

Figure 5.8 Location of strain gages for fatigue measurements

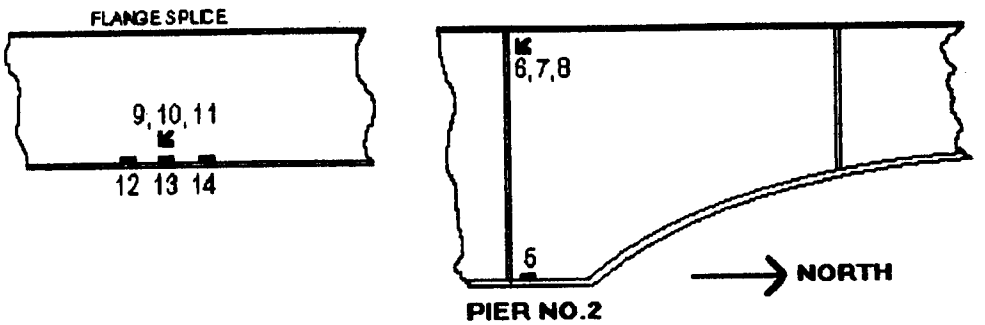

Figure 5.9 Location of strain gages for fatigue measurements

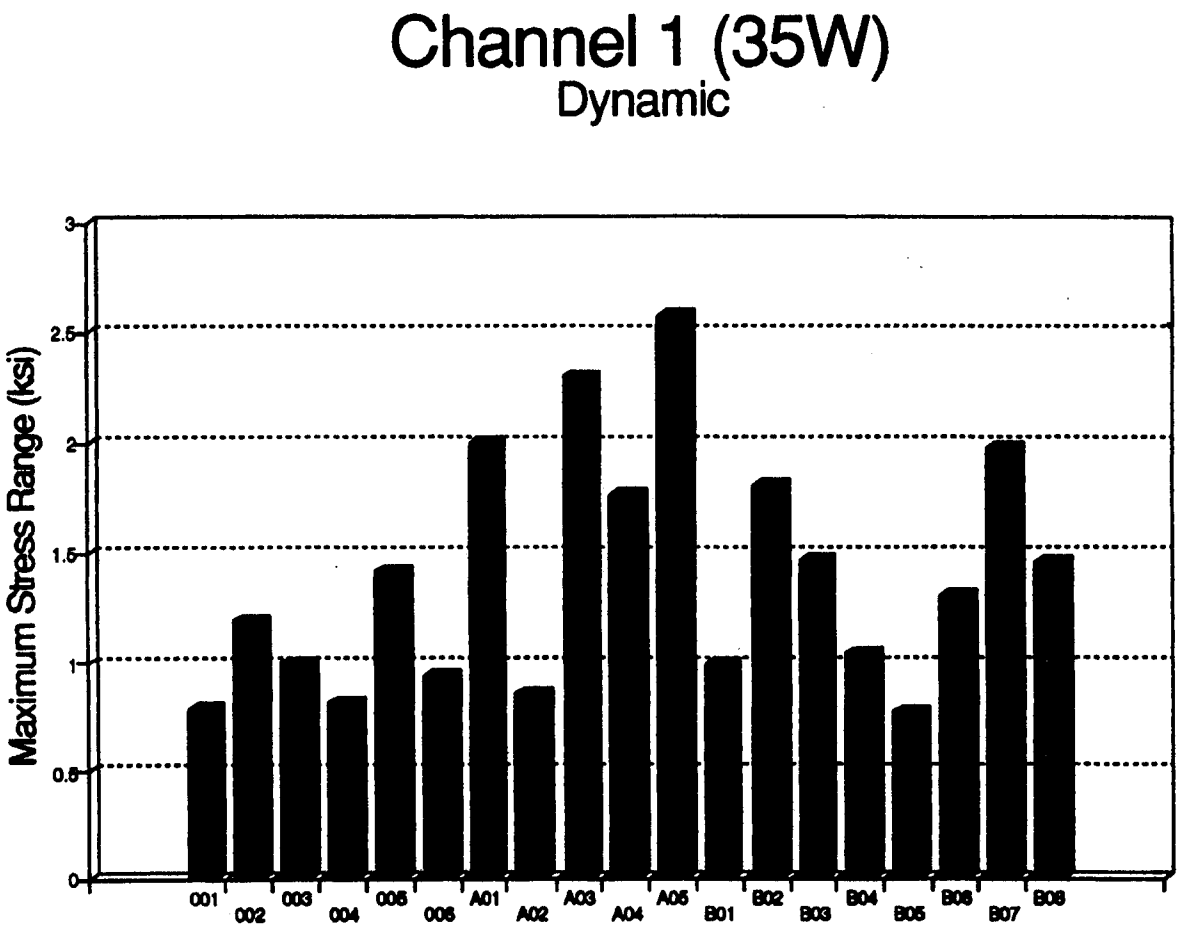

Figure 5.10 Maximum stress range (pier No. 2, bottom flange, beam 2)

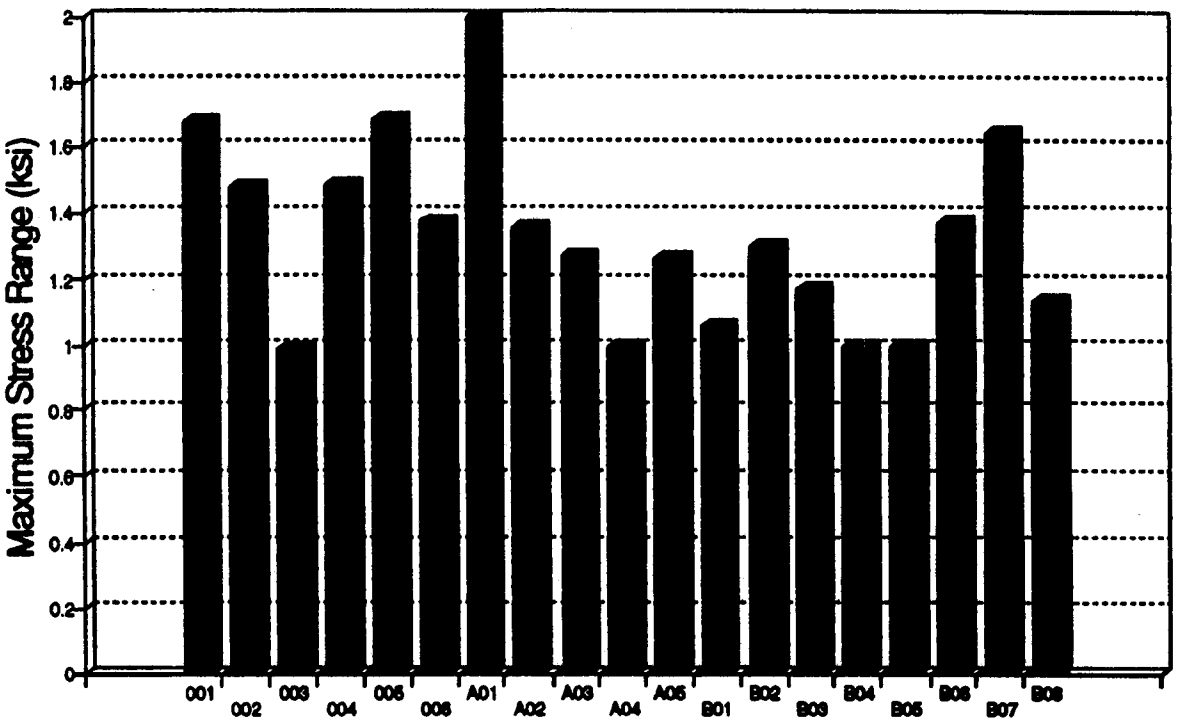

Figure 5.11 Maximum stress range (pier No. 2, bottom flange, beam 2)

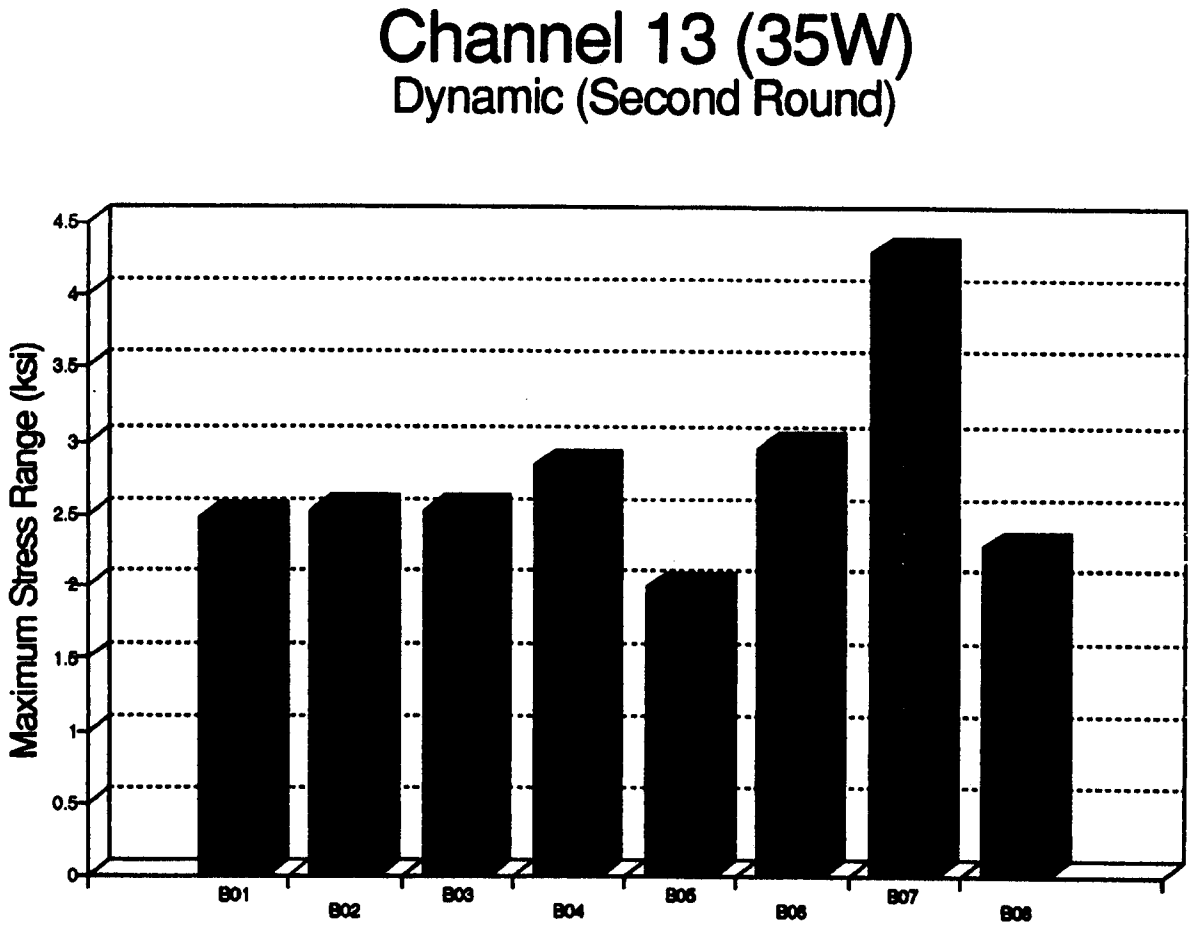

Figure 5.12 Maximum stress range (flange splice, on bottom flange)

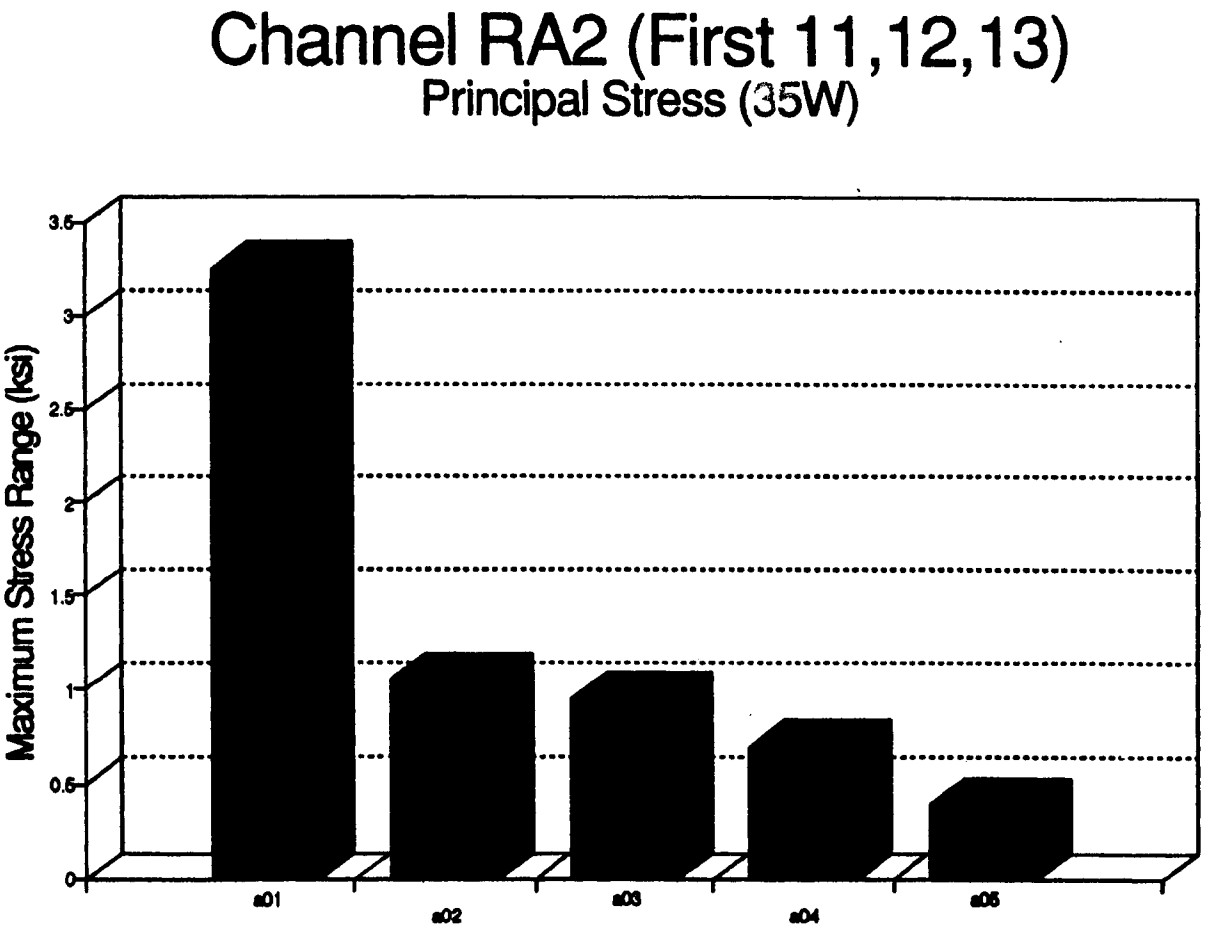

Figure 5.13 Maximum stress range (bottom of web, near stiffener)

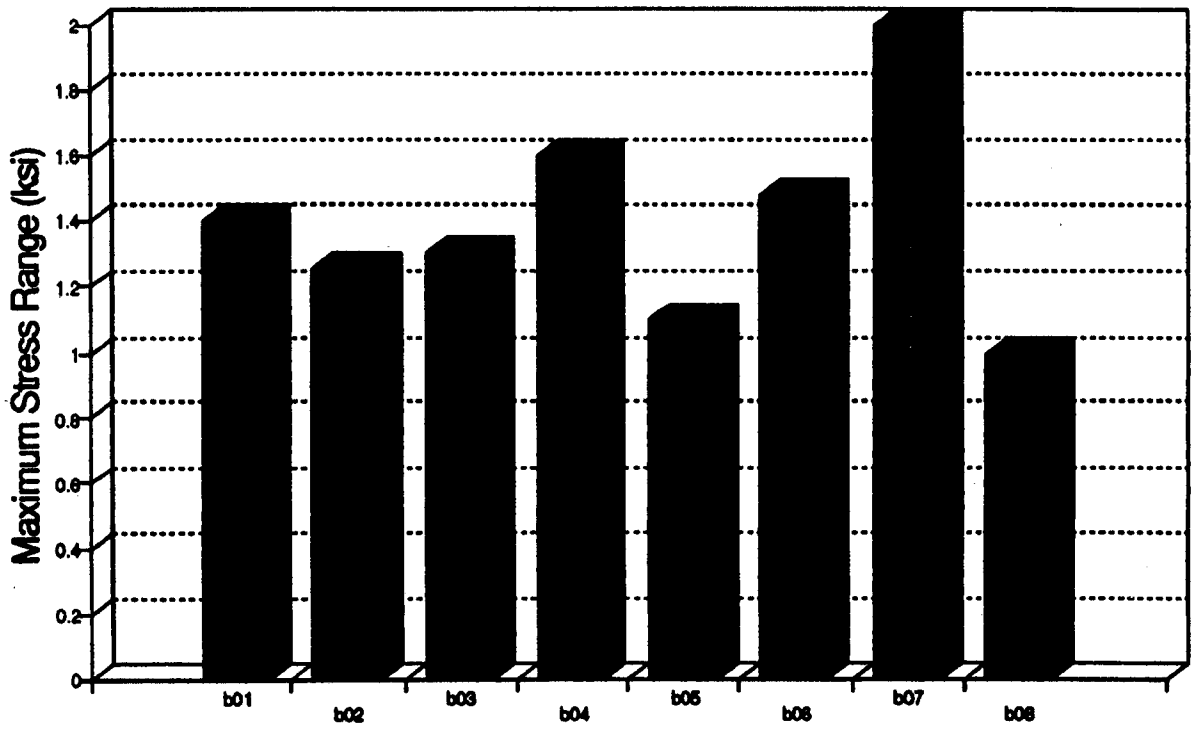

Figure 5.14 Maximum stress range (bottom of web, near flange splice)

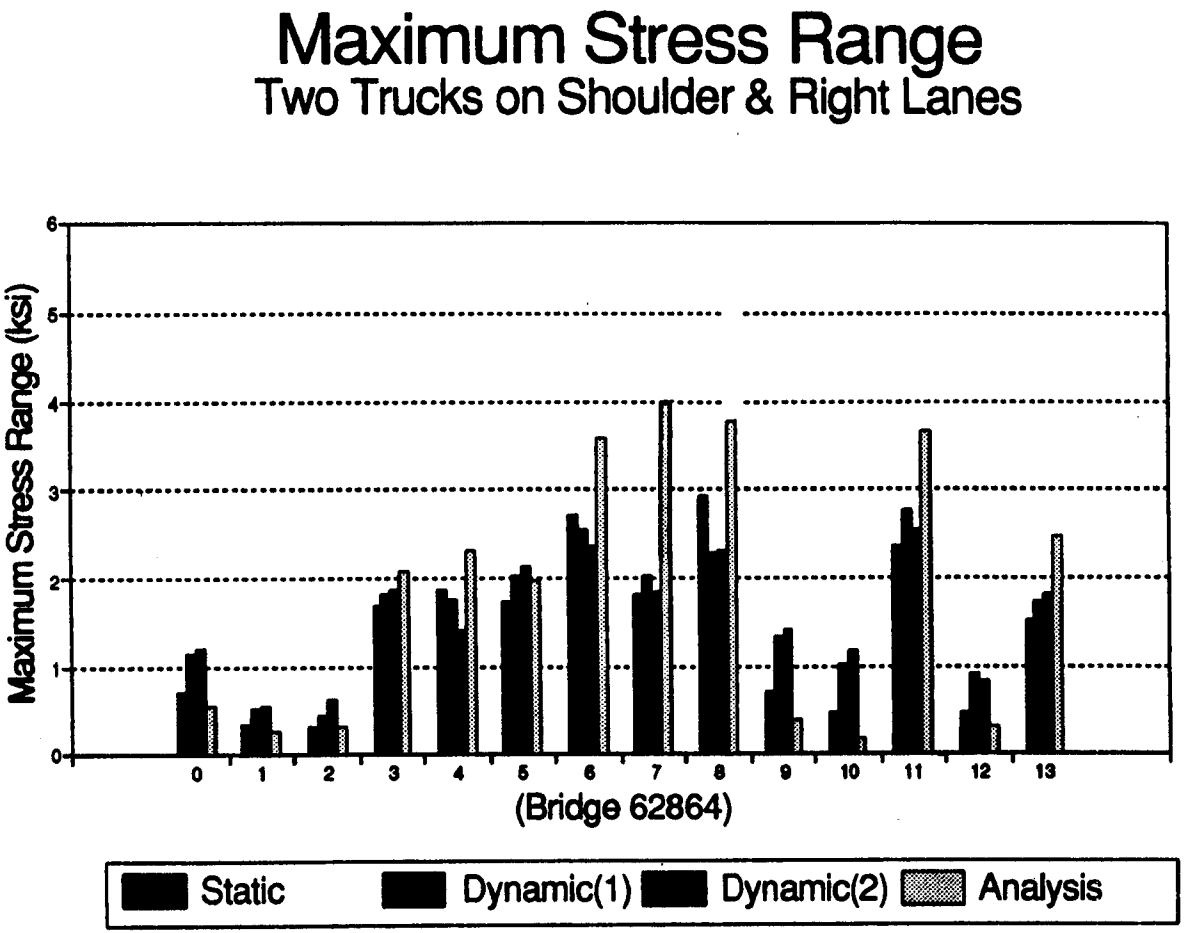

Figure 6.1 Histograms of static and dynamic stress ranges

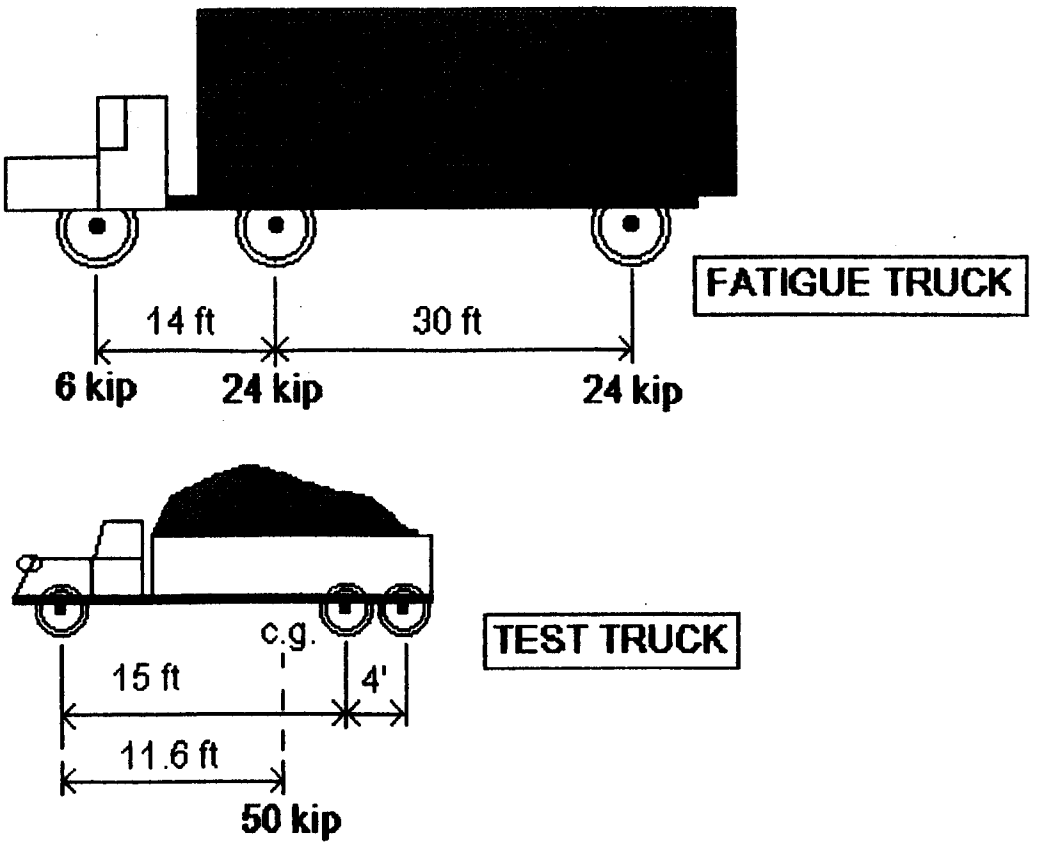

Figure 6.2 Histograms from fatigue truck